Volume 92 • Number 1 • April 2021
Established in 1923 • ISSN 1945-0702

The Chemist

Journal of the American Institute of Chemists

In this Issue

PVC Hose courtesy of Pixabay

Official journal of
The American Institute of Chemists, Inc.
http://www.theaic.org/pub_thechemist_journals/

The Chemist

Established in 1923, The Chemist is the official publication of The American Institute of Chemists, Inc. (AIC). The Chemist was published quarterly in magazine format up until 2006. The Chemist is currently being set up and formatted as an online journal.

The Chemist (ISSN-0009-3025) is published online by The American Institute of Chemists, Inc.

Volume 92 | Issue 1 | 2021

The Chemist

Journal of the American Institute of Chemists

The Chemist (Established in 1923)

Editorial

Alexander G. Zestos

Nayiri Kaissarian

Co-Editors of The Chemist

On May 9, 2019, we attended the Induction of the new American Institute of Chemists (AIC) Pioneer Awardees at the Science History Institute in Philadelphia, PA. Dr. William H. Starnes, Jr. from the College of William and Mary, Dr. Richard Kaner from the University of California Los Angeles (UCLA), and Dr. Peng Chen from Cornell University were the honorees for the AIC Pioneer Award. At the referral of Dr. Starnes, we were soon named the co-editors of The Chemist publication by the American Institute of Chemists. This is a great honor for me as Dr. Starnes was my B.S./M.S. mentor when I was a student at the College of William and Mary in Williamsburg, VA. Since that time, Dr. Starnes and his wife, Dr. Sofia M. Starnes, have remained close family friends. Dr. Starnes has remained as a lifelong mentor for me whose support and advice has helped me tremendously throughout my career.

After a short hiatus, The Chemist returns with a special issue honoring these three remarkable scientists, professors, and awardees in the field of chemistry. The issue begins with an overview of Dr. Starnes' vast accomplishments and work of over fifty years with the poly(vinyl chloride) (PVC) in both industry and academia. Particular attention is paid to the development of ester thiols as thermal stabilizers for PVC.[1] We also detail Dr. Peng Chen's work with Single-Molecule Catalysis and Dr. Richard Kaner's remarkable journey and story with polyaniline nanofibers that detail the journey from laboratory curiosity to commercial products. This issue also includes contributions from Shenoy et. al on Imidazo Pyridine Derivative as a New Corrosion Inhibitor for Mild Steel and Evidence of Macromolecular Structure of Humic Acids from Compost from Campasso and colleagues. We also present Kulkarni's work on Theoretical Validation of Medicinal Properties os Ocimum sanctum and some desert electrochemistry in Jordan where Dr. Amayreh details the construction of a locally used Cactus (Opuntia) Battery. Lastly, this issue includes Barron's work on Animals and the great war and Chen's article on the proper selection and application of mathematical models for estimating occupational exposure to chemicals.

The on-going COVID-19 global pandemic has impacted all of our lives in ways no one could have predicted. The role that chemists and other scientists have played in the response, treatment, and recovery efforts has been paramount. With this issue, we seek to highlight the impact that scientific discovery and advancement can have in our world. We are currently accepting submissions for all types of articles in every field of chemistry for our upcoming issue and sincerely hope that you all consider submitting an article for consideration. We wish you all health and happiness in 2021 and beyond!

Sincerely,
Alexander G. Zestos, Ph.D Nayiri Kaissarian, Ph.D
Co-Editors of The Chemist

References

1. Ge, X.; Culyba, E. K.; Grinnell, C. L.; Zestos, A. G.; Starnes, W. H., Mechanism of action and effectiveness of ester thiols as thermal stabilizers for poly (vinyl chloride). Journal of Vinyl and Additive Technology 2007, 13 (4), 170-175.

The Chemist
Journal of the American Institute of Chemists

Fifty Years with PVC

William H. Starnes, Jr.

Departments of Chemistry and Applied Science, College of William & Mary
Williamsburg, Virginia 23187-8795
(E-mail: whstar@wm.edu)

Abstract: Summarized here are the results of research by the author and his associates on several aspects of the chemistry of poly(vinyl chloride) (PVC), one of the world's most widely used and extensively studied synthetic polymers. The principal topics covered are the molecular microstructure of PVC and its elucidation, the mechanism for the thermal dehydrochlorination of PVC and its autocatalysis by HCl, and the thermal stabilization of PVC by ester thiols, a patented technology that has been licensed for commercialization both domestically and overseas. Special attention is given to the role of free radicals in PVC thermolysis. This article is an invited contribution based on the author's AIC Chemical Pioneer Award address delivered on May 9, 2019.

Key Words: Poly(vinyl chloride), PVC structural defects, PVC thermolysis mechanism, PVC dehydrochlorination autocatalysis, PVC thermal stabilization, ester thiol stabilizers

Introduction

This paper is a condensed version of the Chemical Pioneer Award address titled "Fifty Years with PVC", which was delivered in Philadelphia on May 9, 2019, at the annual meeting of the American Institute of Chemists. The round number in the title is slightly misleading, as the author's work on poly(vinyl chloride) (PVC) actually began in 1973 at AT&T Bell Laboratories ("Bell Labs"). On the other hand, his early ideas for this research were conceived before that time.

The intrinsic thermal stability of PVC is much less than that of the other major commercial synthetic polymers. For that reason, an enormous amount of research, both basic and applied, has been done in order to understand the reason(s) for this problem and to solve it. In fact, thousands of papers have been published in this general area.

Remarkably, though, a clear understanding of the mechanism of the initial thermolysis process remained elusive for more than 60 years after PVC was first commercialized. The present article outlines the work of the author and his associates relating to this mechanism and then comments briefly on a promising approach to thermolysis to describe all of the research that was recognized by the Chemical Pioneer Award. A major concern of this paper is the question of how and to what extent free radicals are involved in the earliest stages of degradation, where the polymer loses most or all of its useful properties.

Overview, Structural Defects, and Nonradical Degradation

Except for the very low concentrations of structural defects it contains, PVC is a conventional head-to-tail polymer made commercially only by free-radical polymerization. In the earliest stage, its thermolysis (equation 1) is just a process of dehydrochlorination involving the sequential loss of HCl from adjacent monomer units, in order to generate a family of conjugated polyene sequences having different lengths. The number of double bonds in these sequences can range from only a few up to 15–20, or even more, depending upon the conditions under which the degradation is occurring. Once initiated, polyene growth is extremely fast, an observation which shows that it involves some sort of "zipper" mechanism in which the loss of an HCl molecule facilitates the loss of HCl from an adjacent monomer unit [1]. The degradation begins slowly at temperatures as low as 100 °C and is autocatalyzed by the evolving HCl [1]. Furthermore, it is now generally agreed to be initiated primarily, if not exclusively, by structural defects that incorporate allylic or tertiary chloride and are situated well away from the ends of the polymer chains [1–3].

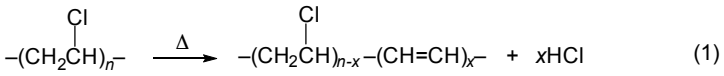

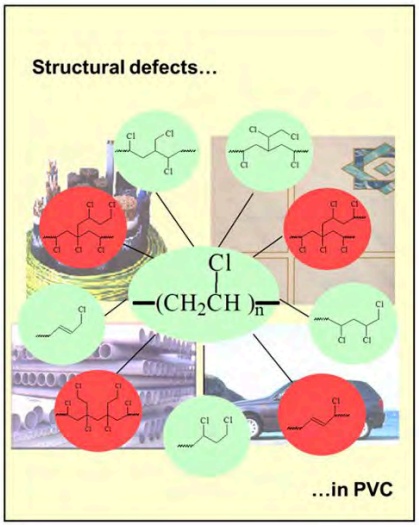

Fig 1. Structural Defects in PVC (drawing by research student J. Zhang)

Figure 1 shows all of the defect structures that are now believed to be present in all samples of commercial PVC [2]. The thermally stable structures are shown in green; those activating thermolysis are in red. By using ^{1}H and ^{13}C NMR spectroscopies, together with chemistry involving, *inter alia,* prior reductive dechlorination of PVC samples with tri-*n*-butyltin hydride or tri-*n*-butyltin deuteride, we were able to deduce the molecular constitutions, concentrations (frequencies of occurrence), and mechanisms for the formation of all of these structural defects, while disproving the occurrence of other defects whose presence had been proposed [1,2]. Some of our findings have been confirmed by other researchers [1,2].

Concurrent and previous studies performed by us and other investigators also led to the conclusion that, in its earliest stage, PVC thermolysis is very likely to involve the ion-pair mechanism of equation 2 or a four-center concerted pathway such as that in equation 3 [1],

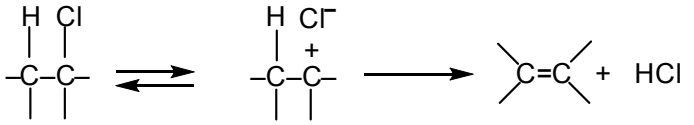

(2)

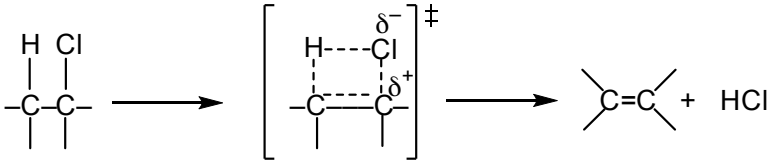

(3)

where the transition state does not necessarily have the symmetry that is shown. In the ion-pair process, discharge of the intermediate by proton transfer creates an internal chloroallylic segment whose instability allows sequential dehydrochlorination to continue rapidly down the chain. This mechanism obviously would be favored by the high thermodynamic stabilities of allylic and tertiary carbocations formed from the unstable structures in Figure 1. The mechanism of equation 3 would be assisted by the same factors and thus can be regarded as quasiionic in nature. A quasiionic mechanism seems most likely to operate in the vapor phase, but its occurrence in media of relatively low polarity (too low to allow the existence of ion pairs) has not been excluded conclusively, even though its operation is "forbidden" by orbital symmetry rules.

Free-Radical Mechanisms Proposed for Polyene Formation

Notwithstanding the considerations just described, a huge amount of experimental evidence points to the possible involvement of free radicals in the early stages of the thermolysis of PVC. Described elsewhere in detail [1,2,4–6], this evidence shows that the thermolysis is accelerated by radical sources and retarded (under certain conditions) by radical scavengers, that radicals are produced during the thermolysis process itself, and that conjugated polyenyl diradicals are present in the thermally decomposed polymer.

In 1954, Arlman [7] proposed a free-radical mechanism for polyene growth during PVC thermolysis. It is shown in equation 4, where the initial value of n is 0. As depicted, it consists of a series of steps in which HCl molecules are eliminated in succession from adjacent monomer units, so as to form a conjugated polyenyl radical that increases in length as the process proceeds. The rate constant $k_{el,n}$ for each Arlman step may vary as a function of n, thereby giving a set of values that can be compared, as discussed below, with the value of a rate constant $k_{el,s,}$ which applies to a "standard" reaction (equation 5) involving the thermolysis of a simple sec-alkyl chloride containing no radical centers or double bonds.

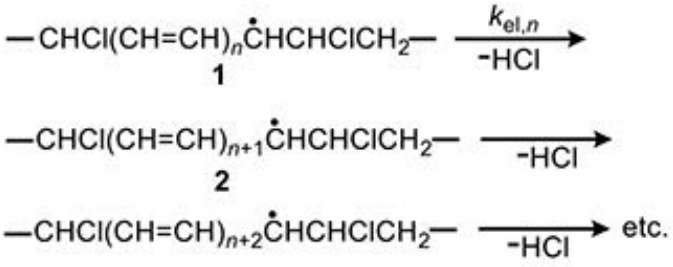

(4)

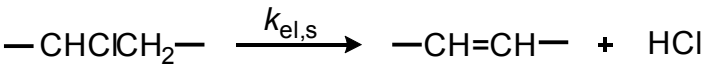

(5)

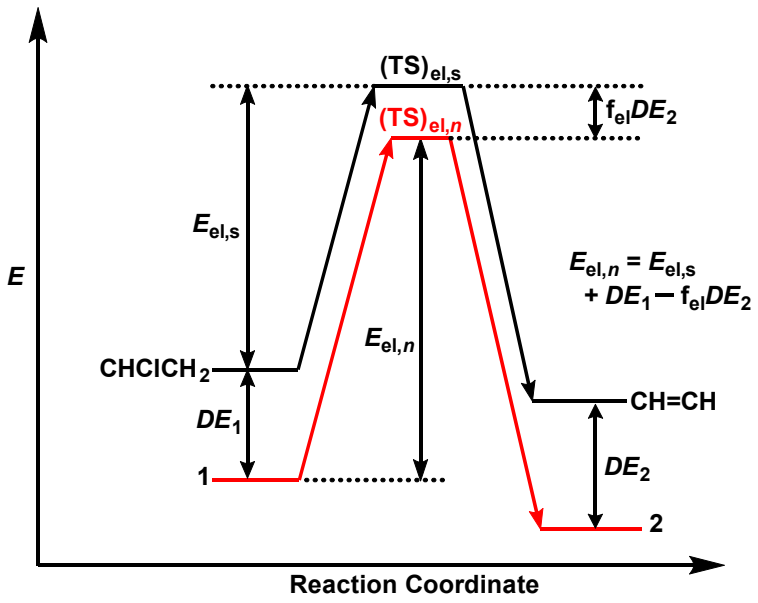

Fig 2. Energy Diagram for Polyene Growth

The energetics of the Arlman scheme can be assessed with recourse to Figure 2, where the energy (E) levels assigned to reactant, transition state (TS), and organic product have no quantitative significance, though they are thought to be accurate in a relative sense. The figure shows that the activation energy for the standard elimination is $E_{el,s}$ and that the ground-state energies of radicals **1** and **2** in equation 4 will be lowered by conjugative stabilization or delocalization (DE_1 and DE_2), except, of course, in the case where $n = 0$. To the extent that the transition state, $(TS)_{el,n}$, for an Arlman elimination (shown in red) structurally resembles **2**, its energy will be decreased by some fraction, f_{el}, of DE_2. Accordingly, the activation energy, $E_{el,n}$, for the Arlman step is given by the expression near the right-hand side of Figure 2.

With these considerations in mind, we can write the Arrhenius equations for the standard elimination (equation 6) and an Arlman step (equation 7) and then combine them to produce equation 8, which could be used with experimental data to predict values of the Arlman rate constant, as a function of n,

$$k_{el,s} = A_{el,s} e^{-E_{el,s}/RT} \tag{6}$$

$$k_{el,n} = A_{el,n} e^{-(E_{el,s} + DE_1 - f_{el}DE_2)/RT} \tag{7}$$

$$k_{el,n} = k_{el,s}(A_{el,n}/A_{el,s}) e^{(f_{el}DE_2 - DE_1)/RT} \tag{8}$$

if the values of f_{el} and the A-factor ratio were known. Since they are not, we will opt instead

for a different approach involving the assignment of values to these two terms that are demonstrably too high. The resulting equation can be used to predict *maximum* values of $k_{el,n}$, which then can be compared with experimental observations in order to test for the validity of the Arlman hypothesis.

First, we will arbitrarily assign a value of 1 to f_{el}. This assumption is patently ridiculous, as the Arlman transition state certainly would not enjoy *all* of the stabilization energy of radical **2**. Next, as regards the *A* factors, we note from Figure 3 that, unlike for the standard elimination,

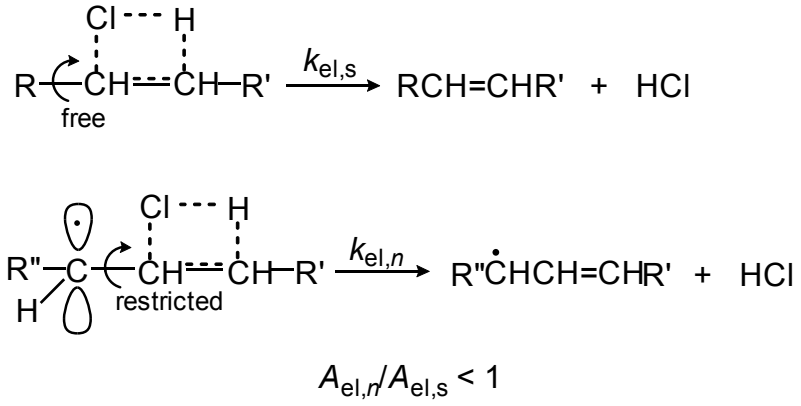

Fig 3. Rotational Effects Influencing Arrhenius *A* Factors

rotation about a proximal C-C bond would be restricted, or perhaps even frozen, in the Arlman transition state, because that would tend to decrease the total energy of the system by maximizing overlap of the incipient π orbital with a *p* orbital (depicted) or a π orbital of the radical segment already present. The concurrent entropic reduction would tend to cause the *A*-factor ratio to be less than 1.

Consequently, assuming it to be 1, together with the assumption that $f_{el} = 1$, converts equation 8 into equation 9, which can be used with confidence to calculate values of $k_{el,n}$ that are too high. Before proceeding to do this, however, it will be convenient to outline a similar analysis of another free-radical process for polyene growth in PVC.

$$k_{el,n} \leq k_{el,s} e^{(DE_{\mathbf{2}} - DE_{\mathbf{1}})/RT} \quad (9)$$

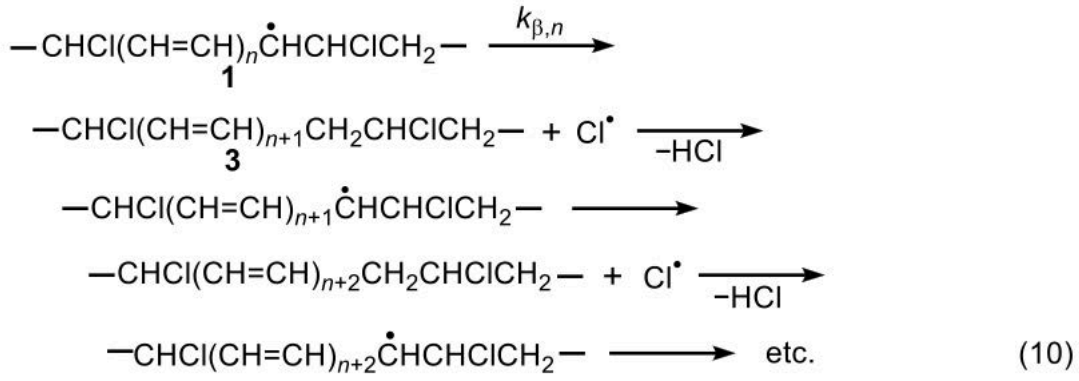

This process (equation 10) was suggested independently by Winkler [8] and by Stromberg et al. [9] in 1959. Like the Arlman mechanism, it starts with radical **1** but requires two steps to form a new double bond and a molecule of HCl. The first step is a β scission process yielding polyene segment **3** and a chlorine atom; the second step involves abstraction, by the chlorine atom, of a weakly bonded allylic methylene hydrogen in **3.** This step gives HCl and a new (and longer) polyenyl radical, whose subsequent β cleavage allows the process to continue in the same way. Regardless of which step is rate-determining, if either of them can be shown to be too slow to account for the experimental rate of polyene growth, then the Winkler-Stromberg mechanism can be regarded as disproven. Accordingly, we will select the β scission step and analyze it by following the procedure used for the Arlman process. In this analysis, the starting species for the standard reaction (equation 11) is

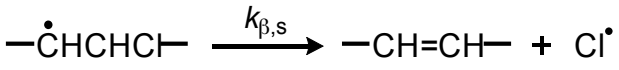

now a *sec*-chloroalkyl radical containing no double bonds, and the Arrhenius expressions for this reaction and the Winkler-Stromberg β scission are equations 12 and 13, respectively. Their combination produces equation 14; and when f_β and the *A*-factor ratio are assigned a value of 1, this equation reduces into equation 15, which should predict inflated values of $k_{\beta,n}$.

$$k_{\beta,s} = A_{\beta,s}e^{-E_{\beta,s}/RT} \quad (12)$$

$$k_{\beta,n} = A_{\beta,n}e^{-(E_{\beta,s} + DE_{\mathbf{1}} - f_\beta DE_{\mathbf{3}})/RT} \quad (13)$$

$$k_{\beta,n} = k_{\beta,s}(A_{\beta,n}/A_{\beta,s})e^{(f_\beta DE_{\mathbf{3}} - DE_{\mathbf{1}})/RT} \quad (14)$$

$$k_{\beta,n} \leq k_{\beta,s}e^{(DE_{\mathbf{3}} - DE_{\mathbf{1}})/RT} \quad (15)$$

Table 1 lists values of the radical delocalization enthalpy (SE_{rad}) and the enthalpy of conjugation (SE_{conj}) for the linear enes and enyl radicals identified in column 1, all of which are conjugated except for C_2. For each chemical species, the sum of its two enthalpies is the *DE* value in column 4. The radical delocalization enthalpies are experimental values from the literature [10]; conjugation enthalpies were determined by multiplying the enthalpy of a single conjugative interaction (15.6 kJ/mol) by the number of these interactions in the species of interest [10,11].

Table 1. Stabilization Energies of Enes and Enyl Radicals

Ene or enyl	SE_{rad} (kJ/mol)	SE_{conj} (kJ/mol)	*DE* (kJ/mol)
C_2	0	0	0
$C_3^{\bullet}$	56.5[a]	0	56.5
C_4	0	15.6	15.6
$C_5^{\bullet}$	70.7[a]	15.6	86.3
C_6	0	31.2	31.2
$C_7^{\bullet}$	80.3[a]	31.2	111.5
C_8	0	46.8	46.8
$C_9^{\bullet}$	86.6[a]	46.8	133.4
C_{10}	0	62.4	62.4

[a] Value from [10]

Values of *DE* corresponding to various values of *n* are listed in Table 2 for radicals **1** and **2** and for polyene **3** in the schemes of Arlman (equation 4) and Winkler et al. (equation 10). When the appropriate DE_1 and DE_2 values and the experimental value of ca. 10^{-7} s^{-1} for $k_{el,s}$ at 175 °C (references cited in [6]) are used in equation 9, the $k_{el,n}$ values in Table 2 ensue. All of them except the one for $n = 0$ are much too low to account for the growth of PVC polyenes, which has an experimental rate constant, k_p, of ca. 10^{-2} s^{-1} at the same temperature (references cited in [6]). Thus the Arlman mechanism can now be dismissed from serious consideration.

Table 2. Delocalization Energies of Reactive Species and Predicted Rate Constants for Reactions in the Arlman and Winkler-Stromberg Schemes for Polyene Growth

	Delocalization energies (kJ/mol)			Maximum rate constants @175 °C (s^{-1})	
n	DE_1	DE_2	DE_3	$k_{el,n}$	$k_{\beta,n}$
0	0	56.5	0	4×10^{-1}	10^6
1	56.5	86.3	15.6	3×10^{-4}	20
2	86.3	111.5	31.2	9×10^{-5}	4×10^{-1}
3	111.5	133.4	46.8	4×10^{-5}	3×10^{-2}
4	133.4	—	62.4	—	5×10^{-3}

At 175 °C, $k_{\beta,s}$ is ca. 10^6 s^{-1} [12]. Insertion of this value and the requisite values of DE_1 and DE_3 for **1** and **3**, respectively, into equation 15 affords the predicted $k_{\beta,n}$ values that appear in Table 2. Though quite high at the outset, they attenuate rapidly with increasing values of *n*, a trend which shows that the β cleavage step of the Winkler-Stromberg mechanism soon becomes too slow to allow the growth of the longer PVC polyenes at the experimentally measured rate. Other strong arguments against the Winkler-Stromberg hypothesis have been presented elsewhere [6].

Effects of Additives on PVC Thermolysis Rates

In order to obtain more information about the mechanism for polyene formation, dehydrochlorination rates of powdered PVC were measured at 180 ° C flowing argon and in the presence of various additives [5].

β–Carotene (**4**, nominally all-trans when purchased) was used as a model for long PVC polyene sequences.

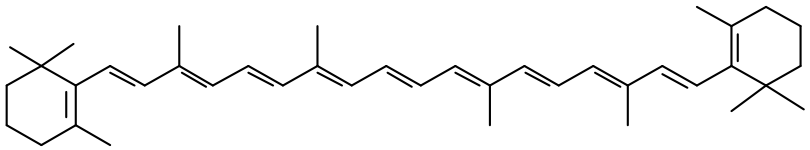

4

Additives "BHT" (an industrial acronym for 2,6-di-*tert*-butyl-4-methylphenol) and triphenylmethane (TPM) were introduced as potential radical scavengers (H-atom donors), and metallic mercury (Hg^o) was used as a potential specific scavenger of atomic chlorine [5 and references cited therein]. The argon was used to prevent air oxidation and to sweep the evolving HCl into a vessel containing water, where it was titrated with standard base in order to measure reaction rates. Argon also had a third (and very important) function, which was to change the HCl concentration in and around the degrading polymer. The higher the argon flow rate, the lower the concentration of HCl, and vice versa.

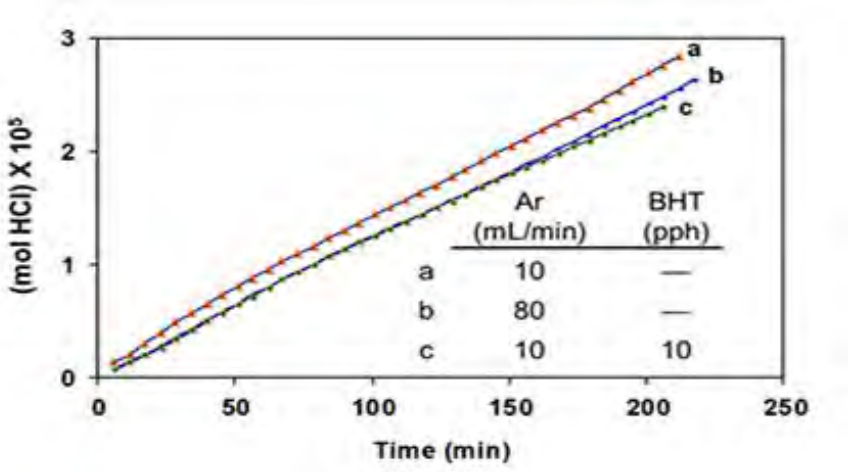

Fig 4A. Kinetic Plots for Dehydrochlorination at 180 °C

In the kinetics experiments of Figure 4A, after 200 min, the extent of dehydro-chlorination was only ca.1.5 mol %. So, at this stage, the polyene concentration was much lower than that. Moreover, the rate (as inferred from the slopes of the plots) was essentially unaffected by a change in HCl concentration (cf. curves a and b) or, when the HCl concentration was relatively high, by the addition of BHT (curve c; pph = parts by weight per hundred parts of polymer). However, the situation changed dramatically when a small amount of **4** was introduced at the outset. As Figure 4B demonstrates, this additive caused a powerful autoacceleration when the concentration of

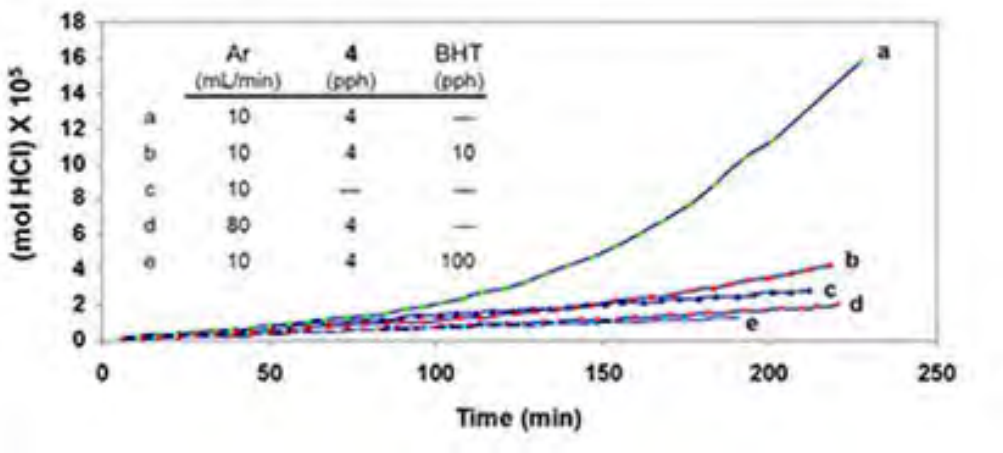

Fig 4B. Kinetic Plots for Dehydrochlorination at 180 °C

HCl was high (cf. curves a and c) but not when it was low (curve d), and the autoacceleration was greatly retarded (curve b) or prevented entirely (curve e) by the initial incorporation of increasing amounts of BHT. Similar results were obtained when TPM was used as the potential radical scavenger (Figure 4C, cf. curves b, c, and e), although the data showed that, in this respect, TPM was only about one-sixth as effective as BHT.

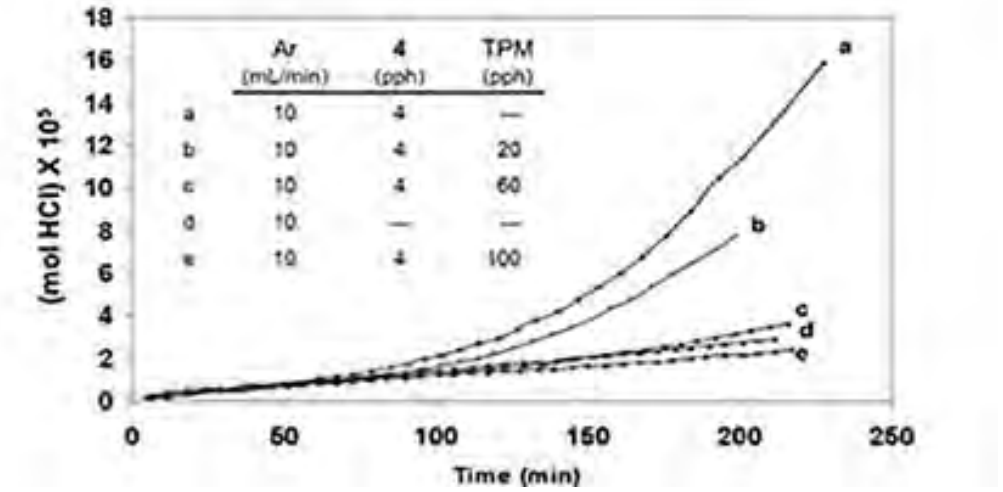

Fig 4C. Kinetic Plots for Dehydrochlorination at 180 °C

Furthermore, when **4** was eliminated, and the reaction was allowed to run for longer times at high HCl concentration, in order to increase the concentration of polyenes derived exclusively from PVC, rate acceleration began at ca. 500 min and continued until ca. 1400 min, when BHT (100 pph) was introduced (Figure 4D). This addition stopped the autoacceleration and reduced the rate to a level that was close to the one observed originally. Finally, as is shown by curves b and d of Figure 4E, when the HCl concentration was high, metallic mercury completely eradicated the autoacceleration caused by **4** and reaffirmed by curves a and c.

In summary, our study of the rate effects of additives showed that in the thermal dehydrochlorination of PVC, (1) autoacceleration is kinetically dependent upon the concentrations of both HCl and conjugated polyenes; (2) autoacceleration results from a process involving free radicals; and (3) dehydrochlorination does *not* require free radicals when autoacceleration is not occurring.

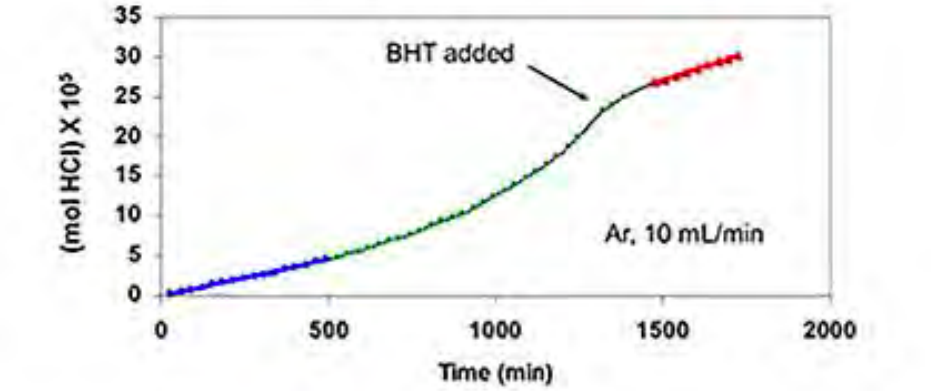

Fig 4D. Kinetic Plots for Dehydrochlorination at 180 °C

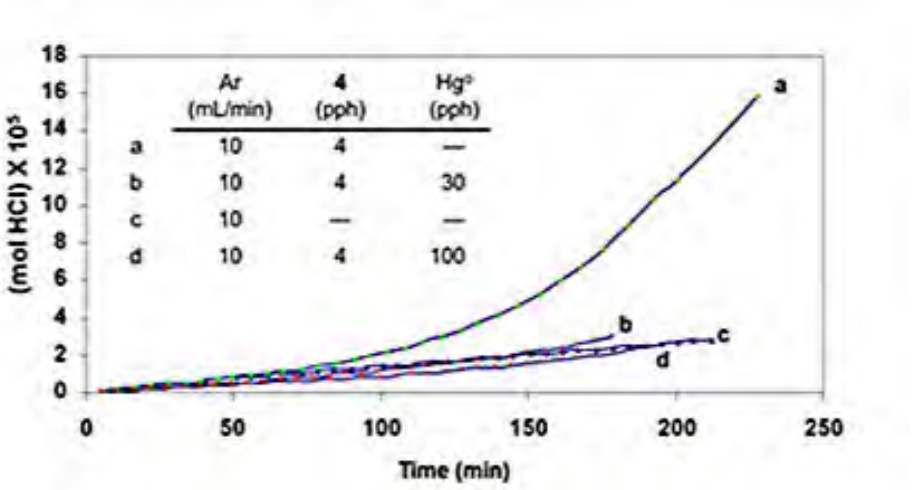

Fig 4E. Kinetic Plots for Dehydrochlorination at 180 °C

Mechanism of Autocatalysis During Thermal Dehydrochlorination

The kinetically active radical species in PVC dehydrochlorination are conceivably cation diradicals, which, if present, would seem most likely to have resulted from the mechanism shown in equation 16 [1,5 and references cited therein]. Another possibility is that the active species are cation monoradicals formed via the reactions in

equations 17 and 18 [5]. Han and Elsenbaumer [13] showed that such a process is apparently a characteristic feature of the protonic acid doping of conjugated polymers,

$$P + H^+ \rightleftharpoons PH^+ \overset{\Delta}{\rightleftharpoons} PH^{\bullet\bullet+} \quad (16)$$

(P = conjugated polyene)

$$P + 2H^+ \rightleftharpoons PH_2^{++} \quad (17)$$

$$PH_2^{++} + P \rightleftharpoons PH_2^{\bullet+} + P^{\bullet+} \quad (18)$$

and very strong evidence for the occurrence of its second step was provided by Kispert and his associates [14–17], who used electrochemical oxidation to generate polyenyl dications from a number of carotenoids and verified their ability to oxidize their neutral precursors, as in equation 18. Kispert et al. [18] also showed that **4** and other carotenoids afforded cation monoradicals when they were treated in solution with an excess of HCl.

The autoacceleration of PVC dehydrochlorination is most likely to begin with the abstraction, by some radical species, of an unactivated methylene hydrogen, in order to generate radical **1** ($n = 0$). This radical then initiates a process like that in equation 10 but involving methylene H abstraction mostly from ordinary monomer units. As a result, new isolated allylic chloride structures are formed throughout the polymer matrix, and their subsequent dehydrochlorination in the usual (nonradical) way then can start the growth of new polyene sequences and thus cause autoacceleration. In this overall scheme, radicals obviously play a very important role, but they are not involved at all in the polyene growth reaction.

The question that now remains to be answered is the nature of the radical(s) in the very first abstraction step. As noted above, Hg^o is a specific trap for chlorine atoms. Therefore, its ability to eliminate autoacceleration completely, rather than merely retard it (Figure 4E), implies that the initial abstraction is performed by atomic chlorine exclusively. This radical species might be formed from any or all of the cation radicals in the system, via equation 19, where P is a conjugated polyene [6].

$$\underset{(PH_2^{\bullet+},\ P^{\bullet+},\ PH^{\bullet\bullet+})}{-\overset{\bullet}{C}H\overset{+}{C}H-Cl^-} \rightleftharpoons -\overset{\bullet}{C}H\underset{Cl}{C}H- \xrightarrow{\Delta} -CH{=}CH- + Cl^{\bullet} \quad (19)$$

The autocatalysis mechanism proposed here is displayed in full in Figure 5, where the starting structure is either an unstable defect (internal allylic chloride, tertiary chloride) or an unactivated monomer unit, and polyene growth is either ionic (as shown) or quasiionic, depending upon conditions. Post-chlorination studies of PVC have shown that H-atom abstraction by chlorine atoms from the unactivated monomer units occurs mostly from methylene moieties rather than chloromethylene groups [19], as Figure 5 emphasizes. However, abstraction from the latter groups could also lead to the formation of unstable defect structures [6]. Figure 5 rationalizes a huge amount of confusing and contradictory data in the literature, and the explanation for autocatalysis by HCl that it provides is pleasingly consistent with the results of an ozonolysis study of degraded PVC, which showed that the autoacceleration of thermal dehydrochlorination was accompanied by a continual increase in the number of polyene sequences [20].

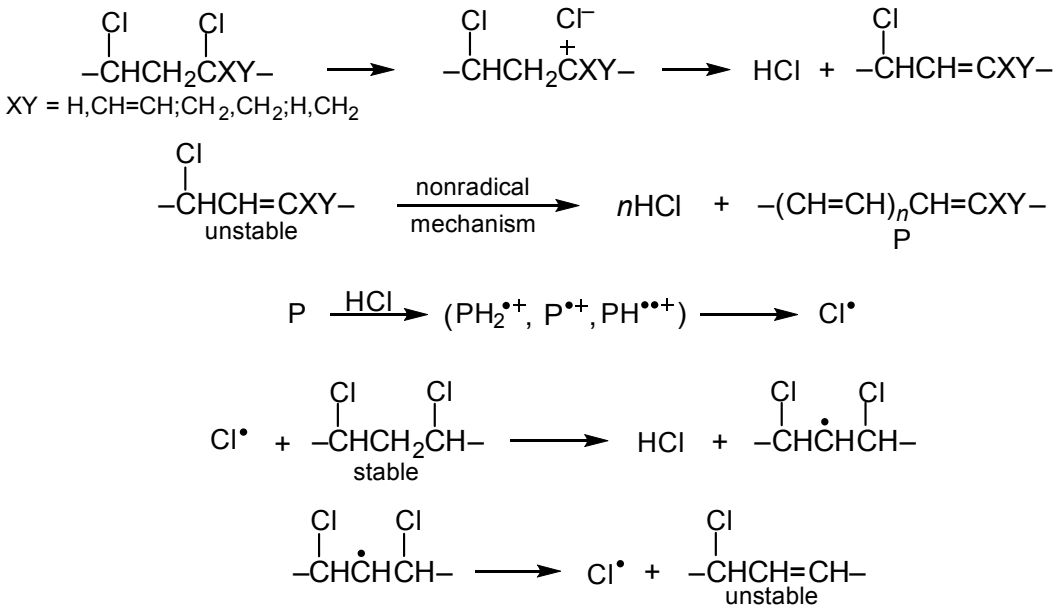

Fig 5. Mechanism of Autocatalysis in the Thermal Dehydrochlorination of PVC

Thermal Stabilization of PVC by Ester Thiols

Some of the additives used traditionally as thermal stabilizers for PVC have raised concerns about their effects on human health and the environment. Thus the replacement of these additives has been increasingly desirable. In an approach to this problem, we

have studied a class of fully organic stabilizers that are commonly known as "ester thiols", because they contain at least one SH function and one or more carboxylate ester groups. The following comments relating to these substances are based on a number of publications (e.g., [21,22]) and patents [23–29], which should be consulted for details.

Our ester thiols are at least as effective as conventional heat stabilizers in both rigid and plasticized PVC. Some of them also are quite useful as plasticizers when they are introduced at high loading levels. Their excellent performance does not require the presence of metallic or nonmetallic costabilizers. However, in certain cases, their effectiveness is increased by the incorporation of such auxiliaries. When purified, the ester thiols do not have unpleasant odors, and their syntheses are usually rapid, straightforward, and inexpensive.

Mechanistic studies with the polymer and with model compounds have shown that a major function of these stabilizers is the deactivation of labile structures by nucleophilic chloride displacement, as exemplified in equation 20. Interestingly, the rate of this reaction increases with increasing

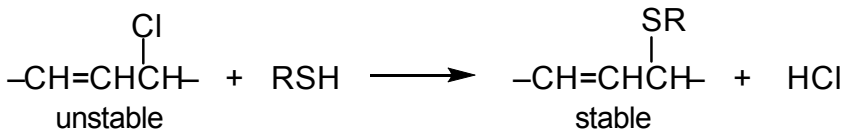

(20)

RSH acidity rather than RSH nucleophilicity. This observation suggests that the displacing species are actually thiolate anions, not the thiols themselves, because the acidities of ester thiols, in general, seem much too low to allow these additives to act as electrophilic catalysts for the displacement process. (Thiolate anion concentration increases, of course, with increasing thiol acidity.)

The ester thiols also stabilize PVC by scavenging free radicals, via H abstraction from SH groups. Moreover, the radical- or acid-promoted addition of these thiols to the double bonds of polyene chromophores not only reduces color, but may deactivate chloroallyl structural segments that are thermally unstable as well.

Our ester thiol patents have been licensed exclusively, for worldwide commercialization, by a company that is incorporated both domestically and overseas.

Concluding Remarks

The topics addressed in this article have been of major concern to us for some time, but they are not the only ones to have attracted our attention. Omitted here from discussion, for example, are our studies of PVC thermolysis at very high temperatures, new smoke suppressants and fire retardants for PVC (performed, in part, in a collaboration

with Prof. R. D. Pike), the polymerization chemistry and microstructures of novel vinyl chloride copolymers, the polymerization chemistry of vinyl acetate, antioxidants and their mechanisms of action, and other areas involving organic and polymer chemistry from a mechanistic point of view.

Considerable progress has now been made toward a full understanding of many aspects of the chemistry of PVC. Nevertheless, this fascinating polymer still seems likely to present researchers with chemical challenges (and surprises!) for many years to come.

Acknowledgments

The author is greatly indebted to his former students, postdoctoral associates, and senior collaborators and colleagues for their invaluable contributions to the research that has now been recognized by the Chemical Pioneer Award. These coworkers are so numerous that their names and affiliations have not been included here. However, many of them are identified in the references. The author also sincerely thanks the following organizations, listed alphabetically, that have supported his research in academia since 1985: Amoco Chemical Co., B. F. Goodrich Co., Colorite Polymers Co., Dow Chemical Co., Edison Polymer Innovation Corp., Egyptian Cultural & Educational Bureau, Elf Aquitaine Inc., GenCorp Foundation, Geon Co., International Copper Assn., Kleerdex Co., National Bureau of Standards, National Science Foundation (Materials Research and Chemistry Divisions), Occidental Chemical Corp., Shell Development Co., Sherwin-Williams Co., Society of Plastics Engineers (four unsolicited grants from the Vinyl Plastics Division), Stockhausen Louisiana Ltd., Stoler Industries, U. S. Department of Defense, U. S. Department of Energy, and Virginia's Center for Innovative Technology.

References

1. Starnes Jr WH. *Prog. Polym. Sci.* 2002, 27, 2133–2170 and references cited therein.
2. Starnes Jr WH. *J. Polym. Sci. Part A: Polym. Chem.* 2005, 43, 2451–2467 and references cited therein.
3. Abreu MRC, Fonseca AC, Rocha NMP, Guthrie JT, Serra AC, Coelho JFJ. *Prog. Polym. Sci.* 2018, 87, 34–69 and references cited therein.
4. Iván B, Kelen T, Tüdös F. in Degradation and Stabilization of Polymers, eds. Jellinek HHG, Kachi H, Elsevier Science, New York, 1989, vol. 2, ch. 8 and references cited therein.
5. Starnes Jr WH, Ge X. *Macromolecules* 2004, 37, 352–359.
6. Starnes Jr WH. *J. Vinyl Addit. Technol.* 2012, 18, 71–75.

7. Arlman EJ. *J. Polym. Sci.* 1954, 12, 547–558.
8. Winkler DE. *J. Polym. Sci.* 1959, 35, 3–16.
9. Stromberg RR, Straus S, Achhammer BG. *J. Polym. Sci.* 1959, 35, 355–368.
10. Doering W von E, Sarma K. *J. Am. Chem. Soc.* 1992, 114, 6037–6043.
11. Doering W von E, Kitagawa T. *J. Am. Chem. Soc.* 1991, 113, 4288–4297.
12. Horowitz A. *ACS Symp. Ser.* 1978, 69, 161–183.
13. Han CC, Elsenbaumer RL. *Synth. Met.* 1989, 30, 123–131.
14. Grant JL, Kramer VJ, Ding R, Kispert LD. *J. Am. Chem. Soc.* 1988, 110, 2151–2157.
15. Khaled M, Hadjipetrou A, Kispert L. *J. Phys. Chem.* 1990, 94, 5164–5169.
16. Khaled M, Hadjipetrou A, Kispert LD, Allendoerfer RD. *J. Phys. Chem.* 1991, 95, 2438– 2442.
17. Jeevarajan JA, Jeevarajan AS, Kispert LD. *J. Chem. Soc., Faraday Trans.* 1996, 92, 1757–1765.
18. Jeevarajan AS, Wei CC, Kispert LD. *J. Chem. Soc., Perkin Trans.* 2 1994, 861–869.
19. Komoroski RA, Parker RG, Shockcor JP. *Macromolecules* 1985, 18, 1257–1265.
20. Martinsson E, Hjertberg T, Sörvik E. *Macromolecules* 1988, 21, 136–141.
21. Starnes Jr WH, Du B, Kim S, Zaikov VG, Ge X, Culyba EK. *Thermochim. Acta* 2006, 442, 78–80.
22. Ge X, Culyba EK, Grinnell CL, Zestos AG, Starnes Jr WH. *J. Vinyl Addit. Technol.* 2007, 13, 170–175.
23. Starnes Jr WH, Du B, US Patent Number 6 667 357, 2003.
24. Starnes Jr WH, US Patent Number 6 747 081, 2004.
25. Starnes Jr WH, Du B, US Patent Number 6 762 231, 2004.
26. Starnes Jr WH, Kim S, US Patent Number 6 927 247, 2005.
27. Starnes Jr WH, Du B, US Patent Number 7 250 457, 2007.
28. Starnes Jr WH, Du B, US Patent Number 7 312 266, 2007.
29. Starnes Jr WH, US Patent Number 7 553 897, 2009.

The Chemist
Journal of the American Institute of Chemists

Polyaniline Nanofibers: From Laboratory Curiosity to Commercial Products

Richard B. Kaner

Department of Chemistry and Biochemistry, UCLA
Los Angeles, CA 90095
(Email: kaner@chem.ucla.edu)

Abstract: My research group began exploring nanostructured polyaniline nearly 20 years ago, right after I heard a lecture given by Dr. Bruce Weiller, an expert in sensors from Aerospace Corp. Bruce explained how the U.S. Air Force was interested in tracking the plumes left from rocket launches, especially as people moved closer to launch sites. One of the byproducts of burning solid rocket propellant is hydrochloric acid (HCl). Therefore, Bruce was interested in detecting HCl using a simple resistive-type sensor device. After Bruce's seminar, I mentioned to him that we were working on the conjugated polymer, polyaniline, which on exposure to a strong acid would undergo over ten orders of magnitude increase in conductivity [1]. Bruce was intrigued and asked me to send him some polyaniline. About three weeks later, he called and mentioned he had both good and bad news. I said, "Please start with the good news," to which he responded that the polyaniline my student had sent could readily detect HCl. Then I asked for the bad news. He replied that the sensors were slow. Clearly what we needed was a high surface area form of our conjugated polymer.

Key Words: Polyaniline, PolyCera® membranes

After discussing the problem with my research group, Jiaxing Huang (who is now a Professor of Materials Science and Engineering at Northwestern University) said that he would take care of this. Very quickly, Jiaxing developed a straightforward method to make nanostructured forms of polyaniline by using interfacial polymerization, an idea related to how Nylon is synthesized [2]. The ingredients for producing polyaniline are the

aniline monomer combined with acid and oxidant, typically ammonium peroxydisulfate (APS). Mixing together all three ingredients produces a highly agglomerated form of polyaniline [3]. Jiaxing's idea was to separate the aniline in an organic solvent from the acid and oxidant, which were dissolved in an aqueous solution. When one solution was placed on top of the other, the reaction kinetics were controlled by the interface, leading to nanofibers. In fact, Jiaxing demonstrated that when the acid was HCl, nanofibers formed with an average diameter of 30 nm and lengths on the order of microns [4,5,6]. Using camphor sulfonic acid produced polyaniline nanofibers with an average diameter of 50 nm, whereas perchloric acid created nanofibers with an average diameter of 120 nm, again with an average length on the order of microns. Note that polyaniline nanofibers had been previously produced by templated growth in zeolites [7] and anopore membranes [8]; however, removing these templates would be needed for applications such as sensors.

Testing by Bruce demonstrated that our new pure nanofibrillar form of polyaniline does indeed respond rapidly when exposed to acids. In fact, we observed a greater than six order of magnitude drop in resistance on exposure to 100 ppm of HCl when compared to the conventional agglomerated form of polyaniline [4]. We next developed ways of detecting weak acids such as hydrogen sulfide (H_2S) by doping the polyaniline nanofibers with nanoparticles of copper chloride ($CuCl_2$) [9]. Upon exposure to H_2S, the dopants were converted to CuS and the strong acid HCl, which could readily be detected. By using more than one resistive sensor we could readily distinguish HCl produced from $CuCl_2$ from HCl itself. In fact, in collaboration with the sensor start-up, Next Dimension, Inc., who used an array of 32 sensor heads, we were able to detect many deadly gaseous species in an effort supported by the U.S. Homeland Security Advanced Research Project Agency (HSARPA). Other deadly agents, such as hydrazine, phosgene and arsine, could be detected simply by adding other agents to the polyaniline nanofibers [10,11,12].

To detect bases such as ammonia, we used the HCl doped form of polyaniline [12,13]. Since these sensors were easy to make, we introduced them into the classroom, in collaboration with Prof. Sarah Tolbert, first for UCLA graduate students in Chem 285 and then for undergraduates in Chem 185. We even produced an instructor's guide so that others can introduce conducting polymers and their use in sensors in their own classrooms [13].

Next, we studied the growth of metal nanoparticles on the polyaniline nanofibers. Since polyaniline is a redox active polymer, upon exposure to chloroauric acid ($HAuCl_4$), the gold in its +3 oxidation state is reduced to gold zero. Since the gold nucleates uniformly across the nanofibers, the size of the gold nanoparticles can be controlled simply by varying the time, temperature and concentration of $HAuCl_4$. By turning off the electrical conductivity with base, these nanostructured gold particles can be used in crossbar type memory devices as we demonstrated in collaboration with Prof. Yang Yang [14]. By applying a potential of >3 V, these devices exhibit a high conductivity on-state that is reversed upon application of -5 V to a low conductivity off-state. The mechanism appears to involve a reversible charge transfer from the gold to the polyaniline [15].

Prof. Paula Diaconescu, who is an expert in catalysis, then asked us to provide her with polyaniline nanofibers decorated with palladium nanoparticles. Her group then examined Suzuki coupling reactions in which aryl halides were shown to react with boronic acid in water with high yields at relatively low temperatures [16]. A semi-heterogeneous mechanism appears to be operative [17].

We then looked at what happens when polyaniline nanofibers are exposed to an intense beam of light. The answer is they melt in a process we termed flash welding [18]. By applying masks, we created interdigited electrodes that could be used for sensors and other electronic devices [19]. Working with Prof. Geoff Spinks and Prof. Gordon Wallace at the Intelligent Polymer Research Institute at the University of Wollongong while carrying out a Fulbright Fellowship in Australia, we controlled the penetration depth of the light to create asymmetric membranes that acted as mechanical actuators upon exposure to acids. Basically, the un-welded side expands when contacted by acid, while the welded side cannot, producing a rotation of up to 720 degrees within 20 seconds in an ~10 cm long piece of flash welded nanofibrillar polyaniline [20]. The rotation is completely reversed on exposure to base.

I presented many of our discoveries on nanostructured polyaniline to UCLA professors at one of our inaugural meetings of the California NanoSystems Institute (CNSI). (Reviews of our work can be found in References 21-23.) After my lecture, Dr. Eric Hoek, then an Assistant Professor of Civil and Environmental Engineering, asked me if I had considered using nanostructured polyaniline for membrane separations. When I mentioned our seminal work on gas separations using traditional polyaniline [24], he was intrigued and wanted to test liquid separations. We began an extremely productive collaboration that has resulted in many advances in conjugated polymer-based membranes [25-32]. Our first major funding for this project came from Abraxis Biosciences headed by Dr. Patrick Soon-Shiong, when we proposed creating a membrane to speed up kidney dialysis. Within two years Eric and I had created a membrane that could accomplish comparable separations to kidney dialysis five times faster. When we asked for further funding to build actual devices, we were told that Patrick was only interested in companies, so we would need to start a company, put together a business plan and present it to his team (as Patrick was by then too busy to meet with us directly). Eric said we should do this as we both had experience with start-up companies. Eric's first company NanoH_2O, Inc. used nanoparticle additives to enhance reverse osmosis membranes [33-34]. NanoH_2O was acquired in 2014 by the Korean company LG Chem for $200M. My first company Fibron, Inc. worked to scale the production of polyaniline nanofibers. We spent over four years perfecting the synthesis of polyaniline nanofibers using a rapid mixing technique as can be seen in Figure 1 [5,35].

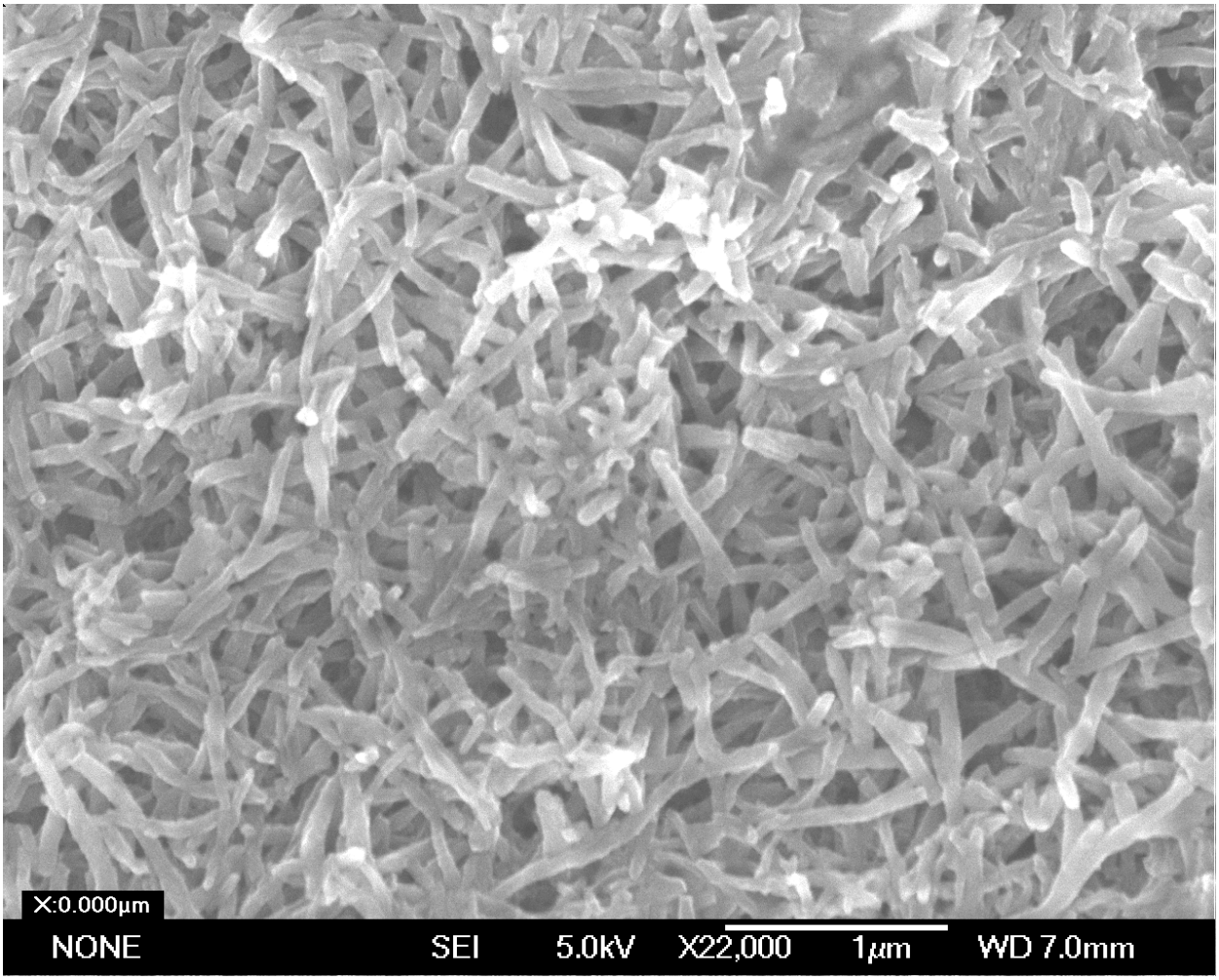

Fig 1. Scanning electron micrograph of polyaniline nanofibers made by adding aniline monomer (0.8 mmol) into a 20 mL solution of 1.0 M hydrochloric acid. After the further addition of 45 mg of the oxidizing agent ammonium persulfate, the reaction was shaken for 5 seconds and left to stand for 24 hours followed by washing with a copious amount of deionized water.

With help from the Korean company, Kolon, we demonstrated the ability to make polyaniline nanofibers on a pilot plant scale of 100 liters per batch. Unfortunately, during the European debt crisis in 2014 one of our European partners pulled out at the last minute of a $5.5 million funding deal with a venture capital group. When none of our initial investors offered to fill in the missing investment, the venture group reneged on the deal and we were forced to liquidate the company. Fortunately, the 'use it or lose it' clause for our intellectual property licensed from UCLA meant that the patents returned to UCLA. Several of these patents formed the basis for the new company Eric and I started called Polycera, Inc. Our name came from a combination of an inexpensive **poly**mer membrane that acts like an expensive **cera**mic membrane. Unfortunately, when developing our business plan, we learned from a physician that the human body can't take kidney dialysis at a faster speed then it is currently done. Although I was dumbfounded that we had not even considered this possibility when starting our project two years earlier, Eric had little hesitation in suggesting that there were even more

important applications for our new membranes, such as cleaning up the mess created by the hydraulic fracturing used to produce oil, known as fracking. It turns out that for every barrel of oil obtained via fracking, 7-10 barrels of oily wastewater are produced; Eric suggested that our membranes could separate this oil from water. We presented our business plan and slide deck to Patrick's associates and received a very positive response with the sentiment that with their blessing there was a 90% Patrick would fund our endeavor. While we waited for a final decision, Eric suggested we travel to Silicon Valley and present our ideas to real venture capitalists. This was an eye-opening experience – heading to Sand Hill Road in the heart of Silicon Valley and acting as *bone fide* entrepreneurs. Patrick then had an epitome in which he decided his funds should be used to further healthcare and while kidney dialysis fell nicely into this arena, clean water did not. In the meantime, we received an enticing offer for funding from a venture group in Silicon Valley. Eric started negotiations and then realized that another company he was involved with – Water Planet, LLC – could make use of our new membranes. Basically, Water Planet had developed a method to separate 99% of oil from water but needed a membrane to clean up the last 1%. They were currently using expensive ceramic membranes and realized that our membranes could handle the same problem much more efficiently. Water Planet offered to buy Polycera, Inc. for the price of the term sheet offered by the venture capital group. This was an offer that made a great deal of sense. So, while my first company Fibron, Inc. failed due to bad timing, my second start-up Polycera, Inc. succeeded due to good timing.

Water Planet went on to scale up our membranes and demonstrate that they reduced the costs associated with cleaning up the mess left from oil fracking by up to 40%. Water Planet liked our name and called their product PolyCera® membranes. Within the past couple years, PolyCera® membranes have been installed in over 100 oil installations around the world. Water Planet recently spun off PolyCera, Inc. as a separate company that is exploring the use of these membranes for other separations from fruit juice to milk products and beyond.

It has been quite a journey from the development of polyaniline nanofibers to solve a problem involving slow sensors to finding a method to clean up the mess created by oil fracking. I hope this article will provide inspiration for other aspiring entrepreneurs.

Acknowledgments

I very much want to thank my students including Jiaxing Huang and collaborators including Bruce Weiller, Yang Yang, Paula Diaconescu, Sarah Tolbert, Geoff Spinks, Gordon Wallace and especially Eric Hoek without whom none of this would have been possible. I also want to thank our sponsors, including the National Science Foundation, the Microelectronics Advanced Research Corp., Homeland Security Advanced Research Projects Agency, Abraxis Bioscience, Boeing and Water Planet.

References

1. Chiang J-C, MacDiarmid AG. *Synth. Met.*, 1986, 13, 193-205.
2. DuPont, Nylon: A DuPont Invention, DuPont International, Public Affairs, 1988, pp 2–3.
3. Huang J, Kaner RB. *Chem. Commun*., 2006, 367-376.
4. Huang J, Virji S, Weiller BH, Kaner RB. *J. Am. Chem. Soc.*, 2003, 125, 314-315.
5. Huang J, Kaner RB. *J. Am. Chem. Soc*., 2004, 126, 851-855.
6. Huang J, Kaner RB. *Angew. Chem.*, *Int. Ed*., 2004, 43, 5817-5821.
7. Wu C, Bein T. *Science*, 1994, 264, 1757-1759.
8. Martin CR. *Acc.Chem. Res.,* 1995, 28, 61-68.
9. Virji S, Fowler JD, Baker CO, Huang J, Kaner RB, Weiller BH. *Small*, 2005, 1, 624-627.
10. Virji S, Kaner RB, Weiller BH. *Chem. Mater.,* 2005, 17, 1256-1260.
11. Virji S, Kojima R, Fowler J, Kaner RB, Weiller BH. *Chem. Mater.*, 2009, 21, 3056-3061.
12. Virji S, Kojima R, Fowler JD, Villanueva JG, Kaner RB, Weiller BH. *Nano Res.,* 2009, 2, 135-142.
13. Virji S, Weiller BH, Huang J, Blair R, Shepherd H, Faltens T, Haussmann PC, Kaner RB, Tolbert SH. *J. Chem. Ed*., 2008, 85, 1102-1104. http://www.jce.divched.org/Journal/Issues/2008/Aug/abs1102.html
14. Tseng RJ, Huang J, Ouyang J, Kaner RB, Yang Y. *Nano Letters,* 2005, 1077-1080.
15. Tseng RJ, Baker CO, Shedd B, Huang J, Ouyang J, Kaner RB, Yang Y. *Appl. Phys. Lett*., 2007, 90, 053101.
16. Gallon BJ, Kojima RW, Kaner RB, Diaconescu PL. *Angew. Chem., Int. Ed*., 2007, 46, 7251-7254.
17. Lemke WM, Kaner RB, Diaconescu PL. *Inorg. Chem. Front*. 2015, 2(35), 1-6.
18. Huang J, Kaner RB. *Nature Materials*, 2004, 3, 783-787.
19. Strong V, Wang Y, Patatanyan A, Whitten PG, Spinks GM, Wallace GG, Kaner RB. *Nano Letters*, 2011, 11, 3128-3135.
20. Baker CO, Shedd B, Innis PC, Whitten PG, Spinks GM, Wallace GG, Kaner RB. *Adv. Mater*., 2008, 20, 155-158.
21. Li D, Huang J, Kaner RB. *Acc. Chem. Res.,* 2009, 42, 135-145.
22. Tran HD, D'Arcy JM, Wang Y, Beltramo PJ, Strong V, Kaner RB. *J. Mater. Chem.,* 2011, 21, 3534-3540.
23. Baker CO, Huang X, Nelson W, Kaner RB. *Chem. Soc. Rev.,* 2017, 46, 1510-1525.
24. Anderson MR, Mattes BR, Reiss H, Kaner RB. *Science,* 1991, 252, 1412-1415.
25. Guillen GR, Farrell TP, Kaner RB, Hoek EMV. *J. Mater. Chem.,* 2010, 20, 4621-4628.
26. Liao Y, Zhang C, Zhang Y, Strong V, Tang J, Li X-G, Kalanter-zadeh K, Hoek EMV, Kaner RB. *Nano Lett.*, 2011, 11, 954-959.

27. McVerry BT, Temple JAT, Huang X, Marsh KL, Hoek EMV, Kaner RB. *Chem. Mater.,* 2013, 25, 3597.
28. Liao Y, Wang X, Chian W, Yu D-G, Li X-G, Hoek EMV, Kaner RB. *Nanoscale*, 2013, 5, 3856-3862.
29. Liao Y, Li X-G, Hoek EMV, Kaner RB. *J. Mater. Chem. A,* 2013, 1, 15390-15396.
30. Liao Y, Farrell TP, Guillen GR, Li M, Temple JAT, Li X-G, Hoek EMV, Kaner RB. *Mater. Horiz.,* 2014, 1, 58-64.
31. Huang X, McVerry BT, Marambio-Jones C, Wong MCY, Hoek E, Kaner RB. *J. Mater. Chem. A,* 2015, 3, 8725-8733.
32. McVerry BT, Anderson M, He N, Kweon H, Ji C, Xue S, Rao E, Lee C, Kaner RB. *Nano Lett.,* 2019, 19(8), 5036-5043.
33. Jeong BH, Hoek EMV, Yan Y, Huang X, Subramani A, Hurwitz G, Ghosh AK, Jawor A. *J. Membr. Sci.,* 2007, 294, 1-7.
34. Lind ML, Ghosh AK, Jeong BH, Hoek EMV. *Langmuir,* 2009, 25, 10139-10145.
35. Li D, Kaner RB. *J. Mater. Chem.,* 2007, 17, 2279-22782.

The Chemist
Journal of the American Institute of Chemists

Single-molecule Catalysis

Peng Chen

Department of Chemistry and Chemical Biology, Cornell University
Ithaca, NY 14853
(Email: pc252@cornell.edu)

Single-molecule imaging approaches have revolutionized the study of chemical and biological systems due to their power of dissecting the real-time behaviors of individual entities. In the past 14 years, my group has pushed the development and application of single-molecule approaches in studying catalysis on single nanoparticles (i.e., heterogeneous catalysis) and catalysis by transition metal complexes in making polymers (i.e., homogeneous catalysis) (Figure 1).

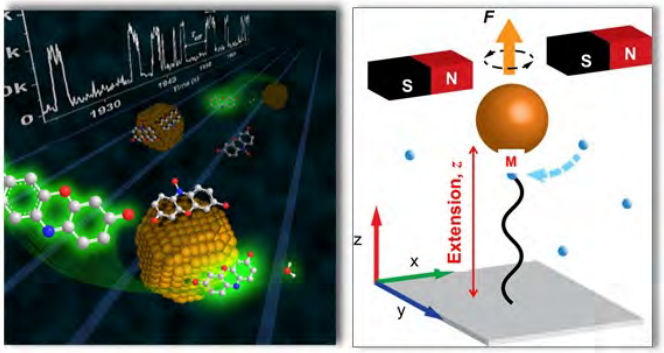

Fig 1. Left: Schematic of using single-molecule fluorescence microscopy to image catalytic reactions on single metal nanoparticles in which the reaction product (green shaded) is fluorescent. **Right:** Schematic of using magnetic tweezers to monitor single polymer growth in real time under catalytic living polymerization reactions in which the polymer is tethered between a magnetic particle and a surface and a transition metal catalyst (M) catalyzes the incorporation of monomers.

For nanoparticle catalysis, due to the intrinsic heterogeneity among individual particles and surface structural dynamics (the latter is particularly relevant for nanometer sized particles), studying their catalytic behaviors at the single-particle level in real time is crucial for understanding their fundamental catalytic properties. Using single-molecule fluorescence imaging combined with a fluorogenic reaction approach (Figure 1, left), we have imaged catalytic reactions on individual nanoparticles at single-turnover resolution in real time under operando conditions. We have discovered temporal activity fluctuations of individual nanoparticles, attributable to their dynamic surface restructuring, whose timescales, energetics, and dependences on particle size and materials were quantified. We have extended the single-molecule imaging approach to screen the activity of catalyst particles in a massively scalable and parallel way with single-particle, sub-diffraction resolution. Using single-molecule localization microscopy, we spatially resolved and mapped reactions on individual particles at nanometer resolution, directly visualizing site-specific activity and uncovering spatial activity gradients within single facets. We further discovered cooperative communication between reactions on the same catalyst particle, in which reactions occurring at different locations on the same catalyst affect each other positively, phenomenologically similar to enzyme cooperativity but mechanistically distinct.

For polymerization catalysis, due to the intrinsic conformational heterogeneity among individual polymer molecules, their growth behavior during polymerization reactions is expected to differ from one to another and from time to time, but it was unknown how they would differ and what the consequences would be. We have developed a magnetic tweezer-based approach (Figure 1, right) to visualize real-time polymer growth at the single-polymer level. Focusing on ring-opening metathesis polymerization catalyzed by a Ru-based transition metal complex, we found that the extension of a growing polymer under a pulling force does not increase continuously but exhibits wait-and-jump steps. These step-wise behaviors are attributable to the formation and unraveling of conformational entanglements from newly incorporated monomers, which only occur under nonequilibrium living polymerization conditions. The configurations of these entanglements appear to play a key role in determining the polymerization rates and the dispersion among individual polymers, raising the possibility to manipulate their configuration to alter polymerization kinetics and dispersion.

The Chemist
Journal of the American Institute of Chemists

Imidazo Pyridine Derivative as a New Corrosion Inhibitor for Mild Steel in Acidic Media

Vranda Shenoy K[a], Reena Kumari P.D[a], Sowmya P.V[b]

[a]Department of Chemistry, Shri Madhwa Vadiraja Institute of Technology and Management Bantakal, India
[b]Department of Chemistry, Mangalore University
Mangala gangothri, India
Address for Correspondence:
[a]Reena Kumari P D
Department of Chemistry, Shri Madhwa Vadiraja Institute of Technology and Management Bantakal, Udupi, Karnataka, India
(Tel: +91 820 2589182; E-mail: kiran_reena@yahoo.com)
ORCID ID: 0000-0001-5607-5106

Abstract: The corrosion inhibition of mild steel (MS) in 0.5 M HCl and 1 M HCl solution by 2-(4-methylphenyl)imidazo[1,2]pyridine was studied at temperature range from 303-333 K by weight loss measurements. The results show that the studied compound exhibits good performance as an inhibitor for MS in both 0.5 and 1 M HCl solution. The inhibitor efficiency of the inhibitor was dependent on concentration as well as temperature of the solution. The adsorption on mild steel surface was explained through Langmuir's adsorption isotherm model. The values of standard free energy of adsorption indicated adsorption of aminopyridine derivative was a spontaneous process and adsorbed chemically as well as physically on the metal surface.

Key Words: Mild steel, imidazo pyridine inhibitors, weight loss method, kinetic parameters, Langmuir adsorption

Ethics Approval
Not applicable as no involvement of human participants or any other biological objects.

Conflicts of Interest
The authors declare no conflict of interest.

Introduction

Mild steel is a key construction component in the petroleum industry and power plants. In most of the industrial processes, mineral acids are widely used for cleaning, pickling and descaling processes. In mineral acids, metallic corrosion represents a lamentable waste of both resources and money; they must be protected. As the dissolution of these components in an acid medium is very high, it may be desirable to use inhibitors to reduce the corrosive attack on metals [1].

Heterocyclic compounds having nitrogen, sulphur or oxygen atoms are of special significance as they often provide superior inhibition along with the presence of polar groups and/or π electrons [2]. These kinds of organic molecules are adsorbed on the surface of the metal, consequently controlling the rate of corrosion.

Imidazo pyridines are essential organic molecules used in the pharmaceutical industry for their antiviral [3], anti-inflammatory [4], anti-bacterial [5], analgesic, antipyretic and anticonvulsant [6] properties. The presence of a N-heterocyclic system makes them well-qualified, excellent inhibitors for mild steel corrosion in an acidic medium [7,8].

The present study explores the use of one of the imidazo pyridine derivatives namely 2-(4-methylphenyl)imidazo[1,2]pyridine as a corrosion inhibitor for mild steel surface in 0.5 and 1 M hydrochloric acid solution using gravimetric analysis. Owing to the simple application, accuracy and reliability, this method was chosen to understand the corrosion inhibitive effect of the inhibitor. The effect of solution temperature, concentration of the acid solution, as well as inhibitor concentration on the electrochemical dissolution of mild steel, were studied and discussed. Kinetic and thermodynamic parameters were also calculated and discussed.

Experimental Procedure

Materials

Test coupons: The weight loss study was performed on mild steel containing (in wt %) C- 0.18, Mn - 0.6, S - 0.05, P - 0.04, Si - 0.1 and Fe - 99.03. The mild steel coupons were mechanically cut, having dimensions 2 cm x 2 cm x 0.5 cm and polished with different grade of emery papers (220, 330, 500, 600, 800,

1000, 1200 grade) for the study. Before immersing in the test solution for the gravimetric study, mild steel coupons were washed with double distilled water, degreased in acetone and dried.

Test solutions: For the gravimetric study, the 0.5 and 1 M HCl electrolyte solutions were prepared by using analytical grade 37% HCl (Merk) solution and double distilled water.

Corrosion inhibitor: 2-(4-methylphenyl)imidazo[1,2-a]pyridine was used as a corrosion inhibitor for the present investigation. The concentration of the inhibitor used for investigation ranged from 50 - 200 ppm. The molecular structure of 2-(4-methylphenyl)imidazo[1,2-a]pyridine is shown in Figure 1.

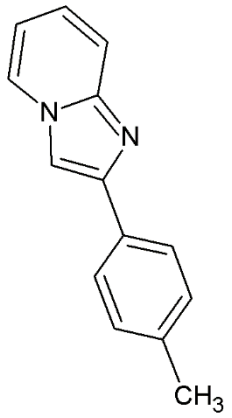

Fig 1. Molecular structure of 2-(4-methylphenyl)imidazo[1,2-a]pyridine

Method

Weight Loss Study: Weight loss measurement was carried out by immersion of precisely weighed mild steel test coupons in the absence and presence of 50, 100, 150 and 200 ppm of the inhibitor in 100 ml of 0.5 and 1 M HCl solution for 2 h. The test coupons were then retrieved from electrolyte, washed with distilled water followed by acetone, dried and reweighed using an analytical balance with the accuracy of ±0.1 mg. The tests were performed in a cell equipped with thermostatic cooling condenser at different temperatures (303 K, 313 K, 323 K and 333 K).

The rate of corrosion (*CR*), and inhibition efficiency (*η%)* are calculated using following equations 1 and 2 [9]:

$$CR(mm/yr) = 87.6\Delta w / Atd \quad (1)$$

where Δw = weight loss in g, A = area of specimen in cm^2 exposed in acidic medium, t = immersion time in h, and d = density of mild steel (g cm^{-3}).

$$\eta\% = (CR_O - CR_i / CR_O) \times 100 \quad (2)$$

where CR_0 and CR_i are corrosion rates for uninhibited and inhibited solution.

Result and Discussion

Effect of Concentration

Corrosion inhibition efficiency ($\eta\%$) of imidazo pyridine derivative and corrosion rate (CR) values calculated by weight loss measurements after 2 h of exposure to both the electrolyte solutions at varying temperatures (303-333 K) are listed in Table 1. The corrosion rates obtained were plotted against different inhibitor concentrations in 0.5 and 1 M HCl solutions are shown in Figures 2(a) and 2(b), respectively.

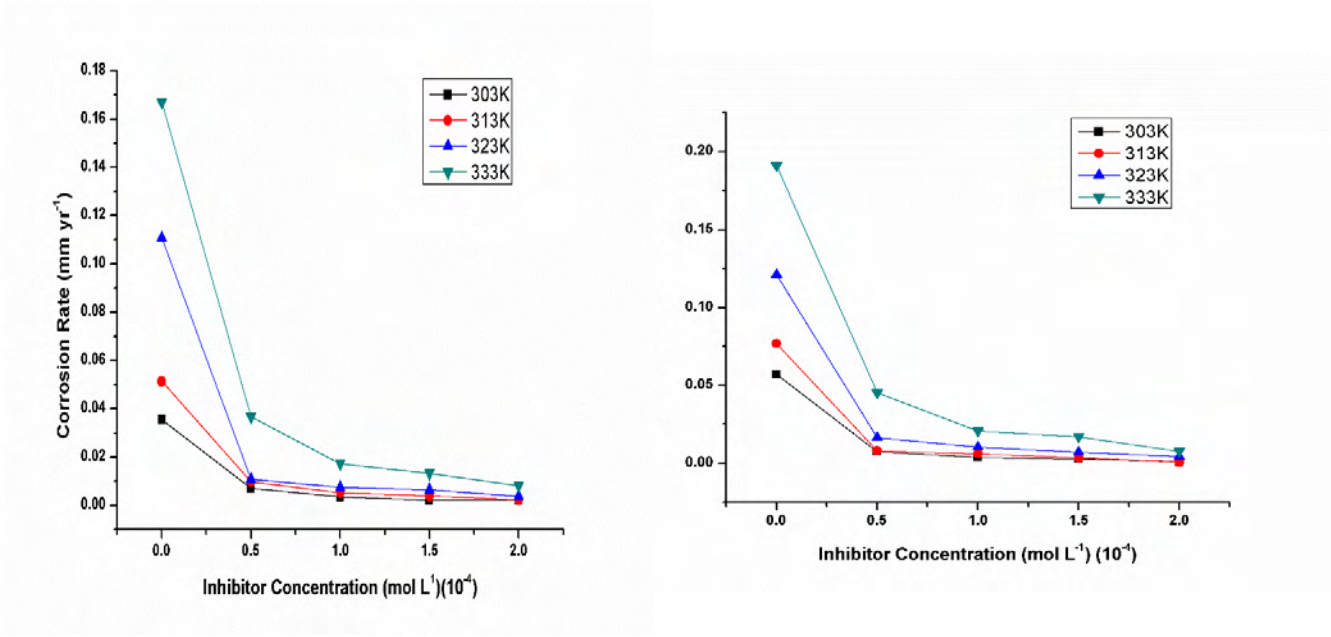

2(a) 2(b)

Fig 2. Variation of corrosion rate with the different concentrations of 2-(4-methylphenyl)imidazo[1,2a]pyridine for mild steel in 0.5 M HCl [2(a)] and in 1 M HCl solution [2(b)]

The data in Table 1 shows that rate of corrosion was much less in the inhibited solution than that of the uninhibited solution. These experimental values prove that as concentration of acid increases, the corrosion inducing property also increases, thereby increasing the corrosion rate of the MS. However, the corrosion rate decreases in the presence of inhibitor, clearly indicating the inhibitive action of imidazo pyridine derivative on corrosion behaviour of mild steel in acidic medium. The inhibition effect could be attributed to the adsorption of the inhibitor molecules/ions from the electrolyte solution at the metal surface. The greater inhibition effect at higher concentration of the inhibitor may be due to an increased rate of adsorption rather than desorption/dissolution of the imidazo pyridine derivative at the metal surface that leads to larger surface area coverage. Thus, the corrosion product formed acts as a protective film that increases the charge transfer resistance at the solid/electrolyte interface region [10].

Table 1. Gravimetric analysis data of 2-(4-methylphenyl)imidazo[1,2a]pyridine at different concentrations in 0.5 and 1 M HCl solution at different temperatures

		0.5 M HCl			1 M HCl		
Temp. (K)	Conc. of Inhibitor (ppm)	ΔW (*g*)	(*η%)*	(*CR*)(mm yr^{-1})	ΔW (*g*)	(*η%)*	(*CR*)(mm yr^{-1})
303	-	0.0743	-	0.0355	0.1204		0.057
	50	0.0150	80.0	7.17x10-3	0.0161	86.6	$7.69x10^{-3}$
	100	0.0073	90.5	3.533x10-3	0.0124	90.3	$5.92x10^{-3}$
	150	0.0046	93.1	2.199x10-3	0.0079	93.7	$3.77x10^{-3}$
	200	0.0044	95.0	1.924x10-3	0.0021	98.25	$1.0x10^{-3}$
313	-	0.1078	-	0.0515	0.1608		0.0768
	50	0.0206	80.8	9.84x10-3	0.0099	93.8	$4.7x10^{-3}$
	100	0.0111	89.7	5.30x10-3	0.0049	96.9	$2.34x10^{-3}$
	150	0.0083	92.3	3.968x10-3	0.0018	98.8	$8.60x10^{-3}$
	200	0.0048	95.6	2.24x10-3	0.0009	99.4	$4x.3010^{-3}$
323	-	0.2315	-	0.1106	0.2534		0.1211
	50	0.0226	90.2	0.0108	0.0194	92.3	$9.27x10^{-3}$
	100	0.0155	93.3	7.4x10-3	0.0100	96.0	$4.781x10^{-3}$
	150	0.00135	94.1	6.49x10-3	0.0078	96.9	$3.729x10^{-3}$
	200	0.0080	96.5	3.84x10-3	0.0055	97.8	$2.62x10^{-3}$
333	-	0.3496		0.167	0.3996		0.1910
	50	0.0770	77.9	0.0368	0.1241	69.0	0.0593
	100	0.0360	89.7	0.0172	0.0492	87.6	0.0235
	150	0.0280	92.1	0.01346	0.0316	92.0	0.0151
	200	0.0168	95.0	8.17x10-3	0.0255	93.61	0.0121

Effect of Temperature

Analysis of inhibition efficiencies at various concentrations of inhibitor at the studied range of temperatures can give us some useful insight into the possible inhibition mechanism of the inhibitor. Table 1 shows variation of corrosion rate with temperature (303-333 K) in 0.5 and 1 M HCl solution in the absence and presence of 2-(4-methylphenyl)imidazo[1,2-a]pyridine.

The data indicate that corrosion rate of the MS increases with increasing temperature in the absence of inhibitor. But, in the presence of inhibitor, inhibition efficiency (*η%)* increases by different amounts at different concentrations of the inhibitor at constant temperature and correspondingly the corrosion rate decreases. But an interesting trend of inhibition was observed when temperature of the medium was increased. In 0.5 M HCl solution, *η%* increased with increasing inhibitor concentration from 303 K to 323 K; however, further raising the temperature did not show noticeable improvement in inhibition performance of the inhibitor. Whereas, in 1 M HCl the enhanced inhibition performance of the inhibitor was seen with the increasing temperature up to 313 K, thereafter inhibitive effect decreased. Hence, based on the above experimental evidence it can be ascertained that the tested imidazo pyridine derivative may serve as a potential inhibitor to protect mild steel metal from acidic attack.

Table 1 shows the overall inhibition efficiency is high for 1 M HCl compare to 0.5 M HCl. This may be due to the ability of the inhibitor to form a protonated complex in an acidic medium, which mainly depends on nature and concentration of the electrolyte and inhibitors. The inhibitor imidazo pyridine derivative in acidic media protonates to form a protonated complex and its population is governed by acid and inhibitor concentration. Compared to 0.5 M HCl, in 1 M HCl solution, the number of protonated species of inhibitor imidazo pyridine derivative is high; Cl^- species are also increased. The Cl^- ions are not only adsorbed by the positively charged iron surface but also facilitate the adsorption process of the protonated inhibitor through an intermediate bridge between the metal and end of protonated inhibitor. Thus, protonated inhibitor species along with the Cl^- ions block the electrochemical active sites of the metal surface and hinder the metal dissolution rate [11].

Corrosion kinetic parameters

Generally, with the effect of temperature, the corrosion of metal in acid media is accompanied by the evolution of hydrogen gas, which is followed by an increase in the metal dissolution process. The effect of temperature on the inhibited metal is a very complex reaction due to rapid desorption reaction of inhibitor on metal surface or decomposition of inhibitor itself [12].

The mechanism of inhibition can be deduced by comparing the Arrhenius equation in the presence and absence of inhibitor. This relationship can be expressed in terms of Arrhenius equation (3) [13-16], where CR is the corrosion rate, Ea is apparent activation energy, R is the molar gas constant (8.314 J mol-1 K-1), T is absolute temperature and A is Arrhenius factor.

$$\log CR = \log A - (E / 2.303RT) \quad (3)$$

A plot of log CR versus 1/T gave a straight line for mild steel in 0.5 M HCl and 1 M HCl solution in the presence and absence of different concentrations of inhibitor as shown in Figure 3(a) and 3(b).

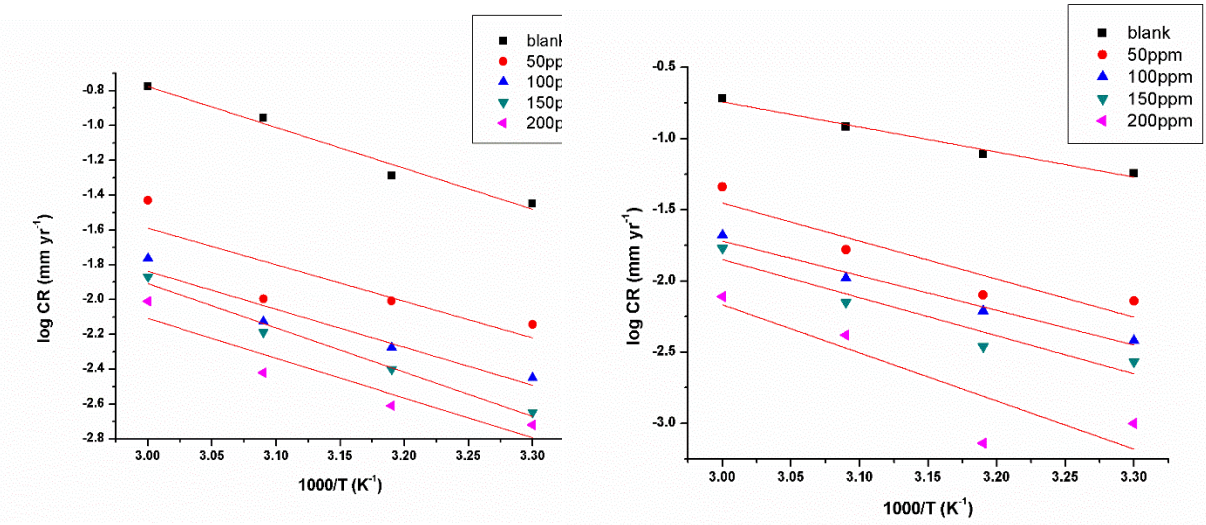

3(a) 3(b)

Fig 3. Arrhenius plot of logCR vs. 1/T in 0.5M HCl in absence and in presence of imidazo pyridine derivative as inhibitor in 0.5 M HCl [3(a)] and in 1 M HCl [3(b)]

The activation energy values (E_a), calculated from the slope of the straight line ($-E_a/2.303R$) for 0.5 and 1 M HCl solutions, are given in Table 2.

Table 2. Thermodynamic activation parameters for the corrosion of mild steel in 0.5 and 1 M HCl in the absence and presence of different concentrations of imidazo pyridine derivative as inhibitor

Inhibitor concentration (M)	E_a (k J mol$^{-1)}$	ΔH* (k J mol^{-1})	ΔS* (J mol^{-1} K^{-1})
0.5 M HCl			
Blank	44.03	42.65	-132.64
$0.5x10^{-3}$	40.26	38.39	-160.78
$1x10^{-3}$	40.26	39.92	-161.00
$1.5x10^{-3}$	48.69	46.68	-142.04
$2x10^{-3}$	43.75	36.97	-175.17
1M HCl			
Blank	33.73	30.15	-169.65
$0.5x10^{-3}$	51.12	48.53	-128.02
$1x10^{-3}$	46.64	44.13	-146.34
$1.5x10^{-3}$	51.12	48.76	-134.96
$2x10^{-3}$	63.18	62.25	-101.83

Generally, lower values of E_a in the inhibited system compared to the blank indicate a chemisorption mechanism, whereas higher values of E_a suggest physisorption [17]. The data in Table 2 shows that in 0.5 M HCl solution, E_a values are less in the presence of lower concentrations of inhibitor compared to uninhibited solution, whereas at higher concentrations these values are slightly more or equal to that of the blank solution. As a result of this, it could be attributed to chemical adsorption at lower concentrations of the inhibitor due to the formation of a strong co-ordination bond between d orbital of iron and inhibitor molecule [18], which controls the charge transfer on the mild steel metal surface. At higher concentrations, physisorption is more likely to take place. But in the case of 1 M HCl, the calculated E_a value for uninhibited solution is less compared to inhibited solution and the range of E_a values (33.73 kJ mol^{-1} to 63.18 kJ mol^{-1}) are lower than the threshold value of 80 kJ mol^{-1} which is required for chemisorption, indicating physisorption takes place [19].

In general, the physisorption process requires the presence of both an electrically charged metal surface and charged inhibitor species in the solution. In the case of chemisorption, this occurs either by charge transfer or by a sharing pair of electrons between a metal atom and inhibitor species [11]. In the present study, the inhibitor imidazo pyridine, which is an organic molecule, protonates in the presence of acidic media, forming cations which exist in equilibrium with corresponding molecular forms, resulting in physical adsorption. This can be explained by considering the continuous process of adsorption and desorption of inhibitor molecules at the metal surface, which is an equilibrium process at a particular temperature. With the increase of temperature, an equilibrium shift takes place leading to a higher desorption rate than adsorption until equilibrium is regained [20]. This explains the decrease in inhibition efficiency with increase in

temperature (physical adsorption), i.e., weak Vander Waal's forces, which disappears at elevated temperatures [21,22]. Thus, in both 0.5 and 1 M HCl solutions inhibition efficiencies increased up to a certain level of temperature, afterwards decreasing, showing a lower reactivity of the inhibitor may be due to desorption or dissolution of the substrate from the metal surface. The enthalpy and entropy of activation for the metal corrosion process are determined using the transition state equation (4) [12].

$$CR = (RT / Nh)\exp(\Delta S^* / R)\exp(-\Delta H^* / RT) \quad (4)$$

where h is Plank's constant (6.626176 x 10^{-34} J s, N is Avogadro's number (6.02252 x 10^{23} mol^{-1}), R is the universal gas constant and T is the absolute temperature. Figure 4(a) and 4(b) show

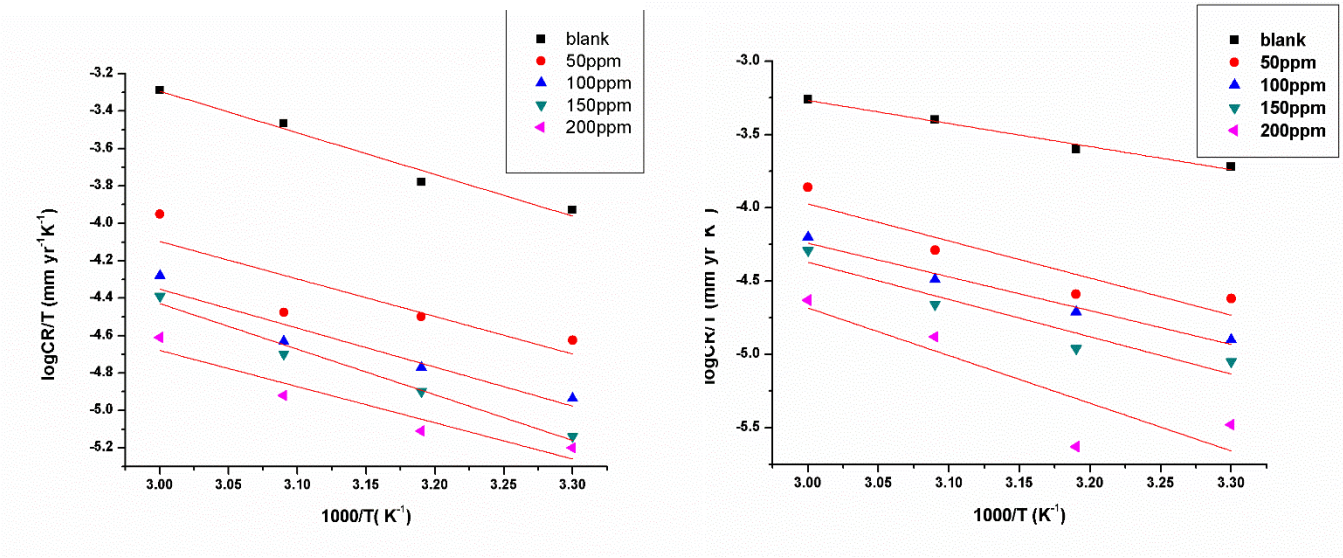

4(a) 4 (b)

Fig 4. Plot of log CR/T vs. 1/T in 0.5M HCl [4(a)] and in 1 M HCl [4(b)] in absence and in presence of the inhibit

the plot of log *CR/T* versus *1/T* for corrosion of mild steel in 0.5 M HCl and 1 M HCl solution in the absence and presence of various concentrations of imidazo pyridine derivative, respectively.

Straight lines with slope of $(\Delta H^{*/} / 2.303R)$ and an intercept of $[\log(R / Nh) + (\Delta S^* / 2.303R)]$ were obtained from which the values of ΔH^* and ΔS^* were calculated and listed in Table 2 for corrosion of mild steel in 0.5 and 1 M HCl solutions. This investigation shows

that the positive value of ΔH^* indicates that corrosion of mild steel in HCl solution is an endothermic process [23]. Large and negative values of entropies (ΔS^*) for both inhibited and uninhibited solution imply that the rate determining step, activation complex, is with association rather than dissociation [24], which results in a decrease of randomness on going from reactants to the activated complex.

Adsorption isotherm and thermodynamic parameters

The electrochemical reaction that takes place on the metal surface can be related to adsorption of the inhibitor, which depends on the nature of the metal surface, electronic characteristics of the metal surface on adsorption, temperature, and electrochemical potential at the metal solution interface [25]. It is a surface phenomenon and can be determined by experimental data.

Electron donor atoms like N, S or O in the molecular structure of the inhibitor favours the greater adsorption on the metal surface. Thus, the adsorption isotherm gives information on the metal-inhibitor interactions. To get the isotherm, the linear relation between degree of surface coverage (θ) values ($\theta = \eta\% /100$) and inhibitor concentration C_{inh} must be determined since surface coverage values are very useful in measuring the adsorption characteristics.

Several attempts were made for various isotherms like Langmuir, Temkin, Frumkin, Flory-Huggins, etc. to fit the θ values. In the present study, the experimental data were best fitted by the Langmuir adsorption isotherm. According to this isotherm, θ is related to C_{inh} using the following equations (5 and 6).

$$\theta / 1 - \theta = K_{ads}.C_{inh} \tag{5}$$

Rearranging equation 5 gives:

$$C_{inh} / \theta = 1 / K_{ads} + C_{inh} \tag{6}$$

where K_{ads} is the equilibrium constant of the inhibitor in adsorption/desorption process, C_{inh} is the concentration of the inhibitor and θ is the surface coverage area. The graph of C_{inh}/θ versus C_{inh} was plotted and fitted straight line was obtained with a slope close to unit as seen in Figure 5a and 5b.

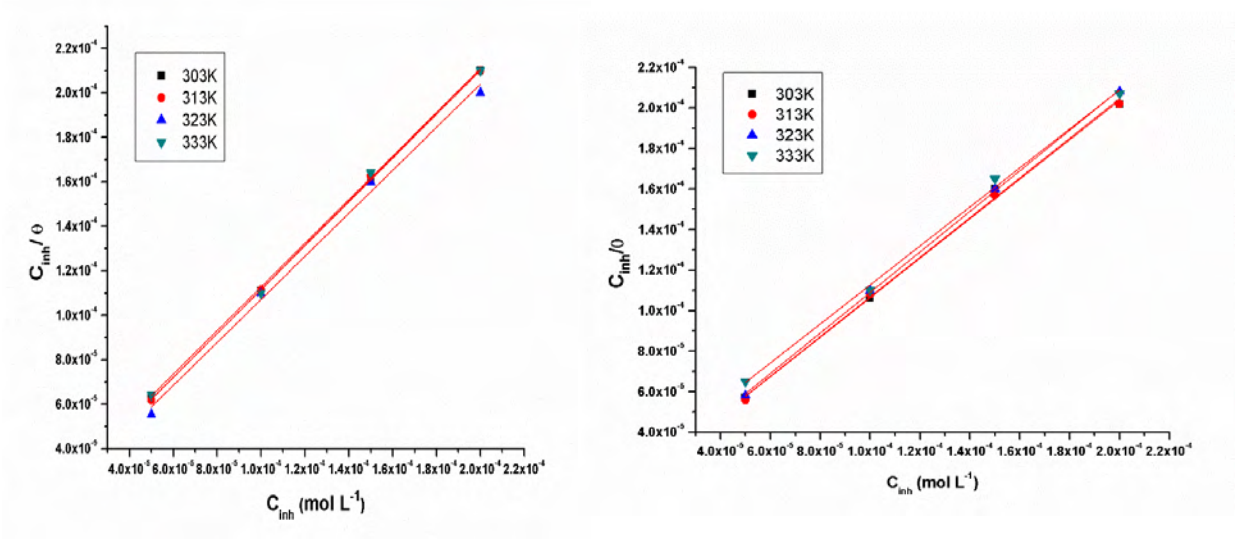

5(a) 5(b)

Fig 5. Langmuir adsorption isotherm plots for the adsorption of imidazo pyridine derivative on mild steel in 0.5 M HCl solution [5(a)] and in 1 M HCl [5(b)] at 303-333 K

The correlation factor $R^2 > 0.9999$ indicating that adsorption of inhibitor on mild steel follows the Langmuir adsorption isotherm. According to this isotherm, adsorbed molecules occupy only one site and there are no interactions with the other adsorbed species [26,27]. The calculated parameters such as equilibrium constant K_{ads}, linear regression coefficient and slopes for 0.5 and 1 M HCl solutions are listed in Table 3.

Table 3. Thermodynamic adsorption parameters for the corrosion of mild steel in 0.5 and 1 M HCl

Temperature(K)	Linear regression Coefficient(R^2)	K_{ads}	slope	ΔG^o_{ads} (k J mol^{-1})
	0.5 M HCl			
303	0.9999	76923	0.9852	-38.29
313	0.9997	80000	0.9909	-39.97
323	0.9930	96150	0.9676	-41.43
333	0.9989	76953	0.9812	-42.40
	1 M HCl			
303	0.9966	111111	0.978	-38.86
313	0.9984	111111	0.974	-40.15
323	0.9995	111111	1	-41.34
333	0.9962	63011	0.962	-42.08

A larger value of K_{ads} shows the more efficient adsorption, hence the better inhibition efficiency [28]. It is evident from the data in Table 5 that, K_{ads} value decreases with increase of temperature showing adsorption of inhibitor 2-(4-methylphenyl)imidazo[1,2]pyridine on

mild steel is unfavourable at higher temperature.

The equilibrium constant K_{ads} is related to the standard free energy of adsorption (ΔG^o_{ads}) using the following equations (7 and 8):

$$\Delta G^o_{ads} = -RT \ln(55.5 K_{ads}) \quad (7)$$

$$\Delta G^o_{ads} = -2.303 RT \log(55.5 K_{ads}) \quad (8)$$

where R is the gas constant and T is the absolute temperature and 55.5 is the molar concentration of water in solution [29]. The (ΔG^0_{ads}) values calculated for the inhibitor in 0.5 and 1 M HCl solutions are summarized in Table 5. The negative values for free energy of adsorption (ΔG^0_{ads}) show the spontaneity of adsorption process [30] and also stability of adsorbed layer on the mild steel surface.

Generally, the value of ΔG^0_{ads} up to -20 kJ mol^{-1} is consistent with physisorption, while those around -40 kJ mol^{-1} or higher associated with chemisorption as a result of sharing or transfer of electrons from inhibitor organic molecule to the metal surface to form a strong coordination bond [30].

In the present case, ΔG^0_{ads}values for 2-(4-methylphenyl)imidazo[1,2a]pyridine inhibitor on mild steel in presence of 0.5 M HCl and 1 M HCl solution ranges from -38.29 kJ mol^{-1} to -42.33 kJ mol^{-1} and -38.86 kJ mol^{-1} to -42.81 kJ mol^{-1}, respectively. This reveals that the process of adsorption involves both physisorption and chemisorptions in particular, the former dominating over the latter. The absolute value of ΔG^0_{ads} increases with an increase in temperature, indicating that adsorption becomes more favourable and also that inhibitor molecules are chemically adsorbing on the mild steel metal surface.

Thermodynamic parameters are important in studying adsorption of organic inhibitor on a metal surface. The enthalpy of adsorption (ΔH°_{ads}) and entropy of adsorption (ΔS°_{ads}) are deduced by a thermodynamic equation (9):

$$\Delta G^o_{ads} = \Delta H^o_{ads} - T\Delta S^o_{ads} \quad (9)$$

The standard enthalpy of adsorption(ΔH°_{ads}) and standard entropy of adsorption (ΔS°_{ads}) are -3.329 kJ mol^{-1} , 0.1379 J mol^{-1} K^{-1}, in 0.5 M HCl and -6.225 kJ mol^{-1}, 0.1835 J mol^{-1} K^{-1}, respectively. The negative values of ΔS°_{ads} indicate that decrease in randomness takes place on going from reactant to metal-adsorbed species.

Conclusion

From the results, it can be concluded that the tested amine derivative, namely 4-methyl imidazo pyridine, shows encouraging inhibitive action on corrosion of mild steel in acidic media. The electrochemical reactive sites formed on the metal surface on exposure to aggressive electrolyte were believed to be effectively blocked by the inhibitor molecules through the adsorption mechanism. The calculated ΔG^0_{ads} values for the inhibitor in both 0.5 and 1 M HCl solutions indicate mixed adsorption with predominant involvement of physisorption. The adsorption was spontaneous and exothermic and best described by the Langmuir adsorption model. The variation of corrosion rates and inhibition efficiencies with the concentration of acid, inhibitor and solution temperatures shows the inhibition tendency of the studied amine derivative on the mild steel surface was controlled by concentration and temperature of the solution.

References

1. Bentiss F, Traisnel M, Lagrenee M. *Corros. Sci*., 2000, 42(1), 127–146.
2. Mernari B, El Attari H, Traisnel M, Bentiss F, Lagrenee M. *Corros. Sci*., 1998, 40(2–3), 391–399.
3. Gueiffier A, Mavel S, Lhassani M, Elhakmaoui A, Snoeck R, Andrei G, Chavignon O, Teulade J-C, Witvrouw M, Balzarini J, De Clercq E, Chapat J-P. *J. Med. Chem.*, 1998, 41(25), 5108–5112.
4. Rupert KC, Henry JR, Dodd JH, Wadsworth SA, Cavender DE, Olini GC, Fahmy B, Siekierka JJ. *Bioorg. Med. Chem. Lett*., 2003, 13(3), 347–350.
5. Rival Y, Grassy G, Michel G. *Chem. Pharm. Bull.*, 1992, 40(5), 1170–1176.
6. Almirante L, Polo L, Mugnaini A, Provinciali E, Rugarli P, Biancotti A, Gamba A, Murmann W. *J. Med. Chem.*, 1965, 8(3), 305–312.
7. Vranda KS, Kumari PDR. 2020, p 040006.
8. Salim R, Ech-chihbi E, Oudda H, El Hajjaji F, Taleb M, Jodeh S. *J. Bio. Tribo. Corros.*, 2019, 5(1), 14.
9. Ji G, Shukla SK, Dwivedi P, Sundaram S, Prakash R. *Ind. Eng. Chem. Res.*, 2011, 50(21), 11954–11959.
10. Ravichandran R, Nanjundan S, Rajendran N. *J. Appl. Electrochem*., 2004, 34(11), 1171–1176.
11. Popova A, Sokolova E, Raicheva S, Christov M. *Corros. Sci*., 2003, 45(1), 33–58.
12. Bentiss F, Lebrini M, Lagrenée M. *Corros. Sci*., 2005, 47(12), 2915–2931.
13. Khedr MGA, Lashien AMS. *Corros. Sci*., 1992, 33(1), 137–151.
14. Schorr M, Yahalom J. *Corros. Sci*., 1972, 12(11), 867–868.

15. Umoren SA, Solomon MM, Udosoro II, Udoh AP. *Cellul*., 2010, 17(3), 635–648.
16. Solomon MM, Umoren SA, Udosoro II, Udoh AP. *Corros. Sci*., 2010, 52(4), 1317–1325.
17. Morad MS, El-Dean AMK. *Corros. Sci*., 2006, 48(11), 3398–3412.
18. Chaieb E, Bouyanzer A, Hammouti B, Benkaddour M. *Appl. Surf. Sci*., 2005, 246(1–3), 199–206.
19. Hamdy A, El-Gendy N Sh. *Egypt. J. Pet*., 2013, 22(1), 17–25.
20. Jamal Abdul Nasser A, Anwar Sathiq M. *Arabian J. Chem*., 2016, 9, S691–S698.
21. Obi-Egbedi NO, Obot IB. *Arabian J. Chem*., 2012, 5(1), 121–133.
22. Obot IB, Obi-Egbedi NO, Umoren SA. *Corros. Sci*., 2009, 51(2), 276–282.
23. Mu, GN, Li X, Li F. *Mater. Chem. Phys*., 2004, 86(1), 59–68.
24. Soltani N, Behpour M, Ghoreishi SM, Naeimi H. *Corros. Sci*., 2010, 52(4), 1351–1361.
25. Villamil RFV, Corio P, Agostinho SML, Rubim JC. *J. Electroanal. Chem*., 1999, 472(2), 112–119.
26. Dehri İ, Özcan M. *Mater. Chem. Phys*., 2006, 98(2–3), 316–323.
27. Eddy NO, Odoemelam SA, Odiongenyi AO. *J. Appl. Electrochem.*, 2009, 39(6), 849–857.
28. Lagrenée M, Mernari B, Bouanis M, Traisnel M, Bentiss F. *Corros. Sci*., 2002, 44(3), 573–588.
29. Quraishi MA, Ahamad I, Singh AK, Shukla SK, Lal B, Singh V. *Mater. Chem. Phys*., 2008, 112(3), 1035–1039.
30. Tang L, Li X, Li L, Mu G, Liu G. *Mater. Chem. Phys*., 2006, 97(2–3), 301–307.

The Chemist
Journal of the American Institute of Chemists

Evidence of Macromolecular Structure of Humic Acids from Compost

Sante Capasso[1], Stefano Salvestrini[1,2*] and Pasquale Iovino[1,2]

[1] Environmental Technologies, University Spin-Off of University of Campania "Luigi Vanvitelli", via Vivaldi 43, 81100, Caserta, Italy.
[2] Department of Environmental, Biological and Pharmaceutical Sciences and Technologies, University of Campania "Luigi Vanvitelli", via Vivaldi 43, 81100, Caserta, Italy

*** Correspondence should be addressed to Stefano Salvestrini**
(Email: stefano.salvestrini@unicampania.it)

Abstract: Humic acids (HA) from compost of domestic-waste origin were characterized by IR and UV-Vis spectra and by elemental analysis. The molecular structure was investigated by treatment with the monocarboxylic acid HCOOH and CH3COOH, dialysis experiments and size-exclusion chromatography (SEC). In contrast to former reports, HCOOH and CH3COOH caused the simple precipitation of HA. SEC experiments gave chromatograms with a broad peak, with an elution volume at the maximum height of the peak very close to that of the globular protein bovine serum albumin, a value slightly above the fractional range of the gel used for SEC tests. The chromatogram profile was found to be independent on HA concentration. The eluted fractions exhibited sharper peaks than the pristine HA sample. It can be concluded that the HA extracted from compost do not consist of relatively small molecules held together by weak intermolecular interactions (as reported in the literature), but rather have a canonical macromolecular structure. The simple approach employed here is proposed as a reference procedure for testing the chemical structure of humic acids of any origin.

Keywords: Humic acids, Hydrodynamic volume, Dialysis, Organic matter, Size-exclusion chromatography

Introduction

Humic substances (HS) are a class of compounds derived from biochemical decomposition of organic matter [1]. They have a backbone of aromatic nuclei and alkyl chains with a diversity of functional groups, notably carboxyl, phenol, hydroxyl, and quinone groups [2]. HS are ubiquitous in surface water, soil and sediments, and are of paramount importance in sustaining plant growth [3]. HS are responsible for the structure and physico-chemical properties of soil and are involved in most processes taking place at soil/water interphase [4]. Moreover, HS are a large fraction of the organic matter in compost, a soil amendment obtained by biological aerobic processing of organic wastes [5].

Humic acids (HA) are the fraction of HS soluble in water at neutral and basic pH. HA interactions with inorganic and organic pollutants have been intensively studied for several decades [6-13]. HA can reversibly bind cations by means of electrostatic interactions, as well as non-ionic compounds including organic pollutants by hydrogen bonds, dipole interactions and hydrophobic effects [14,15]. Dissolved HA are the main carriers of pollutants in water [16]. In addition, HA can strongly influence the retention of pollutants in soil and their bioavailability [17-19]. Because of the occurrence of large void spaces in their three-dimensional structure, HA are able to sequester organic compounds [20]. Thanks to this property, HA are a valid alternative to conventional adsorbent materials [21,22] for low-cost wastewater purification.

HA may undergo conformational changes upon adsorption to solid surfaces [23] and exhibit a colloidal behavior in solution [24]. HA aggregation depends on a diversity of factors including pH, ionic strength, type and concentration of ions [25,26]. Because of this, the molar mass of HA molecules in solution is still a matter of debate [27]. A definition of HA molecular structure is essential for understanding the multi-faceted properties of these compounds and their behavior in the environment.

HA have generally been assigned a macromolecular structure throughout the past century [28-32]. More recently, some authors [33-35] pointed to the lack of clear evidence supporting this view and described HA as supramolecular assemblies of molecules with a mass of about 600 g mol^{-1} [34]. Others [36] suggested that HA solutions consists of both small molecules and macromolecules. Notably, Baalousha et al. [37] reported that HA solutions mainly consist of supramolecular aggregates of relatively small molecules (20 nm diameter) and a minor fraction of isolated larger molecules (30-200 nm).

Von Wandruszka [38] emphasized that the notion of HA solutions consisting of aggregates of small molecules was at odds with a part of the experimental evidence. Indeed, the possibility should be considered that HA samples from different sources, or extracted using different methods, have different molecular structures [39]. Thus, it is a good rule not to extrapolate the properties of a particular sample to the whole class of compounds.

Recent work provided evidence that a commercial HA sample had a macromolecular structure [40]. This paper reports on the molecular structure of HA from compost investigated by treatment with organic acids, dialysis experiments and size-exclusion chromatography.

Materials and Methods

The compost was prepared by composting waste vegetables and fruits following the procedure reported elsewhere [41].

The extraction of humic acids from compost was carried out by basic/acid precipitation method following the procedure reported in [41]. Briefly, 90 g of compost were contacted with 1.0 L of distilled water and the pH was brought to 12.0 by solid NaOH for dissolving HA. Afterwards, the pH of the supernatant was brought to 1.5 by concentrated HCl and the precipitate (HA) was collected and stored.

C, H and N composition was determined by a C, H, N analyzer (PerkinElmer 2400 Series II CHN/O Elemental Analyzer). Ash content was measured by heating the HA at 650 °C for 5 h.
IR spectra were recorded in the range 400-4000 cm^{-1} using pellets of 0.5 mg HA in 100 mg KBr, previously oven-dried at 110 °C for 72 hours. Measurements were carried out on a PerkinElmer Spectrum GX (FT-IR System).

UV-Vis spectra were recorded on a Perkin Elmer, Lambda 40, spectrometer in a 0.20 mol L^{-1} $NaHCO_3$ (pH = 8.6) solution, optical path = 0.50 cm.

The effect of monocarboxylic acids on the HA structure was investigated by adding, drop by drop, pure acetic acid (>98%) or formic acid to 40 mL of HA solution (300 mg L^{-1}, pH = 7.0), down to pH = 2.0. After about half an hour, a sediment started settling at the bottom of the vials. After one day, the precipitate was collected by centrifugation (3,000 rpm for 30 min), washed with deionized water, solubilized in 40 mL of 0.20 mol L^{-1} $NaHCO_3$, and analyzed by UV-Vis spectroscopy. The supernatant obtained by centrifugation was evaporated by a roto-evaporator to eliminate the acetic or formic acid, and the resulting deposit was dissolved in 20 mL of 0.20 mol L^{-1} $NaHCO_3$ and analyzed by UV-Vis spectroscopy.

Dialysis experiments were performed as follows: 60 mL of HA solution, 300 mg L^{-1} in 0.20 mol L^{-1} $NaHCO_3$, were introduced in a dialysis tube with a cut-off of 3.5 kDa or 5.6 kDa (Spectra/por, USA). The bag was put in contact with 60 mL of 0.20 mol L^{-1} $NaHCO_3$, and the whole was periodically and gently shaken.

LP-SECs were performed using Bio-Gel P30 Gel medium with 2.5 - 40 kDa fractional range (Bio-Rad Laboratories, USA), in a column 30 cm in length and 2.5 cm in diameter, eluted with 0.20 mol L^{-1} $NaHCO_3$ (pH 8.6), flow rate 2.0 ml h^{-1}. The eluate was analyzed by absorbance at λ = 450 nm and 280 nm.

The void volume (Vo) and the total available volume (Vt) were measured by blue dextran (molecular weight = 2.0·106 Da) and hydroquinone (molecular weight = 110 Da), respectively. The distribution coefficient (Kd) was computed from the relation Kd = (Vi-Vo)/(Vt-Vo), where Vi is the elution volume of the analyte i.

Results

Characterization of HA sample

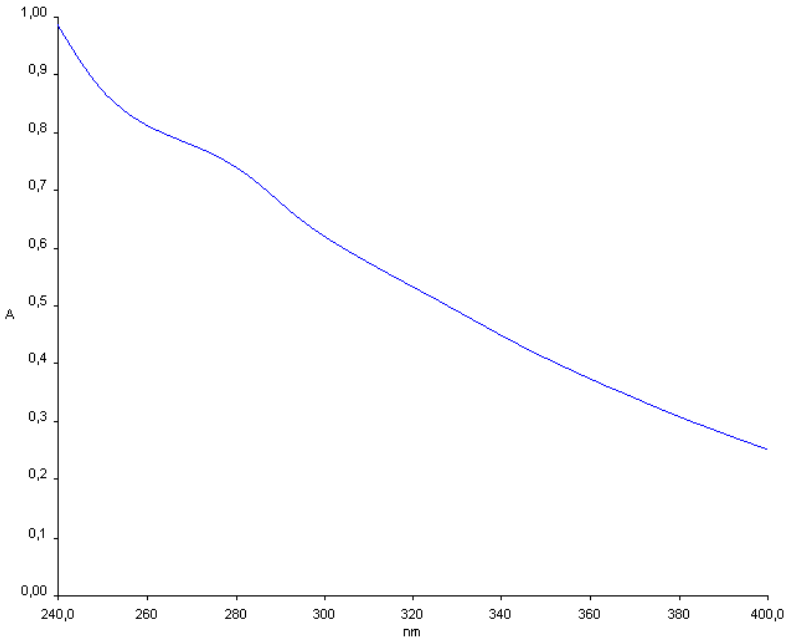

Fig 1. UV-Vis Spectrum of the HA Sample

The shape of UV-Vis spectrum of HA (Figure 1) is characterized by a monotonical absorbance decrease with increasing wavelength, and by a shoulder between 265 and 295 nm prevalently due to aromatic rings. The molar absorption coefficient at 280 nm (ε_{280}) has been used as an index of the degree of aromaticity [42].

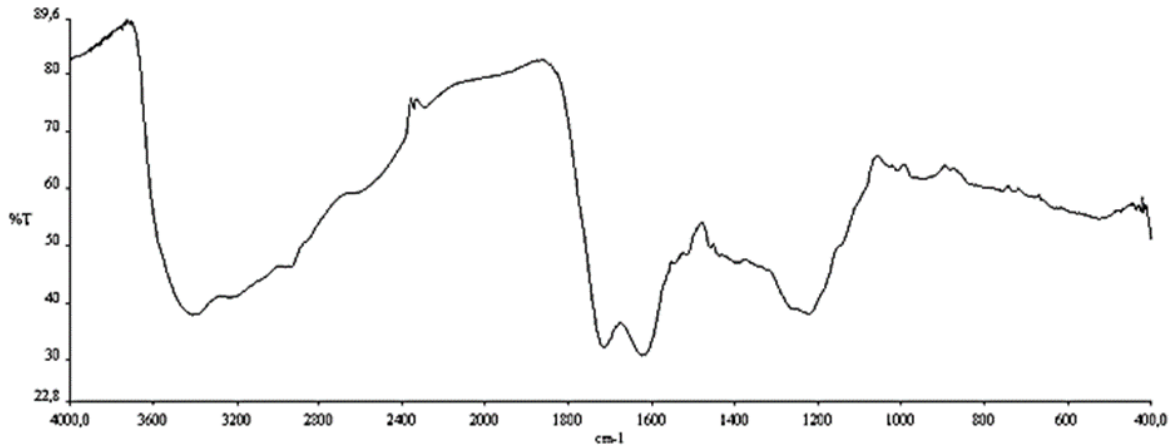

Fig 2. IR Spectrum of the HA Sample

In line with results by Miikki et al. [43], the IR spectrum (Figure 2) displayed distinctive bands at ~ 1200 and 1700 cm^{-1} (carboxyl groups) and 1650 cm^{-1} (unsaturated C=C).

The results of elemental analyses (Table 1) were in agreement with values previously reported for HA from compost [42]:

Table 1. Elemental Analysis of the HA Sample

	Percentage (%)
C	53.1
H	4.9
N	4.5
ash	2.9

Monocarboxylic acid effects on HA structure

The UV-Vis spectrum of the precipitate obtained by acidification with formic or acetic acid was qualitatively and quantitatively indistinguishable, within the experimental error, from that obtained with the starting sample. The absorbance at 450 nm was about 90% of that of the starting solution. The amount of HA present in the supernatant resulted to be negligible.

Membrane dialysis (MD) experiments

HA in $NaHCO_3$ solution was dialysed using membranes with cut-off of 3.5 kDa or 6 - 8 kDa. In either case, UV-Vis analysis did not reveal HA in the outside solution after three weeks.

Size-exclusion chromatography (SEC)

SEC has been commonly employed in work on humic acids [44,45]. The technique sorts the analytes according to their hydrodynamic volume, thus providing information on their molecular size as well as molar mass distribution for poly-dispersed materials. For macromolecules lacking a stable tridimensional structure, the molecular size can be strongly affected by the pH and ionic strength of the solution [34]. In this case, the elution volume depends on the specific eluent composition. Low-pressure SEC has the advantage, in comparison with high-pressure SEC, of permitting the collection of larger volumes of eluate, even with consecutive chromatographies. Figure 3 reports the low-pressure SEC chromatogram of the HA sample.

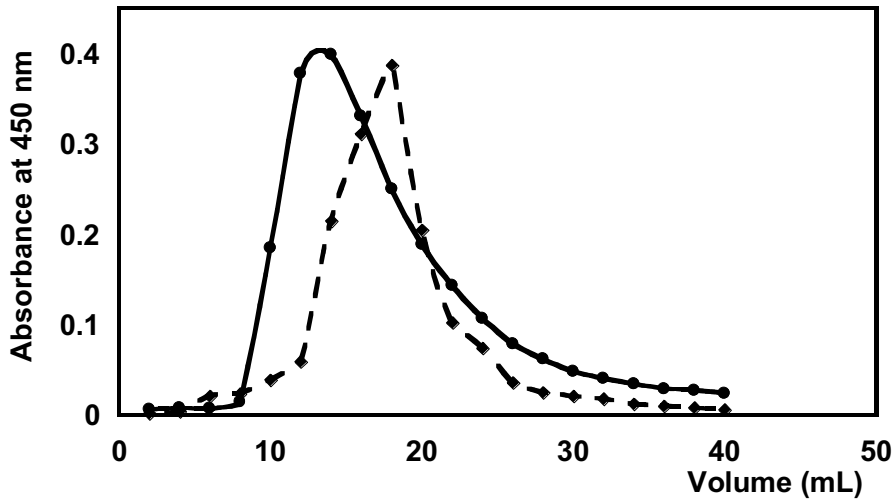

Fig 3. Low-pressure size exclusion chromatogram of HA (500 mg L^{-1}) from compost (unbroken line) and of the eluate fraction 16 - 18 mL (broken line) on a gel with fractional range 2.5 - 40 kDa. For graphical reasons, the absorbance values were multiplied by ten. Column diameter = 2.5 cm, length = 30 cm; flow 2.0 mL h^{-1}, eluent sodium bicarbonate 0.20 M, pH = 8.6, temperature ~ 25 °C.

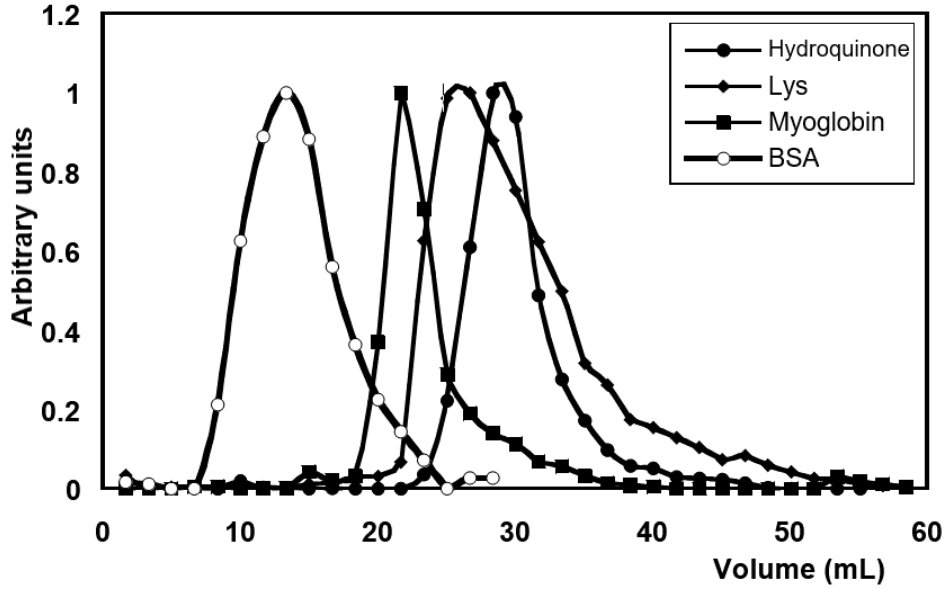

Fig 4. Low-pressure size exclusion chromatograms of some compounds used for the column calibration, BSA = globular protein bovine serum albumin (molecular weight 66.5 kDa), Lys = lysozime from egg (molecular weight = 14.4 kDa), Myoglobin from equine heart (molecular weight 17 kDa), Hydroquinone (molecular weight = 110 Da). The absorbances were normalized at the maximum absorptivity. The chromatogram of blue dextran (not shown) was almost the same as for albumin.

Figure 4 reports the chromatogram of compounds used for calibration. Hydroquinone was chosen as a model of low-molecular- weight humic acids [46]. Myoglobin, BSA and lysozime were chosen because of their sharply different isoelectric points (IP), with the aim to assess the effect of electrostatic interactions with the column. At the experimental pH (8.6), Myoglobin (IP = 7) and BSA (IP = 5) have a negative net charge whereas Lysozime (IP = 11) has a positive net charge. Figure 4 shows that the molar mass had a monotonic trend with the elution volumes, which suggests that column interactions played a negligible role.

The HA chromatogram (Figure 3) is characterized by a broad peak, indicating a wide molecular weight distribution (or the presence of molecular aggregates with different sizes). The elution volume at the maximum height of HA peak nearly coincides with that of the globular protein *bovine serum albumin* (BSA, Figure 4), indicating the predominance in solution of particles with a hydrodynamic volume similar to that of BSA or larger. The molar mass of this protein is slightly higher than the upper value of the nominal fractional range. After this chromatographic run, the fraction corresponding to the eluate from the 18th to the 20th mL of the elution volume, was chromatographed again on the same column (Figure 3). As can be seen, the peak is sharper and more centered in correspondence to the elution volume of the fraction selected. Similar results were obtained with other fractions.

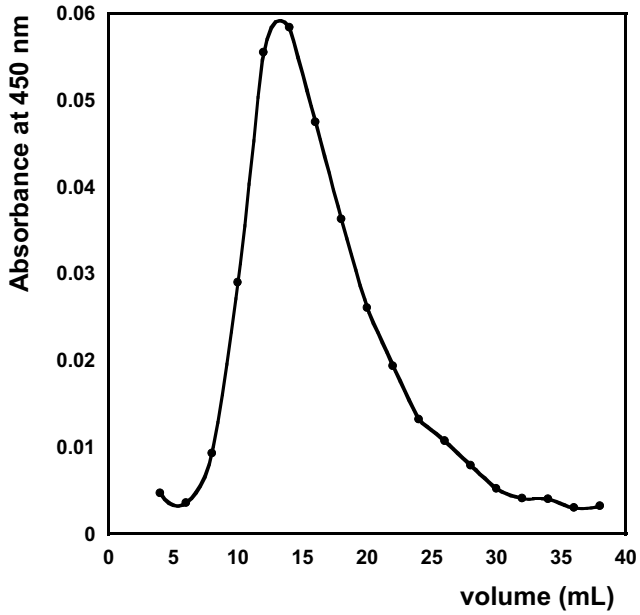

Fig 5. Gel Permeation Chromatogram (Bio-gel P30, 40 KDa) of 50 mg L^{-1} HA in 0.2 M $NaHCO_3$

Interestingly, the chromatogram of a dilute solution of HA (Figure 5) closely mirrors the chromatogram of the more concentrate solution (Figure 3), not considering the lower absorbance of the eluate. This confirms the absence of significant aggregation phenomena under the experimental conditions investigated.

Table 2 reports the distribution coefficient (K_d) of our HA sample, computed in correspondence of the maximum absorbance, and of some proteins.

Table 2. Distribution Coefficient (K_d) on Bio-gel P30, Eluent 0.20 mol L^{-1} $NaHCO_3$

Compound	K_d
Bovine serum albumin	0.04
Humic acids from compost	0.08
Myoglobin from equine heart	0.56
Lysozime from egg	0.82

Discussion

Piccolo and co-workers [47] reported that addition of monocarboxylic acids up to pH 2.0 to a HA solution caused disruption of the HA structure, producing molecules with low molar mass. In contrast, in our experiments the

treatment with formic or acetic acid induced the almost complete precipitation of HA (in line with the well-known acid-base behavior of HA). Moreover, our MD experiments showed that HA molecules did not pass across dialysis membranes with a cut-off of 3.5 or 6-8 kDa. In the hypothesis that our HA sample were an aggregation of small molecules (equation 1), we should have

$$M_n \rightleftarrows M_{n-1} + M \rightleftarrows M_{n-2} + 2M \rightleftarrows \ldots . \rightleftarrows nM \quad (1)$$

observed the molecule *M* diffusing through the membrane up to equilibrium. The behavior actually observed was that expected for macromolecules not for aggregates of small molecules. The size-exclusion chromatograms recorded using a gel with 2.5 - 40 kDa fractional range, led to the same conclusion. Independently of HA concentration, the results indicated a broad molar mass distribution with a prevalence of molecules with a mass close to the upper limit of the fraction range used. Second-run chromatograms of eluate fractions gave sharper peaks, indicating that the starting HA sample was a mixture of macromolecules of different sizes.

The property of HA to charge negatively in solution at neutral and basic pH does certainly not favor molecular association and, were this to occur, the forces involved should be weak. Because of this, the association of small, heterogeneous molecules should have a relatively small variation of the standard Gibbs energy ($\Delta_r G°$), a relatively small association equilibrium constant, and a relatively high rate constant [48]. Thus, the hypothesis that our HA sample were an aggregate of small molecules may be excluded.

Conclusions

The experimental data reported in this paper unambiguously show that the HA analyzed have a macromolecular structure with a broad molar mass distribution and a prevalence of molecules with a hydrodynamic volume close to that of the globular protein *bovine serum albumin* (molecular weight = 66.5 kDa). Our approach requires simple equipment available in any chemical laboratory and may thus become a reference procedure for testing the chemical structure of HA samples of any origin.

Data Availability

Data are available on request (please contact the corresponding author).

Conflicts of Interest

"The authors declare that there is no conflict of interest regarding the publication of this paper."

Funding Statement

This research received no external funding.

Acknowledgements

The authors are grateful to Prof. Roberto Ligrone for very useful discussion of results.

References

1 Flaig W. *Geochim. Cosmochim. Acta*, 1964, 28, 1523–1535.

2 Senesi N, Loffredo E in *Soil Physical Chemistry*, ed. D. L. Sparks, 1999, pp 239–370.

3 Chen Y, Aviad T in *Humic Substances in Soil and Crop Sciences: Selected Readings*, 2015, pp 161–186.

4 Stevenson F in *Humus Chemistry: Genesis, Composition, Reactions*, Wiley, 1994.

5 Diaz W, de Bertoldi LF, Bidlingmaier M in *Compost Science and Technology*, Elsevier, 2007.

6 Senesi N, Testini C, Miano TM. *Org. Geochem.*, 1987, 11, 25–30.

7 De Paolis F, Kukkonen J. *Chemosphere*, 1997, 34, 1693–1704.

8 Carter CW, Suffet IH in *Fate of*

Chemicals in the Environment, 1983, pp 215–229.
9 Pacheco ML, Peña-Méndez EM, Havel J. *Chemosphere*, 2003, 51, 95–108.
10 Tang WW, Zeng GM, Gong JL, Liang J, Xu P, Zhang C, Bin Huang B. *Sci. Total Environ.*, 2014, 468–469, 1014–1027.
11 Salvestrini S. *Environ. Chem. Lett.*, 2013, 11, 359–363.
12 Leone V, Iovino P, Salvestrini S, Capasso S. *Chemosphere*, 2014, 95, 75–80.
13 Iovino P, Leone V, Salvestrini S, Capasso S. *Desalin. Water Treat.*, 2015, 56, 55–62.
14 Senesi N. *Sci. Total Environ.*, 1992, 123–124, 63–76.
15 Chianese S, Fenti A, Iovino P, Musmarra D, Salvestrini S. *Molecules*, 2020, 25.
16 Chiou CT, Malcolm RL, Brinton TI, Kile DE. *Environ. Sci. Technol.*, 1986, 20, 502–508.
17 Lipczynska-Kochany E. *Chemosphere*, 2018, 202, 420–437.
18 Haitzer M, Höss S, Traunspurger W, Steinberg C. *Chemosphere*, 1998, 37, 1335–1362.
19 Rong Q, Zhong K, Huang H, Li C, Zhang C, Nong X. *Appl. Sci.*, DOI:10.3390/app10031077.
20 Schulten HR, Leinweber P. *J. Anal. Appl. Pyrolysis*, 1996, 38, 1–53.
21 Salvestrini S, Vanore P, Bogush A, Mayadevi S, Campos LC. *J. Water Reuse Desalin.*, 2017, 7, 280–287.
22 Canzano S, Capasso S, Di Natale M, Erto A, Iovino P, Musmarra D, *Sustain.*, 2014, 6, 4807–4822.
23 Colella A, de Gennaro B, Salvestrini S, Colella C. *J. Porous Mater.*, 2015, 22, 501–509.
24 Jones MN, Bryan ND. *Adv. Colloid Interface Sci.*, 1998, 78, 1–48.
25 Baalousha M, Motelica-Heino M, Le Coustumer P. *Colloids Surfaces A Physicochem. Eng. Asp.*, 2006, 272, 48–55.
26 Avena MJ, Wilkinson KJ. *Environ. Sci. Technol.*, 2002, 36, 5100–5105.
27 Olk DC, Bloom PR, Perdue EM, McKnight DM, Chen Y, Farenhorst A, Senesi N, Chin YP, Schmitt-Kopplin P, Hertkorn N, Harir M. *J. Environ. Qual.*, 2019, 48, 217–232.
28 Ghabbour G, Davies EA in *Understanding humic substances: advanced methods, properties and applications*, Royal Soci., 1999.
29 Myneni SCB, Brown JT, Martinez GA, Meyer-Ilse W. *Science*, 1999, 286, 1335–1337.
30 Barak P, Chen Y. *Soil Sci.*, 1992, 154, 184–195.
31 Ghosh K, Schnitzer M. *Soil Sci.*, 1980, 129, 266–276.
32 Flaig W in *Soil Components*, ed. J. E. Gieseking, Springer., 1975, pp 1–211.
33 Piccolo A. *Soil Sci.*, 2001, 166, 810–832.
34 Maia CMBF, Piccolo A, Mangrich AS. *Chemosphere*, 2008, 73, 1162–1166.
35 Šmejkalová D, Piccolo A. *Environ. Sci. Technol.*, 2008, 42, 699–706.
36 Baigorri R, Fuentes M, González-Gaitano G, García-Mina JM. *J. Phys. Chem. B*, 2007, 111, 10577–10582.
37 Baalousha M, Motelica-Heino M, Galaup S, Le Coustumer P. *Microsc. Res. Tech.*, 2005, 66, 299–306.
38 von Wandruszka R. *Geochem. Trans.*, DOI:10.1186/1467-4866-1-10.
39 Tombácz E, *Soil Sci.*, 1999, 164, 814–824.
40 Capasso S, Chianese S, Musmarra D, Iovino P. *Environ. - MDPI*, DOI:10.3390/environments7040032.
41 Leone V, Musmarra D, Iovino P, Capasso S. *Water, Air, Soil Pollut.*,

2017, 228, DOI:10.1007/s11270-017-3321-9.
42 Chin YP, Alken G, O'Loughlin E. *Environ. Sci. Technol.*, 1994, 28, 1853–1858.
43 Miikki V, Senesi N, Hänninen K. *Chemosphere*, 1997, 34, 1639–1651.
44 Town RM, Kipton H, Powell J. *Anal. Chim. Acta*, 1992, 256, 81–86.
45 Kawahigashi M, Fujitake N, Azuma J, Takahashi T, Fujitake N, Azuma J, Takahashi T. *Soil Sci. Plant Nutr.*, 1995, 41, 147–150.
46 Liu ZQ, Shah AD, Salhi E, Bolotin J, von Gunten U. *Water Res.*, 2018, 143, 492–502.
47 Piccolo A, Conte P, Cozzolino A. *Eur. J. Soil Sci.*, 1999, 50, 687–694.
48 Atkins PW, De Paula J in *Atkins' physical chemistry*, Oxford University Press, 2010.

The Chemist
Journal of the American Institute of Chemists

Theoretical Validation of Medicinal Properties of *Ocimum sanctum*

P. S. Kulkarni*†, Y.S. Walunj†, N. D. Dongare†

Department of Chemistry, Hutatma Rajguru Mahavidyalaya, Rajgurunagar Pune-410505 MS India
(Tel.: 9850658087, E-mail: pramodskulkarni3@gmail.com)

Abstract: Molecular property and bio-activity scores of ten essential oil constituents present in Ocimum sanctum leaves were predicted using Molinspiration software. For all the essential oil compounds, miLogP values were found to be < 5 for compounds 1-7, indicating their good permeability across the cell membrane, and compounds 8-10 show miLogP values > 5, showing these compounds were not easily permeable across the cell membrane. TPSA in the range of 0.00-66.76 (well below 160Å^2) and n violations = 1 or 0, molecular mass < 500, n rotb < 5 [10], no. of hydrogen bond donors ≤ 5 (the sum of OHs and NHs), no. of hydrogen bond acceptor ≤ 10 (the sum of Os and Ns) were observed for these compounds. This indicates that these compounds were found to obey Lipinski's rule and can easily bind to receptors and were taken further for the calculation of bioactivity scores by calculating the activity score of GPCR ligand, ion channel modulator, nuclear receptor ligand, kinase inhibitor, protease inhibitor and enzyme inhibitor.

Key Words: Molinspiration, *Ocimum sanctum*, bioactivity score, Lipinski's rule

Introduction

Plants are one of the most important sources of medicines. The medicinal plant is very old. The writings indicate the therapeutic use of plants as far back as 4000-5000 B.C. The Chinese were the first to use the natural herbal. In India, however, the earliest references of the usage of plants as medicine appear in

Rigveda, which is supposed to have been penned between 3500-1600 B.C. Later, the properties and healing uses of medicinal plants were analyzed in detail and recorded empirically by the ancient physicians in Ayurveda (an indigenous system of medicine), which is a basic institution of ancient medical science India [1].

O. sanctum, "the holy place", has been experienced from as early as the Vedic period, usually known as "Tulsi", belonging to the family of Lamiaceae. The work is kept sacred by Indians all over the globe as it is an herbaceous plant that is used for religious purposes in accession to its great medicinal values. The plant is an aromatic bushy shrub. It springs up all over India, growing up to 2000 meters in the mounds. It grows in houses, temples, and gardens. Leaves have a sweet, clove-like scent. There are many varieties of this species. It presents in a range of foliage colours (royal and green), leaf shapes and grains, bloom colors, heights and fragrances. The blooms are tiny, purple or white and inflorescence is a long spike. Of all the *Ocimum* species, *O. sanctum* is most widely studied for its pharmacological properties. Traditionally, the leaves are used to treat bronchitis, and gastric, skin and hepatic disorders. Diverse pharmacological properties of *O. sanctum* (for example antidiabetic, immunostimulant, antioxidant, cardioprotection, antifungal) have attracted entrepreneurs to set eyes on this plant. Leaf extract of *O. sanctum* showed significant ability to scavenge free radicals. The industry sector perceives *O. sanctum* not just as a spice used in household kitchens. They, too, view it as a potential lead in the production of drugs that are important to satisfy the insatiable demands of the population. These drugs would be cost effective and quite suitable to millions of our masses, as this herb and its remedies have been in use from ancient times [2]. The leaves contain an essential oil which is composed of eugenol, carvacrol, methylchavicol, limatrol, and caryophylline. The seeds contain oil composed of fatty acids and sitosterol. The roots contain ursolic acid and n-triacontanol. Eugenol – its methyl ether, nerol, caryophyllene, terpinen4-decyladehyde, selinene, pinenes, camphene and α-pinene have been identified in essential oil. To boot, it also contains rosmarinic acid, thymol, linalool, and methyl chavicol and citral [3]. Because of remarkable biological activities of this plant, our aim is to predict the molecular properties and to evaluate the bioactivity scores using Molinspiration [4-6

Materials and Methods

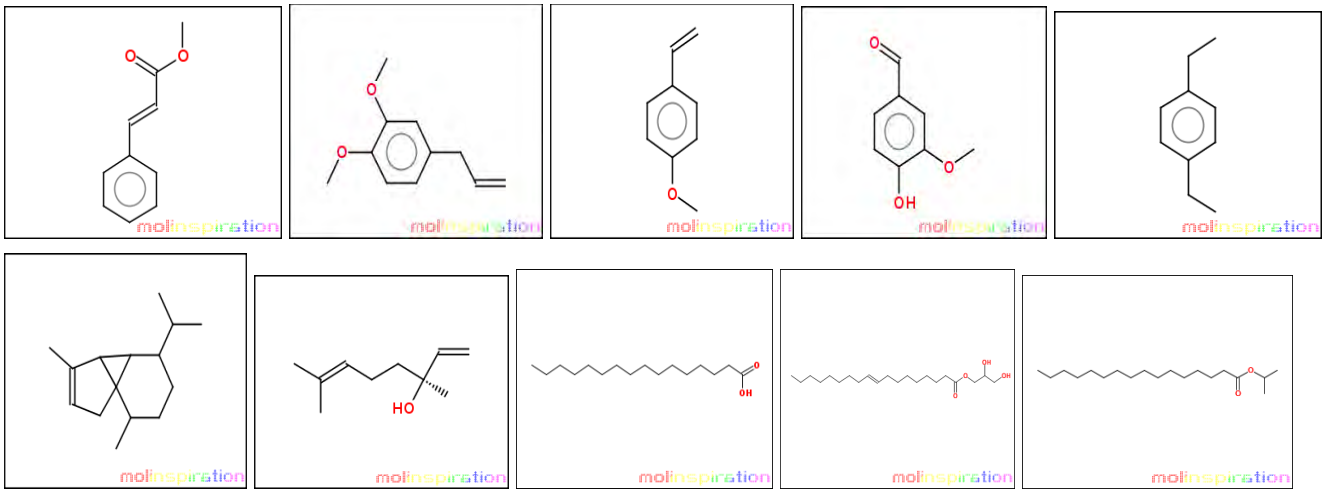

Fig 1. Structures of compound isolated from *O. sanctum*

Structures of all the ten compounds reported from *O. sanctum* were taken from the literature and their structures were drawn using online Molinspiration software (www.molinspiration.com) (Figure 1) for calculation of molecular properties (Log P, total polar surface area, number of hydrogen bond donors and acceptors, molecular weight, number of atoms, number of rotatable bonds, etc.) and prediction of bioactivity score for drug targets (GPCR ligands, kinase inhibitors, ion channel modulators, enzymes and nuclear receptors) [4]. The bioactivity score and drug-likeness properties of the all the ten compounds were compared.

Prediction of bio-activity

1. Molecular properties of nine alkoxy derivative of Naringenin were calculated using Molinspiration and the values are given in Table 1.

Table 1. Calculation of Molecular Properties

S.N	Compound	miLogP	TPSA	natoms	MW	nON	noHNH	nviolations	nrobt	Volume
1	1	2.53	26.30	12	162.19	2	0	0	3	155.99
2	2	2.41	18.47	13	178.23	2	0	0	4	179.67
3	3	2.85	9.23	10	134.18	1	0	0	2	137.32
4	4	1.07	46.53	11	152.15	3	1	0	2	136.59
5	5	3.77	0.00	10	134.22	0	0	0	2	150.77
6	6	5.82	0.00	15	204.36	0	0	1	1	224.82
7	7	3.21	20.23	11	154.25	1	1	0	4	175.59
8	8	7.06	37.30	18	256.43	2	1	1	14	291.42
9	9	6.61	66.76	25	356.55	4	2	1	19	386.27
10	10	8.10	26.30	21	298.51	2	0	1	16	342.34

2. Bio-activity scores of the nine alkoxy towards GPCR ligand, ion channel modulator, nuclear receptor ligand, kinase inhibitor, protease inhibitor and enzyme inhibitors are given in Table 2.

Table 2. Bioactivity Score

S.No	Compound	GPCR Ligand	Ion channel modulator	Kinase inhibitor	Nuclear receptor ligand	Protease inhibitor	Enzyme inhibitor
1	1	-0.92	-0.52	-1.16	-0.69	-1.02	-0.47
2	2	-0.81	-0.38	-1.06	-0.80	-1.14	-0.43
3	3	-1.17	-0.43	-1.25	-1.02	-1.45	-0.68
4	4	-1.20	-0.54	-1.13	-0.91	-1.65	-0.64
5	5	-1.05	-0.40	-1.32	-1.17	-1.22	-0.62
6	6	-0.32	-0.10	-0.71	-0.31	-0.37	-0.16
7	7	-0.73	0.07	-1.26	-0.06	-0.94	0.07
8	8	0.02	0.06	-0.33	0.01	-0.04	0.18
9	9	0.21	0.05	-0.05	0.17	0.15	0.28
10	10	-0.04	-0.07	-0.28	0.05	-0.04	0.06

Lipinski's Rule:

Lipinski's rule of five, commonly known as the Pfizer's rule of five or simply the Rule of five, is a regulation of thumb to estimate drug-likeness or to identify a chemical compound with a certain pharmacological or biological activity that has properties that would make it a likely orally active drug in humans. The principle was designed by Christopher A. Lipinski in 1997. The rule expresses molecular properties vital for a drug's pharmacokinetics in the human body, including their absorption, distribution, metabolism and elimination (ADME) components of the Lipinski's rule [5,6].

Lipinski's rule states:

- Not more than 5 hydrogen bond donors (nitrogen or oxygen atoms with one or more hydrogen atoms)
- Not more than 10 hydrogen bond acceptors (nitrogen or oxygen atoms)
- A molecular weight less than 500
- An octanol-water partition coefficient log P not greater than 5
- No more than one number of violations

Molinspiration

Molinspiration, a web-based software, was used to obtain parameters such as MiLogP, TPSA, and drug-likeness. MiLogP is estimated by the methodology developed by Molinspiration as a sum of fragment-based contributions and correction factors. The MiLogP parameter is applied to check good permeability across the cell membrane. TPSA is related to the hydrogen bonding potential of the compound. Computation of volume developed at Molinspiration is based on group contributors. Number of rotatable bonds measures molecular flexibility. It is a very good descriptor of absorption and bioavailability of drugs. Through the drug-likeness data of a particle the molecular properties and structure features can be checked with regard to known drugs.

Bioactivity score

Bioactivity of the drug can be found out by estimating the activity score of GPCR ligand, ion channel modulator, nuclear receptor ligand, kinase inhibitor, protease inhibitor, and enzyme inhibitor. All the parameters were determined with the aid of Molinspiration drug-likeness score online (www.molinspiration.com). The calculated drug-likeness score of each compound was compared with the specific bodily process of each compound, and the results were

compared with Naringenin. For organic molecules the probability is if the bioactivity score is (> 0), then it is active; if (-5.0-0.0), then moderately active; if (< -5.0), then inactive.

Results and Discussion

a. Molecular property of the Chalcones:

The ten oil constituents obeyed the Lipinski's rule of five and showed good drug-likeness scores. MiLogP values of these oily compounds were found to be < 5 (1.07-5.82 for compounds 1 to 7), indicating their good permeability across the cell membrane. All the derivatives were found to have TPSA and will be below 160Å^2 (100.13), molecular weight < 500, no. of hydrogen bond donors ≤ 5, no. of hydrogen acceptor ≤ 10, n-violations 0, number of rotatable flexible bonds >5.

b. Bioactivity scores of the Chalcones:

The bioactivity scores of the ten compounds have shown the following observations

1. GPCR Ligand: Among the ten compounds were found to be moderately active (≤ 0) and compound no. 8 and 9 shows they are highly active (≥ 0) towards GPCR ligands.
2. Ion channel modulator: Among the ten compounds, compound no. 7-9 were found to be highly active (≥ 0). The remaining compounds were to be moderately active (≤ 0).
3. Kinase inhibitor: All ten compounds were found to be moderately active (≤ 0) towards Kinase inhibitor.
4. Nuclear receptor ligand: Among the ten compounds, compound no. 8-10 were found to be highly active (≥ 0) towards Nuclear receptor ligand. The remaining compounds were to be moderately active (≤ 0).
5. Protease inhibitor: Among the ten compounds, compound no. 9 was found to be highly active (≥ 0) towards Protease inhibitor. The remaining compounds were to be moderately active (≤ 0).
6. Enzyme inhibitor: Among the ten compounds, compound no. 7-10 were found to be highly active (≥ 0) towards Enzyme inhibitor. The remaining compounds were to be moderately active (≤ 0).

Conclusion

In conclusion, ten compounds show highly active to moderate bioactivity score. All compounds obey Lipinski's rule for drug-likeness activity of the molecules.

References

1. Prakash P, Gupta A. *Indian J. Physiol. Pharmacol.,* 2005, 49, 125-131.
2. Mishra T. *J. Med. Plant Stud.*, 2015, 3, 16-19.
3. Singh V, Amdekar S, Verma O. *WebmedCentral Pharmacol.*, 2010, 1, 10. WMC001046 doi: 10.9754/journal.wmc.2010.001046
4. Molinspiration – cheminformatics [last accessed: November 2018] www.molinspiration.com
5. Lipinski CA, Lombardo F, Dominy BW. *P. J. Feeney Adv. Drug Delivery Rev.,* 1997, 23, 3-25.
6. Lipinski CA, Lombardo F, Dominy BW. *P. J. Feeney Adv. Drug Delivery Rev.,* 2001, 46, 3-26.

The Chemist
Journal of the American Institute of Chemists

Constructing a Cactus (*Opuntia*) Battery

Mohammad Ali Amayreh*

Department of Chemistry, Al-Balqa Applied University
19110, Al-Salt, Jordan
(E-mail: mohammad.amayreh@bau.edu.jo)

Abstract: This research aimed to investigate the ability to generate electricity from cutting pieces of cactus plate and studying the electrical properties of the constructed cactus battery. Also, could this battery light LED lamps for a reasonable time? By inserting magnesium (Mg) and copper (Cu) electrodes into cactus pieces and connect them in series, a cactus voltaic cell was constructed. Variations of generated voltage and current were examined for 6 pieces of cactus pieces connected in series as well as 6 electrochemical cells of cactus extract. The results showed that the potential difference of the 6 pieces connected in series decreased from 9.10 V at the beginning of the experiment to 7.35 after 102 hours with 16% of decrement; whereas the current decreased by 67% after 24 hours. The study proved the ability to generate electricity from cut cactus pieces and cactus' extract, as well as its viability as a new inexpensive renewable energy resource. The cactus plates electrolytic solution contents of citric acid are mainly responsible for the production of electricity from chemical reactions between cactus electrolyte and metal electrodes.

Key Words: cactus, battery, voltage, electricity

Introduction

In 1791, Luigi Galvani discovered electrical activity in the nerves of the frogs that he was dissecting. He thought that electricity was of animal origin and could be found only in living tissues [1]. A few years later, in 1800, Alessandro Volta discovered that electricity could be produced through inorganic means. In

fact, by using small sheets of copper and zinc and cloth spacers soaked in an acid solution, he built a battery – the first apparatus capable of producing electricity [1].

Electricity has a central role in our lives and to this day electrochemistry is a standard course of study [1]. Today batteries provide the power for an amazing variety of devices, everything from flashlights to robots, computers, satellites and cars. Inventors and researchers continue to improve the battery, designing batteries that last longer and that are friendlier to our environment [2].

Energy consumption throughout the world, but particularly in industrialized societies, has been steadily increasing. Much of the energy consumed, 97% in the case of the UK, comes from non-renewable sources [3]. The present use of carbon-based non-renewable energy is unsustainable because of the effect of the resultant carbon dioxide (CO_2) emissions on the global climate [3]. Reduction in demand must be part of the solution but alternative energy sources must also be developed. All energy sources come with environmental penalties, whether from the construction of dams and barriers or from the impact of renewable sources such as wind on rural landscapes, but these impacts must be balanced against the necessity of developing low-carbon sources that are both economically viable and, also, secure [3].

Most fruits can conduct electricity because they contain water with various substances dissolved in it. How much electricity they conduct depends on how much water there is and what is dissolved in it. Most fruits have some acid which results in many free ions that allow the flow of electricity, so acidic fruits are quite good conductors of electricity (that is, with low resistance). Lemons and limes are acidic fruits. They contain citric acid which makes them good conductors [4,5].

Organic acids are of great significance in plants. As intermediates in the metabolic processes of the fruits, these acids are directly involved in growth, maturation, and senescence. Fruit juices have a low pH, because they contain high levels of organic acids. The total acid content varies widely, from approximately 0.2% in pear juice to 0.8% in lime. Some of the major acids in fruits include citric, malic, and tartaric acids [6].

Many experiments were carried out to generate electricity from vegetables and fruits. Erika Lindstorm did her experiment which was aimed at finding out which fruit would generate enough electricity to light a light bulb and to discover which fruit would light the bulb the longest. Copper and zinc electrodes were used with a multimeter; the fruit samples were Sunkist lemons, Texas Rio Star grapefruit, hot house tomatoes, Kiwis, and California Navel oranges. After several tests she discovered that the light bulb would not light up with any of the fruits using any of the variables due to the high resistance of the light bulb and because the fruit did not produce enough current [7].

Creating a battery from a lemon is a common project in many science textbooks. Batteries consist of two different metals suspended in an acidic solution. Zinc and copper work well as the metals and the citric acid content of a lemon will provide the acidic solution. Batteries like this will not be able to run a motor or energize most light bulbs. It is possible to produce a dim glow from an LED [4]. Potato was used with zinc and copper electrodes as a battery [8].

In another advanced research project, Professor Chungpin Hovering Liao of National Formosa University in Taiwan has created the world's first chlorophyll organic battery (http://www.ecofriend.org/entry/eco-tech-any-liquid-is-good-for-the-world-s-first-chlorophyll-battery/; http://www.goodcleantech.com/2008/10/chlorophyll_organic_battery_ru.php). The battery can use any liquid, even urine, to power up. It doesn't take much time to start juicing the battery, either. Within 10 seconds of being doused with liquid, the battery starts providing power [9].

Christopher J. Love and other workers studied the source of sustained voltage difference between the xylem of a potted *Ficus benjamina* tree and its soil. They have measured sustained differences of 50–200 mV between the xylem region of a Faraday-caged, intact, potted *Ficus benjamina* tree and its soil, as well as between its cut branches and soils and ionic solutions standardized to various pH values. Using identical platinum electrodes, no correlation between voltage and time of day, illumination, sap flow, electrode elevation, or ionic composition of soil was found, suggesting no direct connection to simple dissimilar-metal redox reactions or transpirational activity. Instead, a clear relationship between the voltage polarity and magnitude and the pH difference between xylem and soil was observed. They attributed these sustained voltages to a biological concentration cell likely set up by the homeostatic mechanisms of the tree. The proposed practical applications of these findings, beyond monitoring pH changes, include a wide variety of trickle chargers for niche, low-power, pulsed, off-grid distributed systems – such as forest fire detectors; environmental sensors; and ''smart dust'' or mesh networked devices – which drastically decrease the need for in-the-field battery changes. Interestingly, ionic flows through micro-fluidic circuits have already been investigated as viable sources of microwatt level electrical power [10].

Aims of the Study

There is currently an upsurge of interest in finding renewable energy resources due to the international rise in the price of oil, which has negative effects on the economies of industrial as well as developing countries. Moreover, the

environmental pollution due to the combustion of fuel is one of the most serious issues worldwide. All countries tend to solve the oil bill problem and to reduce environmental pollution to control global warming by searching for alternative energy resources like wind power, water power, nuclear power, etc.

Jordan is suffering from inconveniently high oil prices: that was one of the most important motives to search for new renewable energy resources.

As a preliminary study that precedes the current project, it was noticed that the cactus stems generate potential difference close to 1 volt. This exciting result encouraged me to carry out further experiments to test the ability to generate electricity from cactus due to the following reasons: (i) the ability to grow it in any location in Jordan and worldwide, even in arid lands and deserts; (ii) its high rate of growth; (iii) the photosynthesis occurs in all its parts which makes it easy to connect the electrodes to the low parts of the cactus stem; and (iv) the dependence on citric acid production along with other acids during photosynthesis which makes it different from the lemon and potato battery or any other kind of citrus batteries.

The current research project was aimed to achieve the following objectives:

- Utilizing the cactus plant as a new renewable energy resource due to its ability to tolerate high temperatures and dry conditions which characterizes Jordan's desert climate.
- Determining the time period for lighting an LED lamp with semi-stable potential difference and current.
- Finding out the possible applications for the electricity which will be generated from cactus.

Experimental

Sample collection

Cactus plates (*Opuntia*) were collected from Kufr' Awan, Irbid district, in the Northern part of Jordan during January-March 2019. All the samples were collected from a house garden of red soil type.

Materials and Methods

Copper electrodes (stripe), magnesium electrodes (stripe), galvanized nails, cactus (*Opuntia*) plates (Figure 1), and a multimeter, 3- & 5-mm diameter LEDs were used for the experiments.

Fig 1. Cactus (*Opuntia*)

To compare the generated potential difference of cactus (*Opuntia*) pieces using different electrodes of copper, magnesium, and zinc. A cactus (*Opuntia*) plate was cut into pieces of ~ 4 × 4 cm, then a copper stripe and zinc were inserted into the cactus pieces to a distance of 2 cm; after that, the electrodes were connected to a multimeter using wires. The readings were then recorded every 5 min for 15 min. The experiment was carried out in triplicate. The above described experiment was then repeated by replacing the galvanized nail electrode with magnesium electrode.

To determine the suitable number of cactus pieces that are enough to light 3 & 5 mm LED lamps, a cactus (*Opuntia*) plate was cut into pieces of ~ 4 × 4 cm, then a copper stripe and a magnesium stripe were inserted into one cactus piece to a distance of 2 cm; after that, the electrodes were connected to light 3 & 5 mm LED lamps using wires. The same steps were repeated by changing the connected number of cactus pieces in series from 1 to 6.

To measure the potential difference for 4 pieces of cactus connected in series, a cactus plate was cut into 4 equal pieces (~ 4 × 4 cm), then copper and magnesium stripes were inserted into the cactus pieces to a distance of 2 cm (the area of the electrode is irrelevant to the generated potential difference). The four pieces of cactus were then joined together so that the copper of the first piece was connected to the magnesium stripe of the second piece. The terminal electrodes of copper and magnesium were then connected to a multimeter as in Figure 2.

Fig 2. Potential Difference Measurement for 4 Pieces of Cactus Connected in Series

To measure the potential difference for 8 pieces of cactus connected in series, a cactus plate was cut into 8 pieces of equal area (~ 4 × 4 cm), then copper strips and galvanized nails were inserted into the cactus pieces to a distance of 2 cm (the area of the electrode is irrelevant to generated potential difference). The 8 pieces of cactus were then joined together so that the copper of the first piece was connected to the magnesium stripe of the second piece. The terminal electrodes of copper and galvanized nail were then connected to a multimeter.

To determine the potential difference variations with time, a cactus plate was cut into 13 pieces of equal size (~ 4 × 4 cm), then copper and magnesium stripes were inserted into the cactus pieces to a distance of 2 cm (the area of the electrode was irrelevant to the generated potential difference). Using wires, the 13 pieces were then joined in a series so that the copper of the first piece was connected to the magnesium stripe of the second piece, then the terminal electrodes of copper and magnesium were connected to a multimeter. The potential difference variations over 40 hours were then recorded.

To determine the current variations with time, a plate of cactus was cut into 13 pieces of equal size (~ 4 × 4 cm), then copper and magnesium stripes were inserted into the cactus pieces to a distance of 2 cm (the area of the electrode was irrelevant to the generated potential difference). Using wires, the 13 pieces were then joined in a series so that the copper of the first piece was connected to the magnesium stripe of the second piece, then the terminal electrodes of copper and magnesium were connected to a multimeter and LED lamp in series. The current variations over 40 hours were then recorded.

To determine how long the LED lamp can continue to light up after 40 hours of continuous lighting, as well as determine the potential difference and current variations with time after 40 hours, a plate of cactus was cut into 6 pieces of equal size (~ 4 × 4 cm), then copper and magnesium stripes were inserted into the cactus pieces to a distance of 2 cm. Using wires, the 6 pieces were then

joined in a series, then the terminal electrodes of copper and magnesium were connected to a multimeter and LED lamp in series to record the current values. When the LED lamp was replaced with a multimeter to record the potential difference values, the LED lamp lit up for over 4 days (100 hours).

To compare the generated potential difference of cactus (*Opuntia*) plates directly from the tree, different electrodes of copper, magnesium, and galvanized nails were used. Cactus (*Opuntia*) plates were selected to be in the middle of the branches (not new plate), then a copper stripe and a galvanized nail were inserted into the cactus pieces to a distance of 2 cm; after that, the electrodes were connected to a multimeter using wires. The readings were then recorded every 5 min for 15 min. The experiment was carried out in triplicate. The above described experiment was then repeated by replacing the galvanized nail electrode with a magnesium electrode.

To determine the ability of using cactus (*Opuntia*) extract to generate electricity, pieces of cactus plate were squeezed to collect their extract in a dish. Then the prepared electrochemical cell, which was built by enveloping a Mg electrode with filter paper and Cu wire, was soaked in cactus extract for about two minutes to become saturated. The same procedure was carried out for another 5 cells. After that, all 6 cells were connected in series to measure the generated potential difference and current variations for a period of 6 hours.

Results and Discussion

The data collected from the cactus experiments are as the following:

Table 1 shows the effect of using different electrodes on the generated voltage values.

Table 1. The Effect of Using Different Electrodes on the Generated Voltage Values

Kind of electrodes	Voltage average of 1st trial (volt)	Voltage average of 2nd trial (volt)	Voltage average of 3rd trial (volt)
Zn/Cu	1.015	0.997	0.972
Mg/Cu	1.570	1.65	1.710

By calculating the voltage average of the (Zn/Cu) cactus cell which was 0.995 V and the voltage average of the (Mg/Cu) cactus cell which was 1.64 V. It was clear that using the Zn/Cu electrode enhanced the potential difference for one cactus electrochemical cell by 39%.

From the experiments which were carried out to determine how many pieces of cactus were needed to light 3 & 5 mm LED lamps, the results presented in Table 2 show that one piece was enough to light up the 3 mm LED lamp, whereas a minimum of two pieces of cactus were required to light up the 5 mm LED lamp. This difference refers to the LED lamp resistance which is increased with the increment of the lamp size. Beside that, the data showed that as the number of the cactus pieces increased, the voltage, the current and the LED lamp luminosity increased.

Table 2. The Correlation Between the Number of Cactus Pieces and the Generated Voltage

Cactus Pieces Number	Voltage (v)	Current (μA) of 3mm LED lamp	Current (μA) of 5mm LED lamp
1	1.57	2.5	-
2	3.03	104.5	38.5
3	4.55	160.0	110.0
4	5.91	220.0	174.2
5	7.45	260.0	207.0
6	9.10	292.0	247.0

The result from Figure 3 shows that the R^2 (Least Square Regression) fit is 0.9993, which indicates an excellent linear fit for the voltage versus number of cactus pieces. In addition, the data for the electrode set and the cactus electrolyte give a linear equation of:

$$Y = 1.503X$$

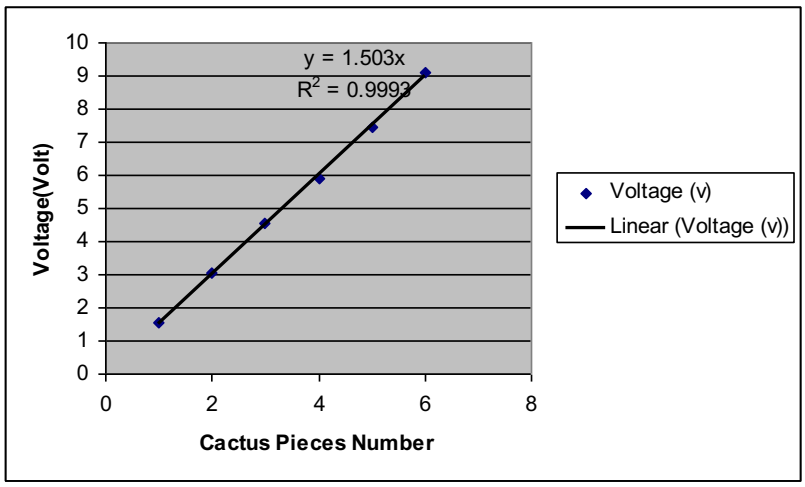

Fig 3. Standard Calibration Curve; The Cactus Pieces Number Versus the Generated Potential Difference

After connecting four cactus electrochemical cells in series using Mg/Cu electrodes, the generated potential difference was enough to light the 5 mm white LED lamp. The potential differences average during the 15-min interval are presented in Table 3

Table 3. The Potential Difference Averages for 4 Cactus Cells in Series Using Mg/Cu Electrodes

Trial No.	1st	2nd	3rd
Potential differences averages	6.73	6.02	5.71

The potential differences average for the three trials was 6.15 V. To determine the importance of using Mg/Cu electrodes, the experiment was repeated by using 8 pieces of cactus as electrochemical cells connected in series with Zn/Cu electrodes. The results obtained are shown in Table 4.

Table 4. The Potential Differences Averages for 8 Cactus Cells in Series Using Zn/Cu Electrodes

Trial No.	1st	2nd	3rd
Potential differences averages	6.73	6.81	6.73

Table 5 shows that the potential difference average for the three trials was 6.76 V. By comparing the potential difference average of 4 cactus electrochemical cells with Mg/Cu electrodes with 8 cactus electrochemical cells with Zn/Cu electrodes, it was clear that the potential difference average for the 8 cells was more than the potential difference average of 4 cells by only 0.27 V despite duplicating the number of pieces.

Table 5. The Potential Difference for 13 Pieces of Cactus Connected in Series

Time (hour)	0	7	12	14	21	25	28	36	37	40	42
Voltage (V)	19.50	18.50	18.30	18.34	18.24	18.36	17.76	17.80	18.00	17.34	7.15

To study the time period of continuously lighting an LED lamp and potential difference stability, an experiment was carried out by connecting 13 pieces of cactus in series. The collected data, as presented in Table 5 and Figure 4, showed a semi-stable potential difference for more than 40 hours, unless the magnesium stripe broke down; then, consequently, the potential difference was decreased to 7.15 V.

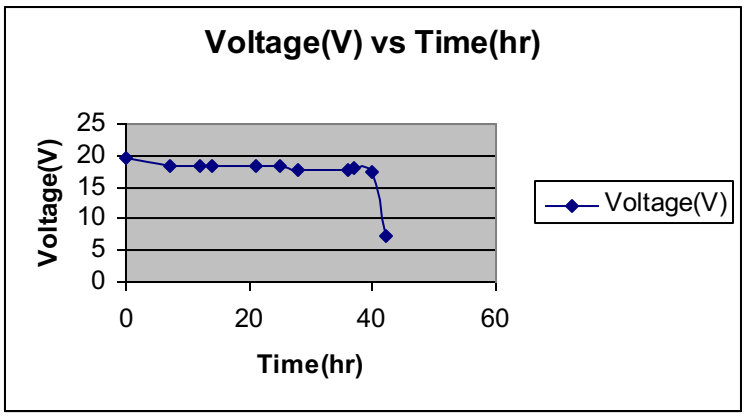

Fig 4. The Correlation Between Voltage and Time for 13 Pieces

Comparing the potential differences over the 40-hour period showed a change in the potential difference at the end of the period by only 11%. The breakdown of the magnesium stripe decreased the potential difference to 7.15 V. This problem can be resolved by using a thicker electrode, hence the lighting time period will elongate.

Figures 5 and 6 showed the correlation between potential difference and time for 6 pieces connected in series for a period of 102 hours.

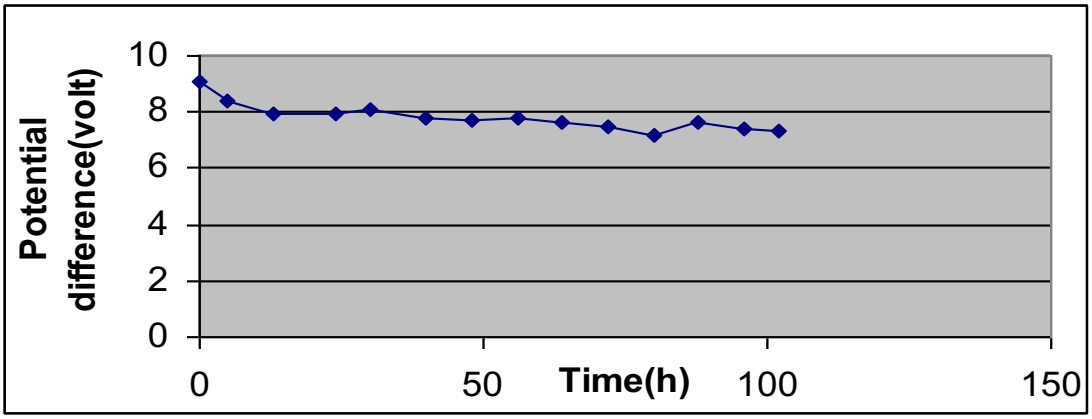

Fig 5. The Correlation Between Voltage and Time for 6 Pieces

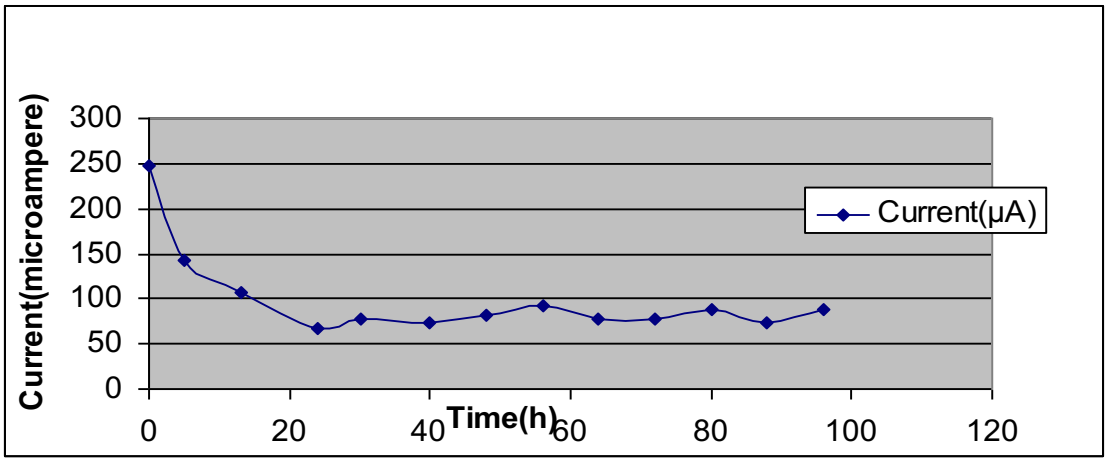

Fig 6. The Correlation Between Current and Time for 6 Pieces

This test was carried out to examine the potential difference and current stability after 40 hours, as is mentioned in Table 5, and to determine the longest period to keep the LED lamp lighting with good luminosity. The results showed that the potential difference decreased from 9.10 V at the beginning of the experiment to 7.35 after 102 hours by a decrement percentage of approximately 16%.

A modified design of cactus battery was carried out as in Figure 7. This design was able to generate electricity for a long time, more than two weeks (336 hours) with continuous LED lamp glow-up. The new design was carried out by increasing the thickness of the magnesium electrode and isolating the cutting cactus pieces into plastic bottles and connects it in series.

Fig 7. The Modified Form of the Cactus Battery by Using Two Plastic Bottles of Cactus Pieces Connected in Series by Using Mg/Cu Electrodes

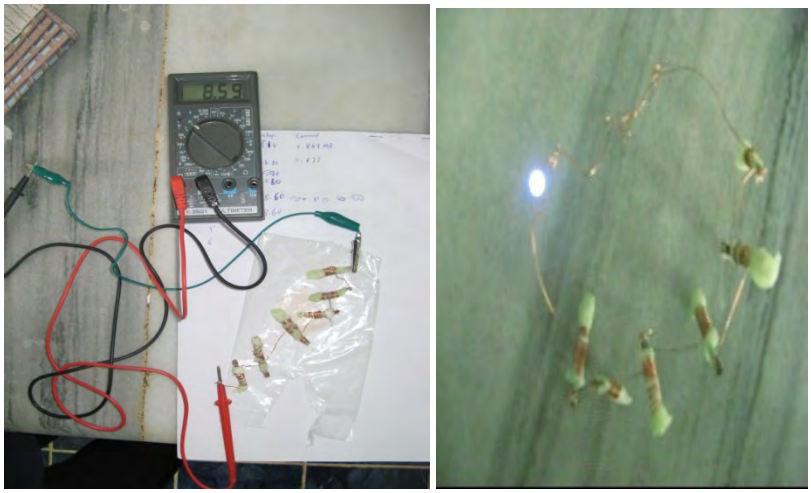

Fig 8. The Modified Form of the Cactus Extract Battery

Another well-modified cactus battery, as shown in Figure 8, can light up the LED lamp brightly.This was built from the same electrodes by using cactus extract instead of cactus plates, as is explained in the procedure. The result of this application has promising future applications like emergency lighting, desktop lighting, etc.

Table 6 shows the voltage and current variation for 6 cactus extract electrochemical cells connected in series. Potential difference average during 6 hours of onetime soaking is 8.64 V, while the current average during 6 hours of onetime soaking was 1 mA.

Table 6. Voltage and Current Variations vs. Time for 6 Cactus Extract Electrochemical Cells Connected in Series

Time(hour)	0	1	2	3	4	5	6
Voltage(volt)	8.81	8.80	8.60	8.60	8.60	8.57	8.52
Current(mA)	1.04	1.18	1.24	1.14	0.91	0.75	0.65

Conclusion

The experiment proved that using Mg/Cu electrodes instead of Zn/Cu electrodes enhanced the generated potential difference by 50%. Moreover, using these electrodes decreased the number of cactus pieces needed to generate the same potential difference by 40%. Regarding the potential difference with time, the results proved the ability to produce a semi-stable high voltage for more than 4 days, where the LED lamp luminosity was still very good. The cut cactus pieces and cactus plate extract could be viable soon due to the low cost of the raw materials, easy applicability, as well as the long-time period of glow-up together with the high current values of cactus battery extract (1 mA). The cactus plate contains substances such as citric acid which under certain circumstances act as electrolytes. The electrons flow through wires from the anode to the cathode. This process generates electricity just the same way as a voltaic battery.

References

1. Piccolino M. *Brain Res. Bull.*, 1988, 46, 381.
2. Science for Environment Policy, "Towards the Battery of the Future", Future Brief 20, Brief produced for the European Commission DG Environment by the Science Communication Unit, UWE, Bristol, 2018. http://ec.europa.eu/science-environment-policy
3. Department for Business, "Energy & Industrial Strategy", UK energy in brief, 2018.
4. Sultana J, Dola K-E, Al Mahmud S. *J. Chem., Biol. Phys. Sci*., 2018, 2, 92.
5. Shittu SA, Ajagbe SA, Oloruntola RF. Conversion of fruit battery. *Int. J. Sci. Eng. Res*., 2018, 9, 1747.

6. Gallander J, “Major Organic Acids in Fruits”, The Science Workbook: Student Research Projects in Food-Agriculture-Natural Resources, College of Agriculture, Ohio State University, 1985.
7. Lindstrom E, “The Electric Fruit”. https://www.autopenhosting.org/lemon/ElectricFruits.pdf
8. Golberg A, Rabinowitch HD, Rubinsky B. Zn/Cu-vegetative batteries, bioelectrical characterization and primary cost analyses. *J. Renewable Sustainable Energy*, 2010, 2, 1.
9. Liao CH, “World’s First Chlorophyll Organic Battery Runs on Any Liquid”, 2008. https://cleantechnica.com/2008/10/31/world-first-chlorophyll-organic-battery-runs-on-any-liquid
10. Christopher JL, Shugugan Z, Andreas M. *PloS One*, 2008, 3, 1. www.plosone.org

The Chemist
Journal of the American Institute of Chemists

Animals & The Great War: The Poisonous Cloud Casualty Statistics

Dean S. Barron

President & Senior Statistician
TwoBlueCats.com
(Email: dsb@twobluecats.com)

Abstract: Famed for trench and gas warfares, The Great War engaged 17 million animals. Horses made up 16 million; the remaining million was an admixture, primarily mules, donkeys, cats, dogs, camels, pigeons, canaries, and goldfish. In the war between the Allied Powers (England, France, Russia) and Central Powers (Germany, Austria-Hungary, Ottoman Empire, Bulgaria), animals transported goods, moused trenches, carried messages, assisted medics, were war mascots, and detected Cl-based gases. Having survived bomb and gas, the canine mascot, Rags, would warn of impending shell attacks by flopping over on his side! This research was initially inspired by Franz Marc's woodcut print, *The Birth of Horses (Geburt der Pferde)*, on exhibit at LACMA in 2018. The artist did not survive the war. Further research revealed the contemporaneous photograph, *German Soldiers and Donkey wearing gas masks* [1]. Upon subsequent research, enter Lutz Haber's opus, *The Poisonous Cloud*, which featured a typeset plot of casualties versus number of gas shells launched. After reconstructing the original data, the final regression analysis was a second order model (R^2=0.62 p-value<0.001) that eclipsed the original (R^2=0.27). This paper explores one confluence of the interrelated animals, art, history, and chemistry, thereby also illuminating the statistical model.

Key Words: Animals and The Great War, The Great War Art, gas shells casualties The Great War, animal gas masks The Great War, regression analysis, Lutz Haber Fritz Haber, chemical warfare, Spanish flu and Étaples

Introduction

The Great War

The Great War raged from 1914 to 1918 between the Allied Powers (England, France, Russia) and the Central Powers (Germany, Austria-Hungary, Ottoman Empire, Bulgaria). Additional nations entered, exited, and switched sides over the course of the war. Further, imperialist possessions, by extension and impressment, became ensnared. The war is particularly famous for featuring trench and gas warfares. Then-novel inventions employed in the war included airplanes, submarines, tanks, and machine guns.The Armistice of 11 November 1918 at 11:11 ended fighting with Germany. Word only reached German East Africa on 14 November, and, even then, the conflict continued there until confirmation was received 25 November. The Treaty of Versailles on 28 June 1919 officially ended the war. Separate armistices and treaties ended the war with Bulgaria, the Ottoman Empire, and Austria-Hungary.

Animals and Art

Artists were among the casualties of the war. *The Birth of Horses (Geburt der Pferde)*, with the primal creation of horse as expressionist Franz Marc (1880-1916) envisioned from the Book of Genesis [2,3], was on exhibit at Los Angeles County Museum of Art (LACMA), in 2018. His philosophy was to paint horses *"wie sie wirklich sind"* [as they really are], not as humans see them [4,5]. During the Great War, Marc was a cavalry messenger [6,7]; he also painted anti-aerial camouflage after Claude Monet and Wassily Kandinsky [8]. Marc was among the artists slated to be withdrawn from battle, but the order was transmitted too slowly [6]. Whilst reconnoitering on horseback at Verdun, a grenade shard fatally struck him [9,7]; his chestnut mare, Eva, survived, however [7]. *Geburt der Pferde* had been part of Marc's contribution to an illustrated Bible project that included Kandinsky, Oskar Kokoschka, Paul Klee, and others [3,7]; the collaboration was left unfinished [3].

Another artist of that era, animal sculptor, Rembrandt Bugatti (1884-1916), was also a victim. He and the animals of *Le Zoo d'Anvers / ZOO Antwerpen* [The Antwerp Zoo] were friends. Once he arranged for the zoo's two Senegalese bushbuck antelopes to be

transported to live with him in his Paris apartment. Although some also lived in the Paris zoological gardens, he bonded with these two, specifically. The pair became his muses and posed for his unique life-size bronze, *Mes Antilopes* [My Antelopes] (1908). Four months later, upon shipping the herd of two back to Anvers, he wrote that he considered them his companions and was coping with separation [10]. Truly, they were *ses antilopes* [his antelopes].

In 1914, the German-imposed *Siège d'Anvers* [Siege of Antwerp] caused food shortages, forcing the zoo to disperse or destroy the animals. Overwhelmed by depression, Rembrandt Bugatti penned this poetically-formatted enjambed entry in his notebook [11]:

"*when even my elephants forgot where to go to die.*"

Rembrandt Bugatti turned on the gas in his studio and died by suicide. *Musée D'Orsay* houses 82 of his works [12]. Posthumously, *Rearing Elephant* (1904) became the ubiquitous Bugatti Royale hood ornament selected by his brother, Ettore (1881-1947), originator of the automobile company [10].

Animals and Census, November 1918

Animals were fundamental to the Great War, especially the 16 million horses, of which only half survived [13]. Field Marshal Douglas Haig, commander of the British Expeditionary Force (BEF) asserted that with more horses, the Allies would have won faster [14]. Simultaneously, he contended that had Germany possessed more equines, they would have prevailed. Overseas horse remounts were not possible for Germany because the British dominated the seas [15].

There were other beasts of burden, 500k cats [16], and 100k dogs [17]. France raised dairy buffaloes [18]. Canaries, rabbits, and mice were carbon monoxide sensors in tunnels [19]. Goldfish tested for residue in runoff water from gas mask cleanings [20]. Pigeons, capable of carrying messages in flight at 114 miles per hour, were placed in baskets for repositioning to the front by dogs [21].

Also encountered, *en passant*, for example, in East Africa, were rhinoceroses, hippopotamuses, impalas, and giraffes. Uninvited were lice, trench mice, rats, tsetse flies, and *Anopheles* mosquitoes.

War mascots were an amalgamation of aspects of modern therapy animal, pet, and soldier. Some were rescued stray dogs and cats [22]; others were goats, kangaroos [21], lions, tigers, and bears. One mascot could be with one human, an entire regiment, or even shared by opposing sides! Famous mascots were the black bear cub, Winnie, from Winnipeg, Canada (inspiration for Winnie-the-Pooh), and dogs Rin Tin Tin, Lassie, Rags, and Sergeant Stubby.

The Escadrille Lafayette, a group of 38 American volunteer pilots within the French Service *Aéronautique* [23], acquired four-month-old lion cub,

Whiskey [24]. A year later, sensing his desire for companionship, the unit adopted a lioness cub, Soda [25]. Whiskey and Soda were the best friends of the squadron flying ace [26]! Ultimately, the pride of two was donated to the *Ménagerie du Jardin des Plantes* in Paris [24].

In 1922, the Great Britain War Office published *Statistics of the Military Effort of the British Empire During the Great War, 1914-1920*. From a limited printing of 250 copies, one extant was donated by the Estate of the late Lady Kemp to the Library of the University of Toronto, and subsequently digitized. The book presents data for both humans and animals.

Sections of the book detailed the remounts and veterinary care. In 1916, for example, the extraordinarily high horse and mule losses in East Africa peaked at 289.5%, due to the tsetse fly. Because rates represented mortality based upon the population at the start of the year, it was >100% due to remounts which continuously repopulated ongoing casualties. A 30 November 1918 census of animals totaled 791,696, cross tabulated by country and by animal species and function [27].

Gas and Gas Masks

Though modern gas warfare was first unleashed in the Great War, it had been considered a half-century earlier for the Crimean War (1853-1856). The British government solicited Michael Faraday for his opinion; he refused on moral grounds [28].

Motivated by the potential horror, both Hague Peace Conferences endeavored to ban such in war: in 1899, *"s'interdiction de l'emploi des projectiles qui ont pour but unique de répandre des gaz asphyxiants ou délétères"* [self-prohibition of the use of projectiles purely used to spread asphyxiating or deleterious gases] (Scott, 1918, p.225), and, in 1907, *"il est notamment interdit:* a. *d'employer du poison ou des armes empoisonnées"* [in particular, it is prohibited: a. use of poison or poisoned weapons] (Scott, 1918, p.116) [29].

The ambitious goal of prohibiting things not yet invented, perforce, led to loopholes, intentional or unintentional. Such apertures for treaty circumvention were exploited by a variety of strategies, such as: cofilling gas shells with high explosives (HE) so as to render the purpose non-unique, releasing non-projectile gas clouds, and selecting irritants not classified as asphyxiating or deleterious [30].

Part of the allure of gas for the Great War, perhaps, was the very nature of the trench: an open vessel awaiting filling. In August 1914, the first gas used was by France [30]: ethyl bromoacetate ($C_4H_7BrO_2$) in *fusils lance-cartouches eclairante* [gas-diffusing rifle cartridges] and *grenades suffocante* [suffocating hand grenades] [31]. The concentration of the lachrymator was intentionally kept too low to be deleterious [31]. However,

because the filling was only an estimated 19 ml per cartridge, it also rendered it ineffective and even undetected [32].

The first effective use of gas was by Germany of chlorine at the Second Battle of Ypres on 22 April 1915. Fritz Haber, the future 1918 Nobel laureate for nitrogen fixation from air, had also developed chlorine gas as a weapon: a chlorine cloud carried by wind after release from canisters. He gathered three future Nobel laureates as assistants (chemist Otto Hahn, physicists James Franck and Gustav Hertz) [33] and personally surveyed the battleground an hour after the cloud had departed [32]. Haber cited the moral defense that response to first gas use by France was permissible [33,30].

A variety of gases were deployed, often by shells, perhaps most notably chlorine (Cl_2), phosgene ($COCl_2$), and mustard ($C_4H_8Cl_2S$). Some shells contained multiple gases, with and without HE, in a variety of permutations.

Prentiss (1937, p.653) estimated total gas casualties at 1.3 million, including 91,198 deaths, dominated by 475,340 and 56k Russian, respectively [34]. This is the baseline assessment.

Post-Czarist Russia's Narkomzdrav Commissariat (НАРодный КОМиссариат ЗДРАВоохранения [People's Commissariat of Health], acronym: НАРКОМЗДРАВ [Narkomzdrav]) disputed the numbers and estimated its gas casualties to have been 90% less (40k total including 6340 deaths) [35]. Substitution into the baseline estimate gives 862k total gas casualties, including 42k deaths. The combined gas and non-gas figures recalculate to 28.1 million total casualties, including 8.3 million deaths. Gas represented 0.50% of all deaths, and nearly 5% of those gassed and symptomatic, died.

At Ypres, the German troops wore crude respirators: mouth pads bathed in sodium thiosulfate ($Na_2S_2O_3$) and taped in place [32]. Rapidly, this evolved into more sophisticated protective gas masks of increasing capability. In January 1916, the BEF issued the PH (Phenate-Hexamine) helmet, consisting of flannel immersed in a solution of phenol (C_6H_5OH), hexamine ($C_6H_{12}N_4$), caustic soda (NaOH), and glycerine ($C_3H_8O_3$) [36,48]. In May 1916 [32], a prototype was finalized of the Small Box Respirator (SBR), the best British gas mask [37]; eventually, 13 million would be issued [32].

From July 1916 until the end of the war, British animals suffered 2431 total casualties from gas, of which 211 were fatal (8.68%) [18]. The French brigade commander during the Ypres chlorine gas attack, Henri Mordacq recounted, "Soon we had to dismount, because the horses, bothered and affected by this, refused to gallop or trot" [30].

In response, a variety of horse masks were developed [18]. As reported in February 1918 [38], the new British horse respirator was an over-the-nostrils sac, soaked in the same solution as the PH helmet [36]. In effect, it had been tested on humans.

Fig 1. German Soldiers and Donkey Wearing Gas Masks During World War One
(photograph by permission of Universal History Archive \ UIG)

The comparable German model was a nosebag that covered both nose and mouth [36]. The donkey in *German Soldiers and Donkey* (Figure 1)[1] appears to be wearing a 1915 German GM-15 *Gummimaske* [rubber mask] gas mask intended for humans [39], a common practice prior to the development of animal-specific ones [40]. Note the eyepieces cover the donkey's nares.

United States patterns were disastrous, fully exhausting a merely trotting horse. Subsequent revisions also proved futile [36].

Dogs, bird carriers, and other animals also wore masks which protected against Cl_2, but, of course, failed universally against mustard [18]. Direct contact with gas residue induced blistering: lips from drinking tainted water; leg, heel, hoof, and frog (a vital anatomical area of the hoof) from treading on it [18,41]. Simply leaving a gassed area was superior to lingering to properly put the gas mask on an animal. Splitting animal groups into smaller subgroups also helped survival, as did construction of anti-bomb walls within stables [18].

The main causes of death for horses and mules were contagious diseases, exhaustion, non-gas combat wounds, accidental injuries, and respiratory diseases [18,42]. There were 2.5 million admissions of horses and mules to BEF Veterinary Hospitals and Convalescent Depots, of which 1.9 million were cured (76%) [42].

The "chief animal plague of active service" was mange, for which the British established a network of dedicated mange hospitals [43]. In some

weeks, mange infected nearly 4% of horses and 2% of mules [18]. The British opted to treat and prevent with repeated immersions in a dipping bath of calcium sulfide (CaS) [18,43]. The French preferred gaseous sulfurous acid (H_2SO_3), administered in a special stable that prevented inhalation of fumes by sealing off the body [44]. Camels were devastated with annual BEF population losses of 30% [45].

The Poisonous Cloud

The Poisonous Cloud [32], by Lutz (contraction of: LUdwig friTZ) Haber, analyzed the chemists, chemistry, weapons, casualties, deaths, political, philosophical, and other aspects of gas warfare in the Great War. (Hereafter, Haber's first names are used for clarity.)

Lutz (1921-2004) was the son of Fritz (1868–1934) and his second wife, Charlotte Nathan (1889-1979). The first wife, Clara Immerwahr (1870-1915), was the first woman to acquire a Ph.D. in chemistry in Germany. She was profoundly impacted by the specter of gas warfare and its associated animal testing [33]; she tried to dissuade Fritz [33,46]. On 02 May 1915, only days after his return from the Cl_2 cloud at Ypres, she committed suicide by shooting herself in the heart with his army pistol in their garden [47].

In 1917, Fritz married Charlotte, a club business manager, and divorced in 1927 [33]. They had two children, Eva Charlotte and Lutz. Owing to enormous cultural and professional pressures, Fritz, Clara, and Charlotte earlier had independently converted from Judaism; nonetheless, were considered Jewish by Nazi Germany. In 1933, Fritz was ordered to dismiss 12 Jewish scientists on his staff [33,48]. He refused, facilitated non-German employment for those scientists [46], submitted a delayed resignation [46], and fled to Switzerland. Fritz had already had Charlotte, Eva Charlotte, and Lutz escape to Lausanne.

In *The Poisonous Cloud*, Lutz lamented that later writers had merely echoed data from old publications without performing their own investigative research [32]. In contrast, Lutz directly accessed original papers and procured recollections from Sir Harold Hartley (1878-1972). Hartley was a surviving Great War Brigadier-General, who had headed the Chemical Warfare Department in the British Ministry of Munitions [49]. Among the documents was one which had recorded German gas shell bombardment data.

Gas Shell Casualty Statistics, September, 1918

Data Reconstruction

Gas shell bombardments and casualties surveys had been a monthly feature in the BEF report, "Hostile Gas Activity," compiled by Hartley's department, copies of which were preserved among his papers. The September 1918 data, with 55 such attacks, was plotted in *The Poisonous Cloud* (Diagram 11.1, p. 283) [32].

The horizontal axis is the number of gas shells (nshells) in the German bombardment; the vertical axis is the resultant BEF casualties (casualties). Some extreme points were listed in a text box.

Sometimes multiple bombardments had identical nshells and casualties. Each data point is represented by a dot, encircled dot, or x, corresponding to one, two, or five observations, respectively. This number (count) weighted the data. Plotted values were extracted by two methods: roller ruler and pdf coordinate measurement.

The roller ruler method, in which a roller ruler is placed on a printout of the scanned physical book copy, has the advantage of handling any non-perpendicular aspects by generating parallel lines that intersect an axis. However, reading that intersection requires interpolation which introduces inaccuracy.

The pdf method, in which the coordinates of each data point are directly read from an open pdf file, has the advantage of inherent precision. Such a pdf is either a scanned copy of the physical book or the publisher released digital version; both require a good original page. For unknown reasons, the published digital graph was slightly rotated or distorted.

The recorded values were from roller ruler, pdf scan, and pdf digital publication; the reconstructed value was defined as the mean of the three. Frequently, a coordinate measurement was exact because the point fell precisely on a grid mark. This occurred for 76% (42/55) of the observations (29 nshells only, 13 both nshells and casualties).

Data Quality Control (QC)

Quality control (QC) included frequency distributions, descriptive statistics, and examination for typographical errors. Upon review, two errors in the original data were discovered, with reconstructed data then remediated as indicated.

First, the minimum casualty: nshells ratio was given as 1:5. In fact, the minimum was 1:5 for nshells ≥1000, but about 1:1 for nshells<1000. This is information is interesting for partitioning (discussed later) but required no emendations.

Second, although N=55 for the September 1918 bombardments, a tally revealed that only 54 appeared in the diagram! The graph combined with the inset textbox totaled the reported 52 nonzero observations, but only two zeros; one zero is missing. Given the careful assignment of point markers, it seems more likely that a point is missing, rather than an encircled dot incorrectly rendered as a dot. Because zero casualties is most likely associated with the smallest possible nshells, the missing point is assigned the value of nshells=100. This is consistent with the original regression (to be introduced as equation 0 [EQN00]) and that 83.3% of the non-missing observations (45/54) are multiples of 100. Zero nshells would not have been a bombardment, at all.

Two additional reconstructed data observations were edited. The book summary table indicated that the nshells to casualty ratio was bimodal for 10 and 20, but pre-QC reconstructed data were unequal (n=7 and n=5). Two observations were extremely close to ratio=20; adjusting those coordinates by <3% each aligned the modes.

Reproducing the Haber Regression

$$\text{casualties} = 49.9 + .02919 * \text{nshells} \qquad \text{(EQN00)} \quad (0)$$

Lutz fit the original data with a first-order linear regression model (equation 0 [EQN00]), hereafter referred to as regrHABER, Figure 2, Table 1) (N=55, R^2=0.27). Correlation between casualties and nshells was 0.533.

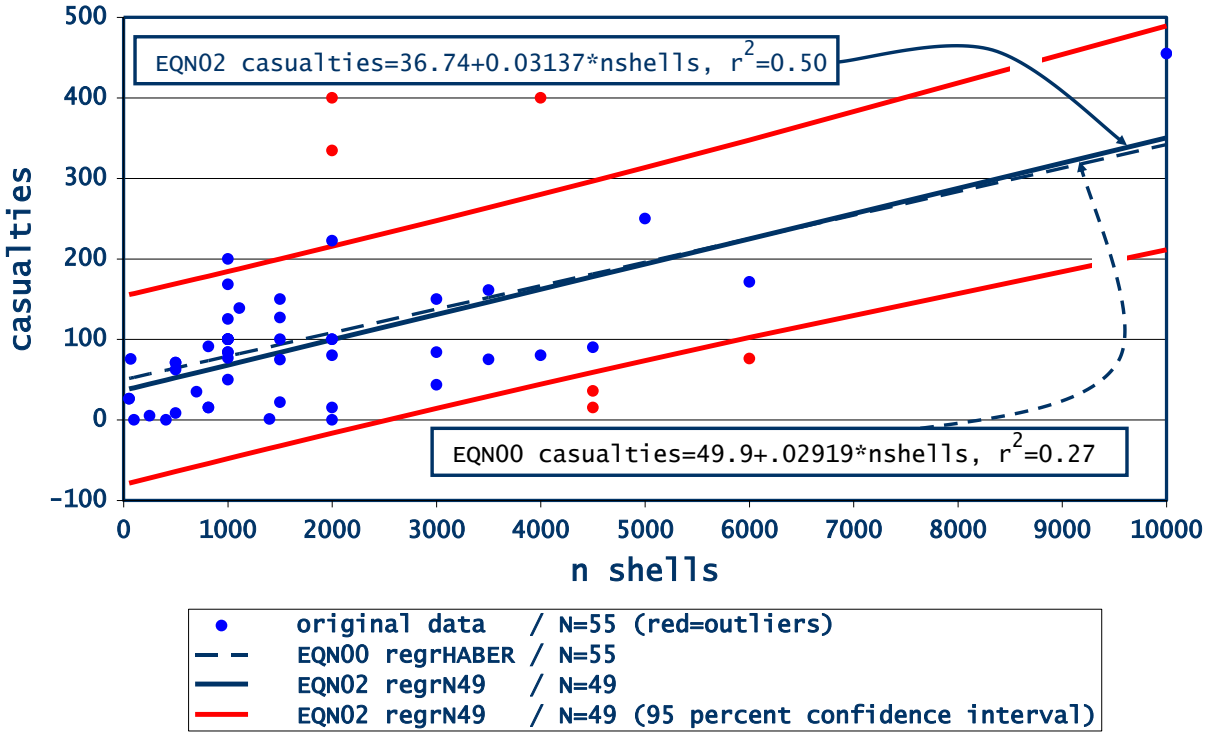

Fig 2. Casualties v. Nshells in Bombardment, Weighted by Count

This plot shows the original data from *The Poisonous Cloud* and original regression (EQN00, regrHABER), first order regression after removing outliers (EQN02, regrN49), and EQN02 95% confidence interval. EQN01 (regrN55REPRO) is nearly superimposable over EQN00 and EQN02, and therefore not shown.

Though not published, the F-statistic and p-value are facilely derivable as $F=18.83$ and $p<0.001$, as calculated from the N and R^2. The $R^2=0.27$ value is interpreted as explaining 27% of behavior. The positive value of the nshells coefficient reflects the positive correlation with casualties, confirming the addition of the nshells=100 casualties=0 value appended in QC (see above).

Table 1. Summary of Regression Models

EQN	MODEL NAME	REGRESSION MODEL	N	R^2	F-value	*p*-value
00	regrHABER	casualties=49.9+.02919*nshells	55	0.27	18.83*	<0.001*
01	regrN55REPRO	casualties=51.668+.02675*nshells	55	0.244	17.146	<0.001
02	regrN49	casualties=36.736+0.0314*nshells	49	0.496	46.301	<0.001
03	regrRATIO	ratiox100=3.678+3108.759*nshells^{-1}	49	0.556	61.006	<0.001
04	regrFINAL	casualties= 84.221+(3.455x10^{-6})*nshells^2+ D*(-49.196) where, D=1, if nshells<1000; D=0, otherwise	49	0.619	37.408	<0.001

***Note.** Value derived; not published in *The Poisonous Cloud*

Using the reconstructed data, the analogous reproduced regression model is quite similar (equation 1 [EQN01], regrN55REPRO, no figure, Table 1) (N=55, R^2=0.244 F=17.146 p<0.001).

(EQN01) casualties=51.668+.027*nshells (1)

Both coefficients of EQN00 lie within the 95% confident intervals (95% CI) for those of EQN01. Correlation is 0.4944, within 10% of published. These similarities are consistent with a sufficiently accurate data reconstruction.

Outliers

Lutz concluded that the data was deficient. The independent variable, nshells, was the tally of the number of newly created shell craters by day, or bursts spotted by night; hence, both imprecise and inconsistent. Consequently, it is especially important to identify any outliers for possible removal.

(EQN02) casualties=36.736+0.0314*nshells (2)

The confidence interval bands from EQN01 were examined for outliers. Not visually obvious, six such observations were conspicuous relative to the 95% CI. After removing them, a first-order linear regression analysis was performed on the reduced dataset (equation 2 [EQN02], regrN49, Figure 2, Table 1) (N=49, R^2=0.496 F=46.301 p<0.001). The six outliers fall outside the 95% CI from

EQN02, validating their removal. The correlation coefficient rises by nearly half to 0.7044.

Casualties to Shells Ratio

The Poisonous Cloud provided some descriptive statistics for the ratio, nshells to casualties. This measure automatically reduced N by three, to 52 from 55, having removed those undefined due to zero casualties in the denominator. Using the reconstructed data, mean=58.10 is not statistically different from the published mean=54 (t=0.151, p-value=0.880). If Lutz had incorrectly used N=55, then the mean would have been 57.11 with N=52.

However, the inverse ratio, nshells to casualties, does not suffer from such limitation. All bombardments have some positive number of shells in the denominator.

For numerical ease, ratiox100 is defined as nshells/casualties multiplied by 100. After removal of outliers, $mean_{ratiox100}$=10.27 (stddev=17.42, N=49). Additional insights are gained by performing regression analysis on ratiox100 as a function of nshells. The best fit is a linear model with $nshells^{-1}$ (equation 3 [EQN03], regrRATIO, Figure 3, Table 1) (N=49, R^2=0.556 F=61.006 p<0.001).

$$\text{(EQN03)} \qquad ratiox100 = 3.68 + 3108.76 * nshells^{-1} \qquad (3)$$

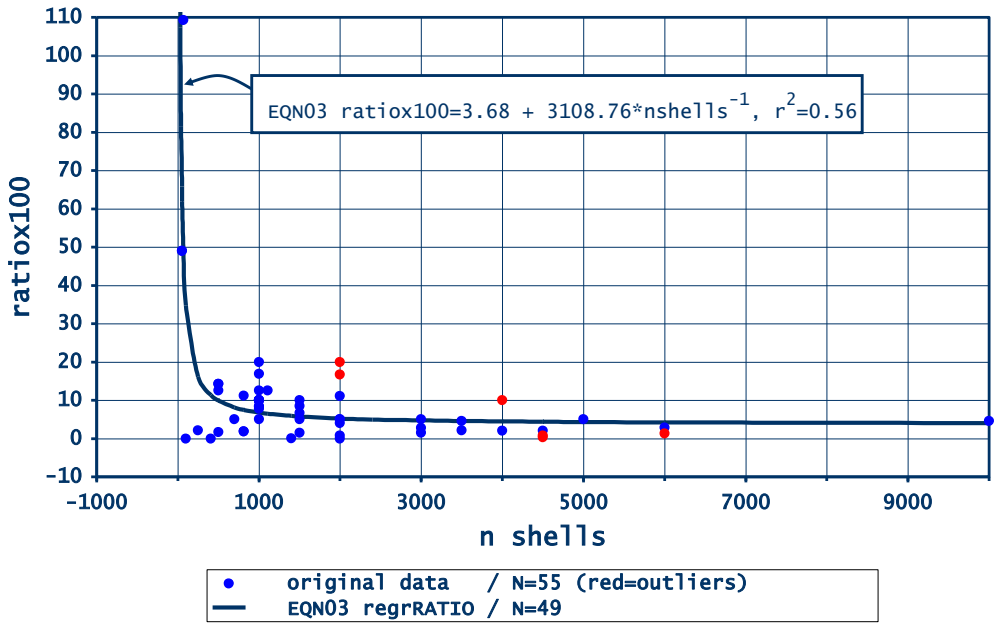

Fig 3. Ratiox100 v Nshells in Bombardment, Weighted by Count
This plot shows the original data and inverse regression (EQN03, regrRATIO). Negative minimum axis values allow viewing at and near 0.

Over the observed nshells values, the difference between the maximum predicted ratiox100, ratiox100$_{max,pred}$ of 61.84 (at nshells$_{min}$=53.45) and ratiox100$_{min,pred}$=3.99 (at nshells$_{max}$=10000), gives a range of 57.86. It is useful to determine the value of nshells for which ratiox100 fell by 95% of this range, a drop of 54.96 (.95x57.86) to 6.88 (61.84-57.86). From EQN03, nshells=970.38 when ratiox100=6.88. The 5% remaining change in ratiox100 for nshells values to 10000 is small enough to consider as essentially constant.

Therefore, partitioning for nshells<1000 is possible. The mean ratio for the nshells<1000 group is 2.94x that of the nshells≥1000 group (Kolmogoroff-Smirnoff KS=0.3857, 1-sided p-value=0.032). The minimum ratios for each group also differ (see above). On this basis, the dummy variable, D, is defined as D=1 for nshells<1000, and D=0 otherwise.

Final Regression

To determine the best regression, models were considered with transformations of both the independent and dependent variables: higher order powers, inverse, logarithmic, and exponentials. Additionally, the possibility of two entirely different models for each side of the nshells=1000 partition was reviewed but rejected. The final model is second-order and includes the dummy variable (equation 4 [EQN04], regrFINAL, Figure 4, Table 1) (N=49, R^2=0.619 where, D=1, if nshells<1000; D=0, otherwise F=37.408 p<0.001).

$$\text{(EQN04)} \quad \text{casualties} = 84.221 + (3.455 \times 10^{-6}) * \text{nshells}^2 + D * (-49.196) \quad (4)$$

The model has two limits at the partition of nshells=1000: approaching from <1000 equals 38.48; from >1000, 87.68. The R^2=0.619 corresponds to the model explaining 61.9% of behavior.

Discussion & Conclusions

Animals

Total combined casualties, animal and human, gas and non-gas, all belligerents, exceeded 36 million in the Great War. An astonishing 20% of the worldwide equine population, 16 million of an estimated 79.25 million [18], was subjugated into service. In the aftermath, there were some positive developments, including the stoppage of scientists and artists placed in direct combat, renewed

attempts to ban chemical warfare, and the rise of animal rights.

At the outset of the war, the Royal Society for the Prevention of Cruelty to Animals (RSPCA) offered its services to the British War Office and was rejected. Unfazed, the RSPCA contributed horse ambulances, saddle pad knitters, and 90 inspectors. Soon thereafter, the existent BEF Army Veterinary Corps proved inadequate and the rejection was retracted. Thus started a comprehensive partnership that lasted even after the war [15]. Of note, socially and politically, women's suffrage and animal rights were often coupled, to the advancement of both [50].

Efforts were made to control populations of unwelcome animals. *Blausäure* (hydrogen cyanide, HCN) was effective, though dangerous, for controlling rodent populations in trenches, flour mills, and railroad cars [48,51]. France even tried to use HCN as a weapon, though unsuccessfully. Fritz Haber led the German anti-rodent research and, after the war, transferred *Blausäure* activities to *DEutsche GEsellschaft für SCHädlingsbekämpfung* [German Society for Pest Control, acronym: Degesch]. Degesh then developed HCN-based Zyklon and Zyklon B [51]. In the Holocaust, Zyklon B was used to murder millions of Jews. "Members of Fritz Haber's extended family, children of his sisters and cousins, were hauled to those camps and killed, poisoned by the fruit of their famous relative's research" [33]. The sisters of Sigmund Freud and Franz Kafka also met their fate in the gas chambers. Once again, international bans on poisonous gases proved ineffective.

From Fritz to Lutz

After Fritz fled Nazi Germany, he met with chemist and future first president of Israel, Chaim Weizmann, and discussed research and Zionism. Weizmann was founding The Daniel Sieff Institute in Rehovot in Mandatory Palestine (now, Weizmann Institute of Science in Rehovot, Israel). Fritz envisaged pensively, telling Weizmann, "When I am gone and forgotten your work will stand, a shining monument, in the long history of our people." Weizmann offered him a position with assurance of "peace and honor. It will be a return home for you - your journey's end," which Fritz "accepted with enthusiasm" [52]. This was not to be; en route Fritz suffered a fatal heart attack [46]. However, his books did make it there; the bequest became the Institute's first library [53,54,46]. Albert Einstein, a great friend since before the Great War, wrote in later correspondence: "It was the tragedy of the German Jew: the tragedy of unrequited love" [33].

A protest banner at a 1968 commemoration of Fritz's birth centennial read: *"Feier für einen Mörder/Haber = Vater des Gaskriegs"* [Celebration for a Murderer/Haber = Father of Gas Warfare]. Lutz was in attendance and, in time, took the incident to heart. He expanded his visits with Sir

Harold Hartley, who by 1970 was living in a nursing home, sharp though fatigued. The collaboration was foundational to *The Poisonous Cloud* [32].

Gas Shell Bombardment Data

Summary statistics reveal the underlying reality: 4484 casualties, 85,583 gas shells - a rate of one casualty per 19 gas shells. The estimated gas mortality rate for 1918 was 2.37% [32], which computes to 106 expected deaths. This is close to one published actual value of 116 for September 1918 [55].

There were data shortcomings alluded to in *The Poisonous Cloud*. The dependent variable, number of casualties, was recorded at Regimental Aid Posts, which were located as close to the front lines as possible, some of which were associated with a Chemical Warfare Section [56]. Patients were counted by virtue of having been medically treated there, but this system excluded gassed combatants killed at the front or captured prisoner. In contrast, equine gas deaths were accurately counted because the horseman documented the cause of death, even those at the front [57]. It does appear, though, that gassed horse-rider duos captured together would not have been counted.

The data recorded only the larger bombardments, however the cutoff was lost. Some important data pertaining to individual bombardments was missing: exact shell contents, rate and duration of fire, and expanse and combatant population of target [32]. Other additional variables that would have enhanced the statistical analysis pertain to gas mask efficacy, supply-chain of gas shells, and Spanish flu.

Mask and anti-gas training reduced the anxiety responsible for the mask removal that created hapless, maskless victims. Prior gas encounters also reduced casualties [58]. Additionally, inadequate human diets caused weight loss, which compromised the seal of the mask, allowing gas to enter [37].

The SBR was an assemblage of 195 parts from over 160 manufacturers [32]! Despite well-orchestrated QC [32], two studies cited by Cook (1998) found failure rates of 25% (N=1082) and 26% (N not cited), respectively [37]. Germany reported 11.5% (N=839) of their masks failed in a survey conducted after the wind reversed direction, turning their chlorine cloud against themselves [59]. Several variables would improve analysis: mask failure rates for BEF and Germany, training, experience, and diet.

The Air Service, American Expeditionary Forces conducted air raids of German railroads and chemical manufacturers. Cl_2 and phosgene manufacturer *Badische Anilin und Sodafabrik* (BASF) was bombed twice in September 1918 [60,61]. Unperturbed availability of gas and materiel to the front would have improved attacks; thus, some measure of supply flow would be useful.

The Spanish flu, first observed in January 1918 [62], was acknowledged on the battlefield as early as May 1918. At the front, it was then considered possibly related to gas mortality [55], and also seems a probable concomitant factor for morbidity. Therefore, variables with Spanish flu incidence, prevalence, and severity would be beneficial for analysis.

Étaples, France was the BEF central depot for humans, horses, and equipment; over 300 trains and 100k combatants traversed daily. En route to the front were fresh draftees, remounts, and arms [63]; returning from the front for reassignment were casualties and survivors of ravaged battalions [63,64]. Approximately 20 hospitals with 22k beds treated up to 40k humans per month [63]; the Neufchatel Veterinary Hospital, with a 1700 animal capacity [65], treated 23k horses, total [66]. Pigs, ducks, geese, and chickens lived in Étaples [67]. Overarching were gas warfare and contamination, including known mutagen, mustard [67]. In 1918, one Canadian newspaper report that "hospitals were drenched with enemy gas," obfuscated the exact location due to wartime censorship; however, the description matched Étaples [68]. Humans were malnourished and overcrowded, *"comme des sardines"* [like sardines] [63], and a landfill graced the base. Wilfred Owens, the British war poet killed in the Great War just one week before the Armistice, wrote of "a vast, dreadful encampment," where human faces were "without expression, like a dead rabbit's" [69]. These adverse conditions were ideal for formation of a reassortant virus within the porcines [67]. Transmission from pigs was likely assisted by continuously present mallard ducks, whose migration was altered by a 1914-1919 climate aberration of torrential rains and cold [70]. Peace, with its ensuing repatriation, facilitated spread of the Spanish flu [67].

A century later, zoonoses continue to plague the world. As with Étaples, pigs, birds, horses, and live animal markets are implicated [71,72]. Generally, viral transmission occurs in sequence: natural host animal, intermediate host animal, human [72]. The pre-human pathways appear to be: COVID-19 (Coronavirus (COV) Disease 2019, virus SARS-CoV-2), horseshoe bat to pangolin; SARS (Severe Acute Respiratory Syndrome, SARS-CoV), horseshoe bat to raccoon dog and masked palm civet; MERS (Middle East Respiratory Syndrome, MERS-CoV), Egyptian cave bat to dromedary camel [72].

Swine flu in pigs (influenza A virus subtype H1N1) appeared shortly after Spanish flu (H1N1) was first described with similar symptoms and mortality [73,71]. Swine flu in humans (H1N1) also appears to have descended from Spanish flu [73] via a cycle of pigs, birds, and farm animals [74].

Regression Analysis

The mean ratiox100 for nshells<1000 was triple that for nshells≥1000. The corresponding dummy variable, D, was statistically significant in the final regression (EQN04, regrFINAL, Figure 4). Such a partition could reflect fundamentals.

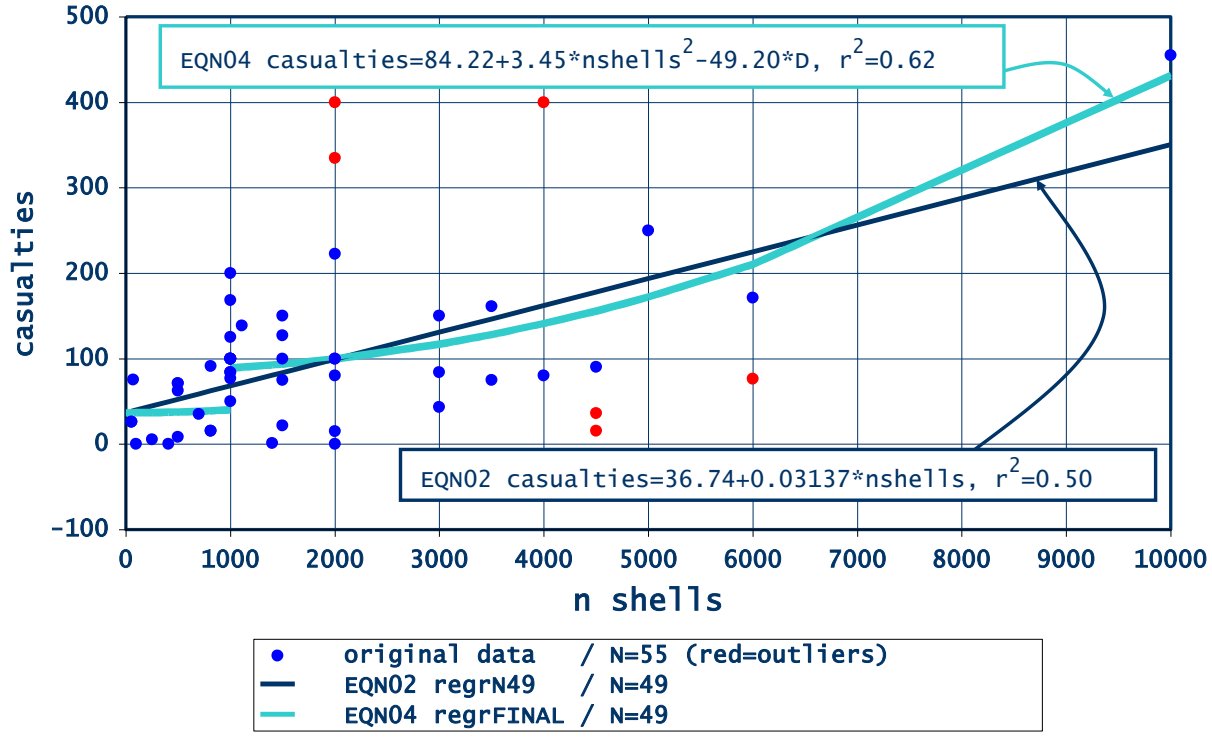

Fig 4. Casualties v Nshells in Bombardment, Weighted by Count
This plot shows the original data and final second order linear regression model with dummy variable, D (EQN04, regrFINAL).

One explanation is that the lower part corresponds to direct hits on a small concentrated group, whilst the upper part corresponds to an unlimited supply of gas shells. There should be a limit of primary casualties equal to the population in the targeted zone, but that data is unavailable.

The Poisonous Cloud concluded that "the explanatory value of the number of shells as a cause of casualties is relatively low," apparently based upon the low R^2=0.27 of the original model (EQN00, regrHABER, Figure 1, Table 1) and suboptimal data quality. The new final model (EQN04, regrFINAL, Figure 3, Table 1) benefits from removal of outliers, a second-order term for nshells, and the dummy variable. The final regression explains 61.9% of the behavior of casualties as a function of number of shells in a bombardment, more than twice the original.

References

1. German Soldiers and Donkey Wearing Gas Masks During World War One [Photograph], Universal History Archive \ UIG, 1915.
2. Marc F, The Birth of Horses (Geburt der Pferde) [Woodcut print], Los Angeles County Museum of Art, Los Angeles, CA, United States, 1913. Woodcut printed in black, red, rose, and green on Japan paper. Image: 8 1/2 x 5 3/4 in. (21.5 x 14.6 cm); Sheet: 13 1/2 x 9 7/8 in. (34.3 x 25.1 cm). The Robert Gore Rifkind Center for German Expressionist Studies (M.82.288.204)
3. Placard for The Birth of Horses (Geburt der Pferde) at Fantasies and Fairy Tales [Exhibition], Los Angeles County Museum of Art, Los Angeles, CA, United States, 2018-2019. https://www.lacma.org/art/exhibition/fantasies-and-fairy-tales
4. Marc F, Lankheit K in Schriften, DuMont, Köln, 1978.
5. Pollmann I in The Interweaving of World and Self: Transformations of Mood in Expressionist and Kammerspiel Film, Amsterdam University Press, Amsterdam, 2018, In Cinematic Vitalism, pp 163-206. doi:10.2307/j.ctv5nph05.7
6. Marc F, Tale of Creation - Genesis II, Joy of Museums Virtual Tours. https://joyofmuseums.com/museums/united-states-of-america/san-francisco-museums/san-francisco-museum-of-modern-art/tale-of-creation-by-franz-marc/
7. Roßbeck B in Franz Marc: Die Träume und das Leben - Biographie, Siedler Verlag, 2015.
8. Newark T in Camouflage, Thames & Hudson, London, 2007.
9. Simmons W. Abstraction and Empathy on the Eve of World War I. *Konturen*, 2013, 5, 3-30. doi:http://dx.doi.org/10.5399/uo/konturen.5.0.3246
10. Horswell E in Rembrandt Bugatti: Life in Sculpture, Sladmore Gallery Editions, London, 2004.
11. Murray GE in Arts of a Cold Sun - Poems, University of Illinois Press, 2003, “Bugatti's Zoo”, pp 25–26. JSTOR, www.jstor.org/stable/10.5406/j.ctt2ttcw4.20. Accessed 17 Sept. 2020.
12. Musée d'Orsay, Collections catalogue - search results, n.d. Retrieved November 9, 2020, from https://www.musee-orsay.fr/en/collections/index-of-works/resultat-collection.html?no_cache=1&zsz=1&zs_r_2_z=3&zs_r_2_w=Bugatti%2C%20Rembrandt&zs_ah=oeuvre&zs_rf=mos_a&zs_mf=21&zs_sf=0&zs_send_x=1&zs_liste_only=1.
13. Bernstein J, Ph.D. Dissertation, Where Beasts’ Spirits Wail: The Great War and Animal Rights, University of Southern California (Literature and Creative Writing), 2014.
14. Singleton J, Britain's Military Use of Horses 1914-1918, *Past & Present*, 1993, 139(1), 178-203.
15. Cooper J in Animals in War, Corgi, London, 2000.
16. Roberts P, Cats in Wartime, 2006. http://www.purr-n-fur.org.uk/featuring/war01.html
17. Suriano MG, Animals in the Great War, Associazione culturale Se, case studies|Se, 2017. https://associazioneculturalese.com/case-studies/gli-animali-nella-grande-guerra/
18. Moore J in Army Veterinary Service in War, Brown, London, 1921.
19. Turner A in Messines, 1917: The Zenith of Siege Warfare, Osprey Publishing, Oxford, 2010.
20. National Geographic, WORLD WAR 1 FACTS, National Geographic Kids, n.d. https://www.natgeokids.com/uk/discover/history/general-history/first-world-war/
21. Bulanda S in Soldiers in Fur and Feathers: The Animals That Served in World War I - Allied Forces, Alpine Publications, Crawford, CO, 2014.
22. Schäfer ED, “Animals, Use of”, in The European Powers in the First World War: An

Encyclopedia, eds. Spencer Tucker, Laura Matysek Wood, Justin D. Murphy, 1996, pp 52-54.
23. Miller RG, Like a Thunderbolt: The Lafayette Escadrille and the Advent of American Pursuit in World War I, Air Force History and Museums Program, Washington, D.C, 2007.
24. Guttman J in SPA 124 Lafayette Escadrille: American Volunteer Airmen in World War I, Osprey Publishing, Oxford, 2004.
25. Flood CB in First to Fly: The Story of the Lafayette Escadrille, the American Heroes Who Flew for France in World War I, Grove Press, 2016.
26. Jablonski E in Warriors with Wings: The Story of the Lafayette Escadrille, Bobbs-Merrill, Indianapolis, 1966.
27. Great Britain, Statistics of the Military Effort of the British Empire During the Great War: 1914-1920, H.M. Stationery Office, London, U.K., 1922.
28. Croddy E, Perez-Armendariz C, Hart J in Chemical and Biological Warfare: A Comprehensive Survey for the Concerned Citizen. Springer New York, New York, NY, 2002.
29. Carnegie Endowment for International Peace, & International Peace Conference in Conférence Internationale de la Paix, 1899, Les Conventions et Déclarations de La Haye de 1899 et 1907, ed. J. B. Scott, Oxford University Press, New York etc, 1918.
30. One Hundred Years of Chemical Warfare: Research, Deployment, Consequences, eds. Bretislav Friedrich, Dieter Hoffmann, Jürgen Renn, Florian Schmaltz, Martin Wolf, Springer, 2017.
31. Trumpener U. The Road to Ypres: The Beginnings of Gas Warfare in World War I. *J. Mod. Hist.*, 1975, 47(3), 460-480. Retrieved August 26, 2020, from http://www.jstor.org/stable/1876002.
32. Haber LF in The Poisonous Cloud: Chemical Warfare in the First World War, Clarendon Press, Oxford [Oxfordshire], 1986, Appendix: A Statistical Note on Gas Shells and Casualties in the BEF, pp 283-284, and see generally.
33. Charles D in Master Mind: The Rise and Fall of Fritz Haber, the Nobel Laureate Who Launched the Age of Chemical Warfare, Ecco, New York, 2005.
34. Prentiss AM, Fisher GJB in Chemicals in War: A Treatise on Chemical Warfare, McGraw-Hill Book Co, New York, 1937.
35. Kohn S, Meyendorff, A in The Cost of the War to Russia: The Vital Statistics of European Russia During the World War 1914-1917, Yale University Press, New Haven, 1932.
36. Moore W in Gas Attack!: Chemical Warfare 1915-18 and Afterwards, Cooper, London, 1987.
37. Cook T. Through Clouded Eyes: Gas Masks and the Canadian Corps in the First World War. *Mater. Hist. Rev*., 1998, (47), 4-18.
38. Gas Masks for the War's Horses. *Sci. Am.*, 1918, 118(5), 103-103.Retrieved September 18, 2020, from http://www.jstor.org/stable/26024062.
39. Catfish. The GM-15 (Gummimaske) 1916. Germany's First WWI Gas Mask. - Civilian Military Intelligence Group [Blog post], 2017, July 18. Retrieved from https://civilianmilitaryintelligencegroup.com/23088/gm-15-gummimaske-1916-germanys-firt-wwi-gas-mask.
40. War Is Boring. Chemical Warfare Hell: Even Horses Needed Gas Masks During World War I [Blog post], 2019, April 2. Retrieved from https://nationalinterest.org/blog/buzz/chemical-warfare-hell-even-horses-needed-gas-masks-during-world-war-i-50232.
41. United States, Bancroft WD, Bradley HC, Eyster JAE, Gilchrist HL, Goldschmidt SA, Hanzlik PJ, ... Wilson DW in The Medical Department of the U.S. Army in the World War, G.P.O., Washington, 1926, vol XIV.
42. Blenkinsop LJ, Rainey JW in Veterinary Services, H.M. Stationery Office, London, U.K., 1925.

43. Smith F. THE WORK OF THE BRITISH ARMY VETERINARY CORPS AT THE FRONTS. *J. R. Soc. Arts*, 1918, 67(3449), 80-92. Retrieved September 18, 2020, from http://www.jstor.org/stable/41347860.
44. Moore L in Animals in the Great War: rare photographs from wartime archives, Pen & Sword Military, Barnsley, U.K., 2017.
45. Pirie-Gordon H, Allenby EHHA in A Brief Record of the Advance of the Egyptian Expeditionary Force Under the Command of General Sir Edmund H. H. Allenby, G. C. B., G. C. M. G., July 1917 to October 1918, H.M. Stationery Office, London, U.K., 1929.
46. Goran M in The Story of Fritz Haber, University of Oklahoma Press, Norman, 1967.
47. King G. Fritz Haber's Experiments in Life and Death. *Smithsonian Magazine*, June 6, 2012. https://www.smithsonianmag.com/history/fritz-habers-experiments-in-life-and-death-114161301/
48. Freemantle M in The Chemists' War: 1914-1918, Royal Society of Chemistry, Cambridge, 2015.
49. Ogston AG. Harold Brewer Hartley, 1878-1972. *Biogr. Mem. Fellows R. Soc.*, 1973, 19, 349-373.
50. Kean H in Animal Rights: Political and Social Change in Britain Since 1800, Reaktion Books, London, 1998.
51. Hayes P in From Cooperation to Complicity: Degussa in the Third Reich, Cambridge University Press, Cambridge, U.K., 2005.
52. Weizmann C in Trial and Error: The Autobiography of Chaim Weizmann, Harper, New York, 1949.
53. Weizmann Institute of Science, Library. Haber Collection, 2020 October 15. https://weizmann.primo.exlibrisgroup.com/discovery/collectionDiscovery?vid=972WIS_INST:972WIS_V1&collectionId=8123966930003596
54. Dunner, J in The Republic of Israel, Its History and Its Promise, Whittlesey House, New York, 1950.
55. MacPherson WG, Balfour A, Elliott TR, Herringham WP, Macpherson WG in Medical Services: Diseases of the War, H.M.S.O, London, 1923, vol 2.
56. Vedder EB in The Medical Aspects of Chemical Warfare: with a Chapter on the Naval Medical Aspects of Chemical Warfare, Williams & Wilkins, Baltimore, 1925.
57. Van der Kloot W. April 1915: Five Future Nobel Prize-Winners Inaugurate Weapons of Mass Destruction and the Academic-Industrial-Military Complex. *Notes Rec. R. Soc. London*, 2004, 58(2), 149-160. Retrieved September 1, 2020, from http://www.jstor.org/stable/4142047.
58. Jones E. Terror Weapons: The British Experience of Gas and Its Treatment in the First World War. *War Hist*ory, 2014, 21(3), 355–375. JSTOR, www.jstor.org/stable/26098580. Accessed 11 Nov. 2020.
59. Foulkes CH in Gas!: The Story of the Special Brigade, Naval & Military Press, East Sussex, 2012.
60. Maurer M in The U.S. Air Service in World War I, Albert F. Simpson Historical Research Center, Maxwell AFB, Ala., 1978, vol 4.
61. BASF, Toxic Gas Production During World War I, n.d. https://www.basf.com/global/en/who-we-are/history/chronology/1902-1924/1914-1918/giftgasproduktion-im-ersten-weltkrieg.html
62. Barry JM. The Site of Origin of the 1918 Influenza Pandemic and Its Public Health Implications. *J. Transl. Med.*, 2004, 2, 3. https://doi.org/10.1186/1479-5876-2-3
63. Office de Tourisme d'Étaples-sur-mer, Sur le chemin de la Première Guerre, 2015.

https://www.tourisme-etaples.com/wp-content/uploads/2015/12/On-the-path-of-the-First-World-War.pdf
64. Gill D, Dallas G. Mutiny at Etaples Base in 1917. *Past & Present*, 1975, (69), 88-112. Retrieved October 18, 2020, from http://www.jstor.org/stable/650297.
65. Krenzelok G, THE ARMY VETERINARY SERVICE DURING THE GREAT WAR, WW1, n.d. rootsweb. http://freepages.rootsweb.com/~gregkrenzelok/genealogy/veterinary%20corp%20in%20ww1/veterinary%20corp%20in%20ww1.html
66. Krenzelok G. (n.d.). U.S. VETERINARY HOSPITAL NO. 6 NEUFCHATEAU, FRANCE WW1. rootsweb. http://freepages.rootsweb.com/~gregkrenzelok/genealogy/veterinary%20corp%20in%20ww1/vchospno6franceww1.html
67. Oxford JS, Lambkin R, Sefton A, Daniels R, Elliot A, Brown R, Gill D. A Hypothesis: The Conjunction of Soldiers, Gas, Pigs, Ducks, Geese and Horses in Northern France During the Great War Provided the Conditions for the Emergence of the "Spanish" Influenza Pandemic of 1918-1919. *Vaccine*, 2005, 23(7), 940-945. ISSN 0264-410X, https://doi.org/10.1016/j.vaccine.2004.06.035.
68. Canadian Great War Project, Extracts from the News, "Canadian Nurses Heroic Under Fire," Crag & Canyon [Banff, Alberta], Saturday, July 13, 1918, transcribed by: M. I. Pirie. http://canadiangreatwarproject.com/transcripts/transcriptDisplay.asp?Type=N&Id=815
69. Owen W, Owen H, Bell J in Collected Letters, Oxford University Press, London, 1967, pp 520-521.
70. More AF, Loveluck, CP, Clifford H, Handley MJ, Korotkikh EV, Kurbatov AV, et al. The Impact of a Six-Year Climate Anomaly on the "Spanish Flu" Pandemic and WWI. *GeoHealth*, 2020, 4(9), e2020GH000277. https://doi.org/10.1029/2020GH000277
71. Brown IH. The Epidemiology and Evolution of Influenza Viruses in Pigs. *Vet Microbiol*., 2000, 74(1-2), 29-46. doi: 10.1016/s0378-1135(00)00164-4. PMID: 10799776.
72. Ye ZW, Yuan S, Yuen KS, Fung SY, Chan CP, Jin DY. Zoonotic Origins of Human Coronaviruses. *Int. J. Biol. Sci.*, 2020, 16(10), 1686–1697. https://doi.org/10.7150/ijbs.45472
73. Weingartl HM, Albrecht RA, Lager KM, Babiuk S, Marszal P, Neufeld J, Embury-Hyatt C, Lekcharoensuk P, Tumpey TM, García-Sastre A, Richt JA. Experimental Infection of Pigs with the Human 1918 Pandemic Influenza Virus. *J. Virol.*, 2009, 83(9), 4287–4296. https://doi.org/10.1128/JVI.02399-08.
74. Fong IW in Emerging Zoonoses: A Worldwide Perspective (Emerging Infectious Diseases of the 21st Century), Springer, 2017.

The Chemist
Journal of the American Institute of Chemists

Proper Selection and Application of Mathematical Models for Estimating Occupational Exposure to Chemicals

Kang Chen[a,b], Linda F. Martin[b]

[a] *Henkel AG & Co. KGaA, 201203, Shanghai, China.*
[b] *Capitol Technology University, 20708, Maryland, USA.*
([*] Corresponding author: tjck6@163.com, kchen@captechu.edu)

Abstract: Improper selection and application of chemical exposure models may increase the personnel exposure to hazardous chemicals or lead to a worthless computational effort and unnecessary high-level personal protection. This study is aimed to demonstrate critical points in chemical exposure models selection and application, discuss disadvantages or uncertainties of models with potential opportunities to improve their accuracy, provide equations derivation processes of interest from readers, and introduce advanced chemical exposure modelling software. These objectives are achieved through detailed review and analysis of various models with different level of complexity. It is noteworthy that there is a high potential for predictions to be biased or even become invalid, especially in application of the well-mixed box (WMB) model, near field-far field (NF-FF) model, turbulent diffusion model and Bayesian decision analysis. These critical findings and recommendations can contribute to some reference value for both chemical risk assessment and engineering control in various scenarios of chemical exposure.

Key Words: Hazardous chemicals, Chemical exposure, Mathematical modelling, Risk assessment

1. Introduction

Mathematical modelling has been adopted as a primary exposure risk assessment tool given its ubiquitous presence in a range of industries in the past decades. The accelerated pace of the development of computational capability might shed light on the simplification of numerical simulations [1-4]. Today, it could be relatively easy to reach impressive accuracy when establishing simple models thanks to high performance computers.

"All models are wrong, but some are useful" is a famous quote often attributed to the British statistician George E.P. Box. The idea of this quote is that no single model

will be perfect or one-size-fits-all, meaning that it will never fully represent the real-world object or process. This leads to the awareness of two limitations of any model, namely the scope of its applicability, and its assumption which is the foundation of incompleteness in information representation. Having said that, even if a model cannot describe exactly the reality it could be fairly useful if it is close enough. Chemical exposure models are of extreme importance to the science and practice of industrial hygiene (IH), and indispensable in implementing exposure risk management programs effectively and efficiently. With robust modelling results, pertinent countermeasures can be proposed for engineering reference to control and reduce hazardous material exposure in various working conditions, even with a very limited exposure sampling number. Furthermore, mathematical modelling can support retrospective exposure estimation for a process that no longer exists, e.g., for the purpose of legal prosecution or epidemiology study. Although models vary in their complexity and application, most of them are time-efficient, cost-effective, and able to diagnose exposures prospectively or retrospectively. Chemical exposure models are also extremely useful as tools for performing quick and preliminary exposure scan that can provide early and timely alert about potential over exposure to hazardous materials in which case further investigations are warranted. On the other hand, if the modelling results suggest that the exposure level is extremely low or trivial, it can also help to prioritize exposure monitoring efforts or justify that there is no necessity for sampling and testing programs. This is critically important considering the high risk and cost of sampling of highly hazardous materials, as well as infeasibility and inaccessibility of industrial hygiene sampling in special working conditions (e.g., in a confined chemical reactor or during transient operations).

2. Models in Chemical Exposure Modelling Publications

Chemical exposure models, like all other mathematical models, are basically falling into three categories: physics-based, data driven and grey-box models from qualitative, semiquantitative to quantitative [5-7]. While there are numerous modelling text books or tutorial guides in the field of chemical industrial hygiene and occupational health, the publication- “Mathematical Models for Estimating Occupational Exposure to Chemicals (Second Edition)” published by American Industrial Hygiene Association (AIHA) draws great attention from both practitioners and professionals because of its comprehensiveness and practicality. Hereinafter, the name of this publication is abbreviated as “AIHA MMEOEC (Second Edition)”. Its most up-to-date version covers almost all three categories of models, including physics-based models (physiochemical model and computational fluid dynamics model), grey-box models (well-mixed box model with/without changing conditions, near field/far field two-box model, turbulent eddy diffusion model and plume air dispersion model), and data driven models (statistical model and Bayesian decision analysis). Refer to Figure 1 for demonstration of these models.

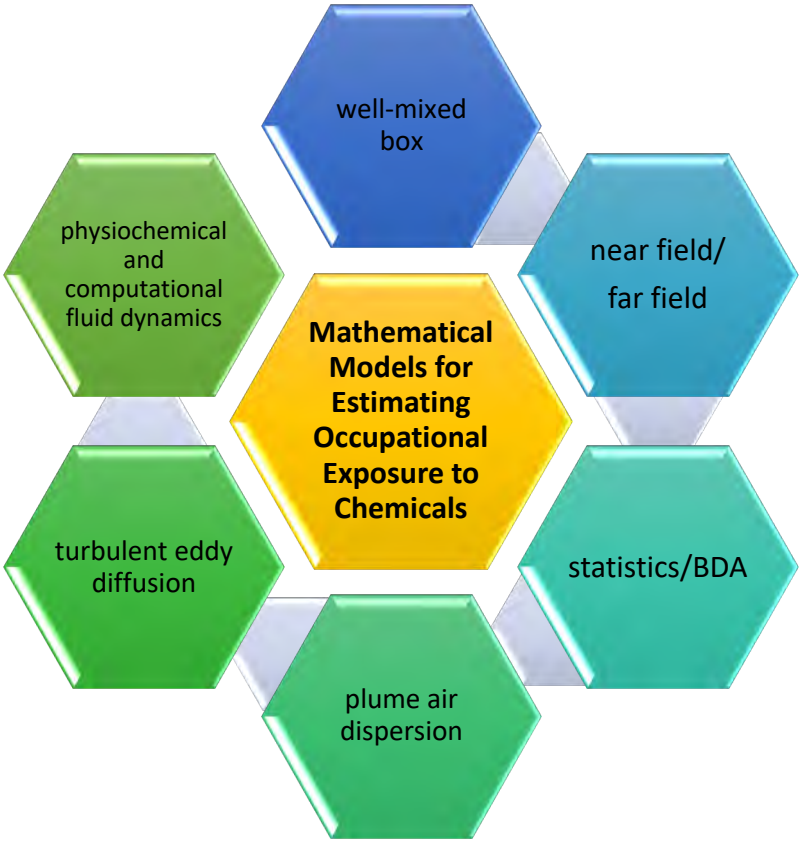

Fig 1. Demonstration of Typical Mathematical Models for Estimating Chemical Exposure

There are multiple opportunities, even for chemical hygiene modelling professionals, to become confused and consequently misunderstand or misapply the principles in model selection and utilization. In this context, the specific purpose of the study is to highlight key points of chemical exposure models selection and application, discuss disadvantages or uncertainties of some models and try to improve their accuracy, identify empirical equations or calculation processes that might lead to misunderstanding or misapplication, demonstrate complete derivation of equations of interest from readers, and introduce newly established modelling and simulation software associated with chemical exposure. In the following sections, all these topics will be discussed respectively in details. While this study was performed mainly based on the AIHA mathematical modelling book, a wider range of topics are analyzed and discussed further in details, and the conclusions could be valuable for both risk assessment and engineering control of hazardous material exposure.

3. Key Points in Chemical Exposure Models Selection and Application

3.1 For a relatively complex indoor environment, the total volume of rooms might be divided into smaller volumes or determined by displacing all solid objects in the room. In many cases of a real chemical laboratory environment, the displaced volume could be significant, but this is often neglected or simplified incorrectly by chemists, which can lead to underestimation of actual concentrations of airborne pollutants and consequently overexposure to hazardous materials due to inadequate protective actions being taken based on the modelling results. It is imperative to raise awareness for all chemists to acquire real data on room volume when the well-mixed room model or computational fluid dynamics model is utilized. Furthermore, in these models, the concentration of contaminants in the make-up air is usually assumed to zero. This might not be true when the outdoor ambient environment is highly polluted together with high potential of outdoor airflow infiltration or reentry into the built environment.

3.2 The well-mixed model is widely recognized as the easiest approach to modeling the indoor chemical contaminant concentrations. Nevertheless, it is a useful approach only if the room air is, indeed, well-mixed or if the contaminant is released at multiple locations throughout a room [8]. The use of mixing factors is discouraged from the author's perspective because they defy the law of conservation of mass and cannot be adequately quantitative. For example, the impact from airflow short circuits might not be mitigated by using a mixing factor and thus variations in pollutant concentration are still exist in the room.

3.3 Although air change is not addressed in the turbulent eddy diffusion models, such kind of removal mechanism in the vicinity of the emission source (e.g., within 1 meter), could be negligible in reducing exposure intensity [9]. Thus, in general, turbulent diffusion models are used to evaluate exposure profile in the near field with the following rules of thumb:

- The concentration value becomes infinite when the distance from the source approaches zero, but an infinite concentration is impossible in the real situation. Thus, the turbulent diffusion models are not appropriate for positions very close to the emission source (e.g., less than 10 cm) [9].
- The turbulent diffusion coefficient (D_T) needs to be calculated carefully and accurately in order to obtain consistent results with the near field (NF) model.
- Contaminants should be released freely without high pressure and thermal energy. Specifically, modeling dispersion via advective air flow and turbulent diffusion is much more difficult than if there is no advective flow due to lack of a closed-form equation that describes the contaminant concentration at various locations and time periods [10-11]. This might answer the question that why only the steady state (time-independent) concentrations are calculated in the current IHMOD software [12].
- Cross-drafts and middle-field effects are not considered in the near field and far field (NF-FF) model, which leads to less adaptability in terms of the concentration gradients compared with the turbulent diffusion model. Figure 2 [9] demonstrates the difference in pollutant concentration gradients within the first 5 mins for a real

case of toluene exposure. The NF-FF model is mainly applied to scenarios of exposure to chemicals with acute toxicity, especially in an imperfectly mixed indoor environment.

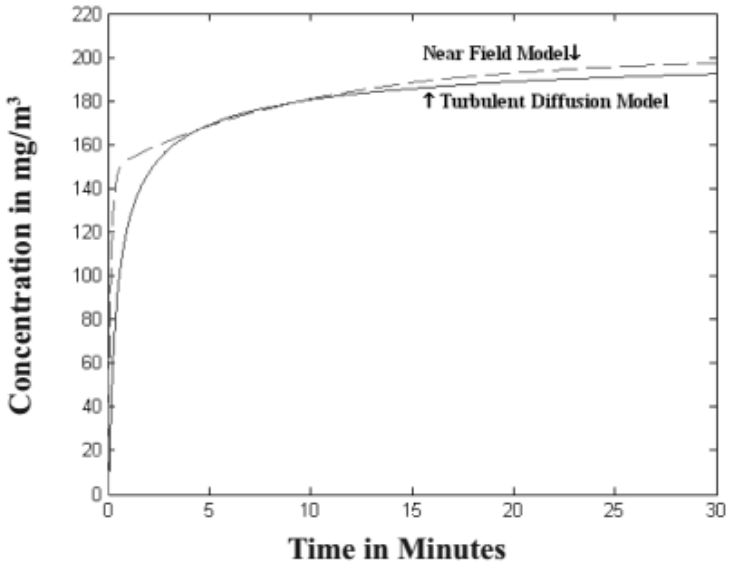

Fig 2. The Comparison of Concentrations as Predicted by the Near Field/Far Field Model Versus the Hemispherical Turbulent Diffusion Model for a Toluene Emission Scenario

3.4 A recently developed modelling freeware (Expostats) for Bayesian decision analysis (BDA) has drawn great attention from the chemical hygiene community [13-15]. BDA has been used in the interpretation of chemical exposure measurements as it renders quantitative integration of professional judgement [16-19] together with data gained from numerical simulations or previous measurements, which permits us to calculate decision probabilities with small sample sizes, even for a single measurement [20-21]. As it is claimed that comparing arithmetic mean to the chemical occupational exposure limit (OEL) is less conservative than comparing the exceedance fraction to 5%, this new tool selects the latter criteria which is numerically equivalent to comparing the estimated 95th percentile to the OEL. Compared with several tools mentioned in the AIHA MMEOEC (Second Edition) (e.g., IHSTAT and IH Data analyst), its assessment output is presented through a risk gauge with a needle indicating the probability value within the related risk category, which can facilitate an easy understanding of the pertinent exposure risk even for general public. Another merit is that this toolkit extends from only left-censored data to interval- and right-censored data and can complete the pretreatment of non-detects in chemical hygiene samples [22-24]. Suitability of the lognormal model for the case under investigation is one important limitation of this tool, and readers might need to consider quasi nonparametric upper tolerance limits (UTLs) for exposure evaluations if measurement results are predominantly below the exposure limit or if their distribution cannot be assumed to comply with parametric assumptions [25].

4. Disadvantages or Uncertainties Of Models and Solutions to Improve Their Accuracy

4.1 In the example 2.4 in the AIHA MMEOEC (Second Edition), the total volume of compressed gas released to the indoor environment is simply calculated by nominal cylinder volume times the ratio between gas cylinder internal pressure and external atmospheric pressure. Nevertheless, chemical industrial standards suggest that the coefficient of compression for the gas investigated under different temperature and pressure should be considered during the calculation to address the real situation [26], through which the final leakage concentration could be obtained more accurately.

4.2 Although the equation (6-3) and (6-4) in the AIHA MMEOEC (Second Edition) describe the time-dependent chemical concentrations in the near and far field, respectively, it is recommended to consider the variability of contaminant generation rate, especially when temperature plays an important role (e.g., large-scale outdoor coating operation during different time periods in a day). In such kind cases, the relationship between temperature and time, i.e., temperature ~ F(time), should be setup firstly and then refer to the equation 6 in this study to establish the function expression between the contaminant generation rate (G) and time, i.e., G ~ f (temperature) ~ f (F(time)).

4.3 The AIHA IHSTAT software uses the Natrella formulas to derive the tolerance factor *k* in calculating UTL 95%, 95%, in which case the chemical samples number should be relatively large (e.g., more than 10) in order to keep adequate accuracy of the modelling outputs [27,28]. It is recommended that pertinent alert should be posted regarding the requirement of the sampling size in the user guide, or preferably another algorithm based on non-central *t*-distribution might be utilized to obtain more accurate results for smaller sampling quantity [28,29]. The major improvement of this alternative algorithm lies in its calculation of the approximate tolerance factor *k* for one-sided tolerance intervals by the following set of formulas:

$$\delta = z_p\sqrt{N} \quad (1)$$

$$k = \frac{t_{\gamma,N-1,\delta}}{\sqrt{N}} \quad (2)$$

where δ is the non-centrality parameter, z_p is the critical value of the normal distribution, γ is the probability and N is the number of sampling.
The disadvantage of the non-central *t*

method is that it depends on the inverse cumulative distribution function for the non-central *t* distribution. This function is not available in many statistical and spreadsheet software programs, but it is available in the software Dataplot and R [28].

5. Derivation Process of Empirical Equations in Chemical Exposure Modelling

5.1 The general form of the equation (4-20) in the AIHA MMEOEC (Second Edition) for determining the average exposure concentrations over time is shown below based on the author's derivation process as well as another teaching note from Mark Nicas [30].

$$C_{avg} = C_{A,in} + \frac{G_A}{Q} + \frac{V}{Q(t-t_0)} \times \left(C_{A,r,0} - C_{A,in} - \frac{G_A}{Q}\right) \times \left(e^{-\frac{Qt_0}{V}} - e^{-\frac{Qt}{V}}\right) \quad (3)$$

Where:

C_{avg}: Time-averaged concentration of chemical A in room air
$C_{A,in}$: Concentration of chemical A in supply air
G_A: Generation rate of chemical A
Q: Ventilation rate
t: Time, t_0: Initial time
$C_{A,r,0}$: Concentration of chemical A in room air at time t_0

By integrating the well-mixed box (WMB) equation above from time $t = 0$ to time $t = t$, it could be easy for readers to find that the equation (4-20) in the AIHA MMEOEC (Second Edition) is incorrect and its right form can be derived as below:

$$C_{avg} = C_{A,in} + \frac{G_A}{Q} + \frac{V}{Qt} \times \left(C_{A,r,0} - C_{A,in} - \frac{G_A}{Q}\right) \times \left(1 - e^{-\frac{Qt}{V}}\right) \quad (4)$$

Further, the limitation of the current equation (4-20) in the AIHA MMEOEC (Second Edition) is that it can only be applied for the scenario $t_0 = 0$. Without reminders or application notes, readers may assume that this equation can be applied to all scenarios just because t_0 and t can be defined as any value, and consequently incorrect average exposure concentrations are obtained.

5.2 The derivation process of the equation for calculating emission rate under various temperature in the example 5.1 and the equation (5-14) in the AIHA MMEOEC (Second Edition) are shown below, respectively, in detail.

Transform the Clausius-Clapeyron equation [31,32] $\frac{\frac{1}{p}dp}{dT} = \frac{\Delta H}{RT^2}$ into $\frac{d(\ln p)}{dT} = \frac{\Delta H}{RT^2}$;
then change the differential part into its derivative form, we obtain $[\ln p(t)]' = \frac{\Delta H}{RT^2}$,
$\therefore \ln p(t) = \frac{-\Delta H}{R} \times T^{-1}$, using T_1 and T_2 representing two different temperatures, the following equations are derived:

$$p(T_1) = e^{-\frac{\Delta H}{RT_1}} \text{ and } p(T_2) = e^{-\frac{\Delta H}{RT_2}} \quad (5)$$

Where:

ΔH is the molar enthalpy of vaporization, R is the molar gas constant, $p(T_1)$, and $p(T_2)$ are the vapor pressure under the absolute temperature T_1 and T_2, respectively.

Finally, the relationship between the emission rate $G(T)$ and the room temperature is expressed as:

$$\frac{G(T_2)}{G(T_1)} = \frac{p(T_1)}{p(T_2)} = e^{-\frac{\Delta H}{R}\left(\frac{1}{T_2}-\frac{1}{T_1}\right)} \quad (6)$$

5.3 The derivation process of the equation (5-14) in the AIHA MMEOEC (Second Edition) hereinafter is relatively complex:

Step one, rewrite the equation (5-13) in the AIHA MMEOEC (Second Edition) as:
$(t)' + \frac{Q}{V} \times C(t) = \frac{\alpha M_0}{V} \times e^{-\alpha t}$;

Step two, insert the exponential term "$e^{\frac{Q}{V}t}$" in order to formalize the derivative term below:

$$C(t)' \times e^{\frac{Q}{V}t} + \frac{Q}{V} \times e^{\frac{Q}{V}t} \times C(t) = \frac{\alpha M_0}{V} \times e^{\left(\frac{Q}{V}-\alpha\right)t}$$

$$\therefore \left[C(t) \times e^{\frac{Q}{V}t}\right]' = \frac{\alpha M_0}{V} \times e^{\left(\frac{Q}{V}-\alpha\right)t};$$

Step three, by integrating both left and right side of the equation above, the following transformation can be derived:

$$C(t) \times e^{\frac{Q}{V}t} = \int \frac{\alpha M_0}{V} \times e^{\left(\frac{Q}{V}-\alpha\right)t}\, dt = \frac{\alpha M_0}{V}\left[\frac{1}{\frac{Q}{V}-\alpha} e^{\left(\frac{Q}{V}-\alpha\right)t} + C_{onst}\right];$$

Step four, based on previous assumption $C(0) = 0$ and thus the constant of integration C_{onst} can be obtained as 1/(α-Q/V);

Finally, rearrange all the terms and the equation (5-14) is obtained as

$$C(t) = \frac{\alpha M_0}{Q-\alpha V}\left[e^{-\alpha t} - e^{-\frac{Q}{V}t}\right];$$

Further, the integral form of the equation (5-14) should be constructed in order to know the time averaged concentration without consideration of back-pressure as below.

$$C_{avg} = \frac{\int_{t_1}^{t_2} \frac{\alpha M_0}{Q-\alpha V}\left[e^{-\alpha t} - e^{-\frac{Q}{V}t}\right] dt}{t_2 - t_1} \quad (7)$$

Where α is the emission rate constant, M_0 is the initial contaminant mass in the source, all the other parameters are the same as those defined in the equation 3, previously.
5.4 While solving the error function (ERF) directly in the section 7.5 of the book is fairly difficult without proper mathematical software packages, approximation of cumulative normal distribution function (CNDF) could be relatively simple as below [33-35]:

$$\varphi(z) \cong \frac{1}{2} + \frac{1}{2}\sqrt{1 - exp\left(-\sqrt{\pi/8}\, z^2\right)}, \text{ where } z \geq 0 \quad (8)$$

and the relationship between the error function and $\varphi(z)$ is:

$$\varphi(z) = \frac{1}{2} + \frac{1}{2} erf\left(\frac{z}{\sqrt{2}}\right), \text{ where } z \geq 0 \quad (9)$$

To eliminate "$\sqrt{2}$", let $x = \frac{z}{\sqrt{2}}$, then $z = \sqrt{2}x$

$$\therefore\ \varphi\left(\sqrt{2}x\right) = \frac{1}{2} + \frac{1}{2} erf(x) \quad (10)$$

The above equations 8 and 10 are coupled in order to solve the error function as below:

$$erf(x)\ = 2\varphi\left(\sqrt{2}x\right) - 1 \cong 1 + \sqrt{1 - exp\left(-\sqrt{\pi/_8}\,2x^2\right)} - 1 \cong \sqrt{1 - exp\left(-\sqrt{\pi/_2}\,x^2\right)} \quad (11)$$

Finally, the following concentration equation in terms of radial distance *r* from the pollutant emission source and time *t* is derived and provides values close to those computed by the exact equation based on the error function:

$$C(r,t) \cong \frac{G}{2\pi D_T r} \times \left[1 - \sqrt{1 - exp\left(-\sqrt{\pi/_{32}}\,\frac{r^2}{D_T t}\right)}\right] \quad (12)$$

While there are no details on derivation of the equation (7-9) in the AIHA MMEOEC (Second Edition), the equation 12 above provides relatively accurate and easy understanding reference on solving the chemical turbulent eddy diffusion model.

6. Misleading or Incomplete Information

6.1 The US EPA website linkage provided in the section 3.4 "Evaporation from Open Surfaces" of the book is not valid and the correct on-line resource for the molecular diffusion coefficient in the air should be directed to: https://www3.epa.gov/ceampubl/learn2model/part-two/onsite/properties.html, and then select "Diffusivity in air and water" column for more details.

6.2 The parameter "$K_l \times V$" in Rule #19a in the Appendix I and the factor K in the equation (4-8) in the AIHA MMEOEC (Second Edition) should be consolidated as "K_{sink}" as both of them have the same meaning to represent the rate of contaminant loss through sinks [36-38], through which can enhance content coherency and readership.

7. Discussion and Conclusion

In this article, multiple mathematical models for chemical occupational exposure evaluation are reviewed systematically and analyzed further in terms of model election, output accuracy and derivation process, which facilitate a better understanding and correct application of different models for chemists or chemical engineers. There are numerous tricks and traps for chemical practitioners or professionals to make imperfect or even incorrect decisions, especially using the WMB model, turbulent eddy diffusion model, NF-FF model, statistical model and Bayesian decision analysis as explained and highlighted above. This critical analysis shines new light onto the application and optimization of mathematical models for chemical occupational exposure evaluation through demonstrating how model predictions could be biased and effective solutions to prevent those misapplications.

There are some recognized challenges or limitations in the present research, which should be addressed in future work. Chemical exposure models investigated in this study only represent a relatively small number of models in real applications due to either research focus or resource limitation. There may be a wider range of exposure scenarios in the emerging chemical industries, including but not limited to exposure to nanoparticles, radioactive chemicals, active pharmaceutical ingredients (APIs) and biochemical active substances (BAS). Recommendations for future work include, first, research on mathematical modelling of dermal exposure to chemicals should be encouraged and scrutinized because physical exposure measurement can be quite challenging considering the uncertainties associated with attempting to quantify real dermal exposure. Currently, there is no scientific method or "golden standard" of measuring the results of the body's exposure to chemicals through dermal contact [39,40]. Therefore, it provides great opportunity and space for the application of dermal exposure models to the chemical community. Additionally, the emerging topic on modelling of combined physiochemical exposure becomes promising and deserve to be further analyzed (e.g., ototoxic chemicals and noise) [41-43]. Last but not least, it is equally important to develop a good mathematical model than knowing how to interpret the results. And here is where the expert interactions are more needed, knowing how to illustrate the results successfully to not only the chemical practitioners but also the general workforce who are concerned with their personal exposure to chemicals.

Acknowledgments

The authors thank Prof. Jérôme Lavoué from University of Montreal, Christopher Packham, FRSPH, FIIRSM from EnviroDerm Services and Dr. Paul Hewett from Exposure Assessment Solutions, Inc. for their technical guidance and professional comments in the field of chemical exposure modelling.

References

1 Shiling Z, Paul P, Liangbo H, Parmesh V, Richard L, Larry B. “CFD modeling of flammable refrigerant leaks inside machine rooms: Emergency ventilation rates for different size chillers". *Sci. Technol. Built Environ.*, 2018, 24(8), 878-885. DOI: 10.1080/23744731.2018.1448676.

2 Stern F, Wilson RV, Coleman HW, Paterson EG. “Comprehensive approach to verification and validation of CFD simulations—part 1: methodology and procedures”. *J. Fluids Eng.*, 2001, 123(4), 793-802. DOI: 10.1115/1.1412235.

3 Chen K, Yang JL, Zhang HB, Zhang WJ. “Low level noise analysis in laboratory fume hood”. *J. Chem. Health Saf.*, 2017, 24(1), 2–7. DOI: 10.1016/j.jchas.2016.03.002.

4. Kang C, Weize W, Wenjun Z. “Investigation of influential factors on laboratory fume hood containment performance”. *Sci. Technol. Built Environ.*, 2020, 26(3), 387-399. DOI: 10.1080/23744731.2019.1637192.

5 Abdul A, Farrokh JS. “Review of modeling methods for HVAC systems”. *Appl. Therm. Eng.*, 2014, 67(1–2), 507-519. DOI: 10.1016/j.applthermaleng.2014.03.055.

6 Abdul A, Farrokh JS. “Gray-box modeling and validation of residential HVAC system for control system design”. *Appl. Energy*, 2015, 137, 134-150. DOI: 10.1016/j.apenergy.2014.10.026.

7 Abdul A, Farrokh JS. “Black-box modeling of residential HVAC system and comparison of gray-box and black-box modeling methods”. *Energy Build.*, 2015, 94, 121-149. DOI: 10.1016/j.enbuild.2015.02.045.

8 Heinsohn RJ in “General Ventilation Well-Mixed Mode”, Industrial Ventilation Engineering Principles, John Wiley & Sons, Inc., New York, 1991, ch. 5. ISBN-13: 978-0471637035.

9 American Industrial Hygiene Association in Mathematical Models for Estimating Occupational Exposure to Chemicals, American Industrial Hygiene Association, Virginia, 2009. ISBN: 978-1-935082-10-1.

10 Nicas M, Armstrong TW. “Computer implementation of mathematical exposure modeling”. *Appl. Occup. Environ. Hyg.*, 2003, 18(8), 566–571. DOI: 10.1080/10473220301417.

11 Nicas M. “Modeling turbulent diffusion and advection of indoor air contaminants by Markov chains”. *Am. Ind. Hyg. Assoc. J.*, 2001, 62(2), 149-158. DOI: 10.1080/15298660108984617.

12 http://www.aiha.org/Content/InsideAIHA/Volunteer+Groups/EAScomm.htm, AIHA IH MOD software, accessed 9/8/2020.

13 Jérôme L, Lawrence J, Peter K, Hugh D, France L, Frédéric C, Gautier M, Tracy K. “Expostats: A Bayesian toolkit to aid the interpretation of occupational exposure measurements”. *Ann. Work Exposures Health*, 2019, 63(3), 267–279. DOI: 10.1093/annweh/wxy100.

14 Gurumurthy R. “Progress in Bayesian statistical applications in exposure assessment”. *Ann. Work Exposures Health*, 2019, 63(3), 259–262. DOI: 10.1093/annweh/wxz007.

15 Eun GL, Diana MC. “Adoption of exposure assessment tools to assist in providing respiratory protection recommendations”. *Ann. Work Exposures Health*, 2020, 64(5), 547-557. DOI: 10.1093/annweh/wxaa023.

16 Susana GH, Mariscala MA, Javier GR, Dale OR. “Working conditions, psychological/physical symptoms and occupational accidents. Bayesian network models”. *Saf. Sci.*, 2012, 50(9), 1760-1774. DOI: 10.1016/j.ssci.2012.04.005.

17 Ramachandran G, Vincent JH. “A Bayesian approach to retrospective exposure assessment”. *Appl. Occup. Environ. Hyg.*, 1999, 14(8), 547–557. DOI: 10.1080/104732299302549.

18 Sottas PE, Lavoué J, Bruzzi R, David V, Nicole C, Droz PO. “An empirical hierarchical Bayesian unification of occupational exposure assessment methods”. *Stat. Med.*, 2009, 28(1), 75–93. DOI: 10.1002/sim.3411.

19 Banerjee S, Ramachandran G, Vadali M, Sahmel J. “Bayesian hierarchical framework for occupational hygiene decision making”. *Ann. Occup. Hyg.*, 2014, 58(9), 1079–1093. DOI: 10.1093/annhyg/meu060.

20 Jones RM, Burstyn I. “Bayesian analysis of occupational exposure data with conjugate priors”. *Ann. Work Exposures Health*, 2017, 61(5), 504–514. DOI:

10.1093/annweh/wxx032.
21 Paul H, Perry L, John M, Gurumurthy R, Sudipto B. “Rating exposure control using Bayesian decision analysis”. *J. Occup. Environ. Hyg.*, 2006, 3(10), 568-581. DOI: 10.1080/15459620600914641.
22 https://expostats.ca/site/app-local/NDExpo, NDExpo, a JavaScript Web application that implements the robust ROS (regression on order statistics) censored data treatment approach, accessed 9/8/2020.
23 Dennis RH in “Computing Summary Statistics and Totals”, Statistics for Censored Environmental Data Using Minitab® and R, 2nd Edition, Wiley, New Jersey, 2012, ch. 6. ISBN: 978-0-470-47988-9.
24 Dennis RH. “More than obvious: better methods for interpreting nondetect data”. *Environ. Sci. Technol.*, 2005, 39(20), 419A–423A. DOI: 10.1021/es053368a.
25 Charles BD, Paul FW. “‘Quasi Nonparametric’ upper tolerance limits for occupational exposure evaluations”. *J. Occup. Environ. Hyg.*, 2015, 12(5), 342-349. DOI: 10.1080/15459624.2014.995301.
26 CSBTS (China State Bureau of Quality and Technical Supervision). Industrial nitrogen (GB/T 3864-2008). CSBTS: Beijing, China, 2008.
27 Selvin S, Rappaport SM, Spear R, Schulman J, Francis M. “A note on the assessment of exposure using one-sided tolerance limits”. *Am. Ind. Hyg. Assoc. J.*, 1987, 48(2), 89-93. DOI: 10.1080/15298668791384445.
28 National Institute of Standards and Technology (NIST). Product and Process Comparisons, NIST/SEMATECH e-Handbook of Statistical Methods, NIST, Maryland, 2013, ch. 7. DOI: 10.18434/M32189.
29 CSBTS (China State Bureau of Quality and Technical Supervision). The tables of quantiles of the noncentral t-distribution (GB/T 15932-1995). CSBTS: Beijing, China, 1995.
30 Nicas M. PH 270A Indoor Air Quality Models, teaching notes, 2020.
31 David RL in CRC Handbook of Chemistry and Physics (82nd Edition), CRC Press, Inc., Florida, 2001. ISBN: 978-0849304828.
32 John AD in Lange′s Handbook of Chemistry (15th Edition), McGraw-Hill, Inc., New York, 1999. ISBN: 0-07-016384-7.
33 Aludaat KM. “Alodat M.T. A note on approximating the normal distribution function”. *Appl. Math. Sci.*, 2008, 2(9), 425-429.
34 Eidous OM, Shareefa RA. “New approximations for standard normal distribution function”. *Commun. Stat.—Theory Methods*, 2020, 49(6), 1357-1374. DOI: 10.1080/03610926.2018.1563166.
35 Wang JJ, Yang ZL. “Review of approximating functions to cumulative normal distribution function”. *J. Comput. Appl. Math.*, 2014, 34(S2), 83-84, 90. DOI: 1001-9081(2014)S2-0083-02.
36 Jayjock MA, Doshi DR, Nungesser EH, Shade WD. “Development and evaluation of a source/sink model of indoor air concentrations from isothiazolone-treated wood used indoors”. *Am. Ind. Hyg. Assoc. J.*, 1995, 56(6), 546-557. DOI: 10.1080/15428119591016773.
37 Salma I, Dosztály K, Borsós T, Söveges B, Weidinger T, Kristóf G, Péter N, Kertész Zs. “Physical properties, chemical composition, sources, spatial distribution and sinks of indoor aerosol particles in a university lecture hall”. *Atmos. Environ.*, 2013, 64, 219-228. DOI: 10.1016/j.atmosenv.2012.09.070.
38 He C, Morawska L, Gilbert D. “Particle deposition rates in residential houses”. *Atmos. Environ.*, 2005, 39(21), 3891-3899. DOI: 10.1016/j.atmosenv.2005.03.016.
39 European Agency for Safety and Health at Work (EU-OSHA). Occupational skin diseases and dermal exposure in the European Union (EU-25): policy and practice overview, EU-OSHA, Belgium, 2008. ISBN: 978-92-9191-161-5.
40 Konstantinos MK, Suzanne S, Angelos NT, Remy F, Ilianna C, Pelagia A, Kyriaki M, Dag R, Michael R, Ulrich P, Gianna L, Anja B, Urs S, Rianda MGE. “Comparison of measurement methods for dermal exposure to hazardous chemicals at the workplace: the SysDEA project”. *Ann. Work Exposures Health*, 2020, 64(1), 55–70. DOI: 10.1093/annweh/wxz085.
41 Chen K, Zhang HB, Zhang WJ. “Measures to alleviate fume hood noise”. *Am. Lab.*, 2018, 50(3), 10-13.
42 Chang SJ, Chen CJ, Lien CH, Sung FC. “Hearing loss in workers exposed to toluene and noise”. *Environ. Health Perspect.*, 2006,

114(8), 1283–1286. DOI: 10.1289/ehp.8959.
43 Choi YH, Kim K. “Noise-Induced hearing loss in Korean workers: Co-Exposure to organic solvents and heavy metals in nationwide industries”. *Plos One*, 2014, 9(5), e97538. DOI: 10.1371/journal.pone.0097538.

The AIC Code of Ethics

Approved by the AIC Board of Directors, April 29, 1983

The profession of chemistry is increasingly important to the progress and the welfare of the community. The Chemist is frequently responsible for decisions affecting the lives and fortunes of others. To protect the public and maintain the honor of the profession, the American Institute of Chemists has established the following rules of conduct. It is the Duty of the Chemist:

1. To uphold the law; not to engage in illegal work nor cooperate with anyone so engaged;

2. To avoid associating or being identified with any enterprise of questionable character;

3. To be diligent in exposing and opposing such errors and frauds as the Chemist's special knowledge brings to light;

4. To sustain the institute and burdens of the community as a responsible citizen;

5. To work and act in a strict spirit of fairness to employers, clients, contractors, employees, and in a spirit of personal helpfulness and fraternity toward other members of the chemical profession;

6. To use only honorable means of competition for professional employment; to advertise only in a dignified and factual manner; to refrain from unfairly injuring, directly or indirectly, the professional reputation, prospects, or business of a fellow Chemist, or attempting to supplant a fellow chemist already selected for employment; to perform services for a client only at rates that fairly reflect costs of equipment, supplies, and overhead expenses as well as fair personal compensation;

7. To accept employment from more than one employer or client only when there is no conflict of interest; to accept commission or compensation in any form from more than one interested party only with the full knowledge and consent of all parties concerned;

8. To perform all professional work in a manner that merits full confidence and trust; to be conservative in estimates, reports, and testimony, especially if these are related to the promotion of a business enterprise or the protection of the public interest, and to state explicitly any known bias embodied therein; to advise client or employer of the probability of success before undertaking a project;

9. To review the professional work of other chemists, when requested, fairly and in confidence, whether they are:
    a. subordinates or employees
    b. authors of proposals for grants or contracts
    c. authors of technical papers, patents, or other publications
    d. involved in litigation;

10. To advance the profession by exchanging general information and experience with fellow Chemists and by contributing to the work of technical societies and to the technical press when such contribution does

not conflict with the interests of a client or employer; to announce inventions and scientific advances first in this way rather than through the public press; to ensure that credit for technical work is given to its actual authors;

11. To work for any client or employer under a clear agreement, preferable in writing, as to the ownership of data, plans, improvements, inventions, designs, or other intellectual property developed or discovered while so employed, understanding that in the absence of a written agreement:
    a. results based on information from the client or employer, not obtainable elsewhere, are the property of the client or employer
    b. results based on knowledge or information belonging to the Chemist, or publicly available, are the property of the Chemist, the client or employer being entitled to their use only in the case or project for which the Chemist was retained
    c. all work and results outside of the field for which the Chemist was retained or employed, and not using time or facilities belonging to a client or employer, are the property of the Chemist;

12. Special data or information provided by a client or employer, or created by the Chemist and belonging to the client or employer, must be treated as confidential, used only in general as a part of the Chemist's professional experience, and published only after release by the client or employer;

13. To report any infractions of these principles of professional conduct to the authorities responsible for enforcement of applicable laws or regulations, or to the Ethics Committee of The American Institute of Chemists, as appropriate.

The Chemist
Journal of the American Institute of Chemists

Manuscript Style Guide

The Chemist is the official online refereed journal of The American Institute of Chemists (AIC). We accept submissions from all fields of chemistry defined broadly (e.g., scientific, educational, socio-political). *The Chemist* will not consider any paper or part of a paper that has been published or is under consideration for publication anywhere else. The editorial office of *The Chemist* is located at: The American Institute of Chemists, Inc. 315 Chestnut Street Philadelphia, PA 19106-2702, Email: aicoffice@theaic.org.

Categories of Submissions

RESEARCH PAPERS

Research Papers (up to ~5000 words) that are original will only be accepted. Research Papers are peer-reviewed and include an abstract, an introduction, up to 5 figures or tables, sections with brief subheadings and a maximum of approximately 30 references.

REPORTS

Reports (up to ~3000 words) present new research results of broad interest to the chemistry community. Reports are peer- reviewed and include an abstract, an introductory paragraph, up to 3 figures or tables, and a maximum of approximately 15 references.

BRIEF REPORTS

Brief Reports (up to ~1500 words) are short papers that are peer-reviewed and present novel techniques or results of interest to the chemistry community.

REVIEW ARTICLES

Review Articles (up to ~6000 words) describe new or existing areas of interest to the chemistry community. Review Articles are peer-reviewed and include an abstract, an introduction that outlines the main point, brief subheadings for each section and up to 80 references.

LETTERS

Letters (up to ~500 words) discuss material published in The Chemist in the last 8 months or issues of general interest to the chemistry community.

BOOK REVIEWS

Book Reviews (up to ~ 500 words) will be accepted.

Manuscript Preparation

RESEARCH PAPERS, REPORTS, BRIEF REPORTS & REVIEW ARTICLES

- **The first page** should contain the title, authors and their respective institutions/affiliations and the corresponding author. The general area of chemistry the article represents should also be indicated, i.e. General Chemistry, Organic Chemistry, Physical Chemistry, Chemical Education, etc.

- **Titles** should be 55 characters or less for Research Papers, Reports, and Brief Reports. Review articles should have a title of up to 80 characters.

- **Abstracts** explain to the reader why the research was conducted and why it is important to the field. The abstract should be 100-150 words and convey the main point of the paper along with an outline of the results and conclusions.

- **Text** should start with a brief introduction highlighting the paper's significance and should be understood to readers of all chemistry disciplines. All symbols, abbreviations, and acronyms should be defined the first time they are used. All tables and figures should be cited in numerical order.

- **Units** must be used appropriately. Internationally accepted units of measurement should be used in conjunction with their numerical values. Abbreviate the units as shown: cal, kcal, µg, mg, g (or gm), %, ^{o}C, nm, µm (not m), mm, cm, cm^{3}, m, in. (or write out inch), h (or hr), min, s (or sec), ml [write out liter(s)], kg. Wherever commonly used units are used their conversion factors must be shown at their first occurrence. Greek symbols are permitted as long as they show clearly in the soft copy.

- **References and notes** should be numbered in the order in which they are cited, starting with the text and then through the table and figure legends. Each reference should have a unique number and any references to unpublished data should be given a number in the text and referred to in the references. References should follow the standards presented in the AIC Reference Style Guidelines below.

REFERENCE STYLE GUIDELINES

References should be cited as numbers within square brackets [] at the appropriate place in the text. The reference numbers should be cited in the correct order throughout the text (including those in tables and figure captions, numbered according to where the table or figure is designated to appear). The references themselves are listed in numerical order at the end of the final printed text along with any Notes. Journal abbreviations should be consistent with those presented in Chemical Abstracts Service Source Index (CASSI) (http://www.cas.org) guide available at most academic libraries.

- **Names** and initials of all authors should always be given in the reference and must not be replaced by the phrase *et al*. This does not preclude one from referring to them by the first author, et al in the text.

- **Tables** should be in numerical order as they appear in the text and they should not duplicate the text. Tables should be completely understandable without reading the text. Every table should have a title. Table titles should be placed above the respective tables.

  Table 1. Bond Lengths (Å) of 2-aminophenol

- **Figure legends** should be in numerical order as they appear in the text. Legends should be limited to 250 words.

  Figure 1. PVC Melt Flow Characterized by Analytical Structural Method

- **Letters and Book Reviews** should be clearly indicated as such when being submitted. They are not peer-reviewed and are published as submitted. Legends should be placed after/under the respective figures.

- **Journals -** The general format for citations should be in the order: **author(s), journal, year, volume, page**. Page number ranges are preferred over single values, but either format is acceptable. Where page numbers are not yet known, articles may be cited by DOI (Digital Object Identifier). For example:

  Booth DE, Isenhour TL. *The Chemist*, 2000, 77(6), 7-14.

- **Books -** For example:

  Turner GK in *Chemiluminescence: Applications*, ed. Knox Van Dyke, CRC Press, Boca Raton, 1985, vol 1, ch. 3, pp 43-78.

- **Patents** should be indicated in the following form:

  McCapra F, Tutt D, Topping RM, UK Patent Number 1 461 877, 1973.

- **Reports and bulletins, etc. -** For example:

  Smith AB, Jones CD, *Environmental Impact Report for the US*, final report to the National Science Foundation on Grant AAA-999999, Any University, Philadelphia, PA, 2006.

- **Material presented at meetings -** For example:

  Smith AB. Presented at the Pittsburgh Conference, Atlantic City, NJ, March 1983, paper 101.

- **Theses -** For example:

  Jones AB, Ph.D. Thesis, Columbia University, 2004.

- For material presented at a meeting, congress or before a Society, etc., but not published, the following form should be used:

  Jones AB, presented in part at the 20th American Institute of Chemists National Meeting, Philadelphia, PA, June, 2004.

- For material accepted for publication, but not yet published, the following form should be used:

  Smith AB. *Anal. Chem*., in press

- For material submitted for publication but not yet accepted the following form should be used:

  Jones AB, *Anal. Chem*. submitted for publication.

- For personal communications the following should be used:

  Smith AB, personal communication.

- If material is to be published but has not yet been submitted the following form should be used:

  Smith AB, unpublished work.

Reference to unpublished work should not be made without the permission of those by whom the work was performed.

Manuscript Selection

The submission and review process is completely electronic. Submitted papers are assigned by the Editors, when appropriate, to at least two external reviewers anonymously. Reviewers will have approximately 10 days to submit their comments. In selected situations the review process can be expedited. Selected papers will be edited for clarity, accuracy, or to shorten, if necessary. The Editor-in-Chief will have final say over the acceptance of submissions. Most papers are published in the next issue after acceptance. Proofs will be sent to the corresponding author for review and approval. Authors will be charged for excessive alterations at the discretion of the Editor-in-Chief.

Conditions of Acceptance

When a paper is accepted by *The Chemist* for publication, it is understood that:

- Any reasonable request for materials to verify the conclusions or experiments will be honored.

- Authors retain copyright but agree to allow *The Chemist* to exclusive license to publish the submission in print or online.
- Authors agree to disclose all affiliations, funding sources, and financial or management relationships that could be perceived as potential conflicts of interest or biases.
- The submission will remain a privileged document and will not be released to the public or press before publication.
- The authors certify that all information described in their submission is original research reported for the first time within the submission and that the data and conclusions reported are correct and ethically obtained.
- The Chemist, the referees, and the AIC bear no responsibility for accuracy or validity of the submission.

Authorship

By submitting a manuscript, the corresponding author accepts the responsibility that all authors have agreed to be listed and have seen and approved of all aspects of the manuscript including its submission to *The Chemist*.

Submissions

Authors are required to submit their manuscripts, book reviews and letters electronically. They can be submitted via email at aicoffice@theaic.org with "Submission for consideration in *The Chemist*" in the subject line. All submissions should be in Microsoft® Word format.

Copyright Assignment & Warranty Form for The Chemist

It is the policy of *The Chemist* to require all contributors to transfer the copyright for their contributions (hereafter referred to as the manuscript) to The American Institute of Chemists, Inc. (hereafter referred to as The AIC) the official publisher of *The Chemist*. By signing this agreement you assign to The AIC to consider publishing your manuscript the exclusive, royalty-free, irrevocable copyright in any medium internationally for the full term of the copyright. This agreement shall permit The AIC to publish, distribute, create derivative works, and otherwise use any materials accepted for publication in *The Chemist* internationally. A copy of the Copyright and Warranty Form for *The Chemist* will be sent to the author(s) whose manuscript is accepted for publication. The AIC will not publish any accepted manuscript in *The* Chemist without its author(s) fully complying with this requirement.

For further information or if you can any questions please contact the Publisher of *The Chemist* at (215) 873-8224 or via email at publications@theaic.org.

Website: http://www.theaic.org/ Email: aicoffice@theaic.org Phone: 215-873-8224

Announcements

INVITATION TO AUTHORS

Authors are invited to submit manuscripts for ***The Chemist,*** the official online refereed journal of The American Institute of Chemists (AIC). We accept submissions from all fields of chemistry defined broadly (e.g., scientific, educational, socio-political). *The Chemist* will not consider any paper or part of a paper that has been published or is under consideration for publication anywhere else.

Research Papers (up to ~5000 words) that are original will only be accepted. Research Papers are peer-reviewed and include an abstract, an introduction, up to 5 figures or tables, sections with brief subheadings and a maximum of approximately 30 references.

Reports (up to ~3000 words) present new research results of broad interest to the chemistry community. Reports are peer- reviewed and include an abstract, an introductory paragraph, up to 3 figures or tables, and a maximum of approximately 15 references.

Brief Reports (up to ~1500 words) are short papers that are peer-reviewed and present novel techniques or results of interest to the chemistry community.

Where to Send Manuscripts?

Please submit your manuscripts by email (aicoffice@theaic.org) to the attention of:

The Editor-in-Chief, The Chemist
The American Institute of Chemists, Inc.
315 Chestnut Street,
Philadelphia, PA 19106-2702
Email: aicoffice@theaic.org

Review Articles (up to ~6000 words) describe new or existing areas of interest to the chemistry community. Review Articles are peer-reviewed and include an abstract, an introduction that outlines the main point, brief subheadings for each section and up to 80 references.

Letters (up to ~500 words) discuss material published in *The Chemist* in the last 8 months or issues of general interest to the chemistry community.

Book Reviews (up to ~ 500 words) will be accepted.

American Institute of Chemists

www.TheAIC.org

From its earliest days in 1923 to the present, the American Institute of Chemists has fostered the advancement of the chemical profession in the United States.

The Institute has a corresponding dedication "to promote and protect the public welfare; to establish and maintain standards of practice for these professions; and to promote the professional experience through certification as to encourage competent and efficient service."

The AIC engages in a broad range of programs for professional enhancement through the prestigious Fellow membership category, awards program, certification programs, meetings, publications and public relations activities.

Advertising: Send insertion orders and advertising materials to AIC. Visit The AIC Web site for additional information at www.TheAIC.org.

The American Institute of Chemists, Inc.
315 Chestnut Street, Philadelphia, PA 19106-2702.
Phone: (215) 873-8224 | Fax: (215) 629-5224 | E-mail: aicoffice@TheAIC.org